Dissertation zur Erlangung des Doktorgrades
der Fakultät für Chemie und Pharmazie
der Ludwig-Maximilians-Universität München

Structural and Biochemical Characterization of Eukaryotic mRNA Decapping Activators

Humayun Sharif

aus

Sangla Hill in Pakistan

2014

Erklärung

Diese Dissertation wurde im Sinne von §7 der Promotionsordnung vom 28. November 2011 von Frau Prof. Dr. Elena Conti betreut.

Eidesstattliche Versicherung

Diese Dissertation wurde eigenständig und ohne unerlaubte Hilfe erarbeitet.

München, den 5. Juni 2014

.....

Humayun Sharif

Dissertation eingereicht am 5. Juni 2014

Erstgutachter: Prof. Dr. Elena Conti

Zweitgutachter: Prof. Dr. Karl-Peter Hopfner

Mündliche Prüfung am 29. Juli 2014

To my beloved mother,

Without her, this journey would not have been possible.

Contents

List of Figures

Introduction

Results

Extended Discussion

List of Tables

Introduction

Results

Abbreviations

ADP	adenosine diphosphate
ARE	AU-rich elements.
ATP	adenosine triphosphate
ATPase	ATP hydrolase
DNA	deoxyribonucleic acid
Edc3	enhancer of decapping 3
FRET	Fluorescence resonance energy transfer
HEAT	Huntingtin, elongation factor 3 (EF3), protein
repeat	phosphatase 2A (PP2A), and the yeast kinase
	TOR1 repeat
MIF4G	middle domain of eukaryotic initiation factor 4G
MR	molecular relplacement
mRNA	Messenger RNA
NGD	no-go decay
NMD	nonsense-mediated decay
nt	nucleotides
Pat1	topoisomerase 2-associated protein
Pab1	poly(A)-binding protein
PCR	polymerase chain reaction
poly(A)	polyadenylate
r.m.s.d.	root mean square deviation
RNA	ribonucleic acid
RNAi	RNA interference
RNase	ribonuclease
RNP	Ribonucleoprotein
SF2	superfamily II
SKI	superkiller
snRNA	small nuclear RNA
TAP	tandem affinity purification
TRAMP	Trf4/5-Air1/2-Mtr4 polyadenylation complex

SLiMs	small linear motifs
Xrn1	5'-3' exoribonuclease 1

Summary

In eukaryotes, mRNA turnover starts with the truncation of 3′ poly(A) tail and proceeds with either 3′-to-5′ degradation by the exosome complex or with decapping followed by 5′-to-3′ degradation by Xrn1. mRNA decapping is catalyzed by the decapping enzyme complex Dcp1-Dcp2 and is regulated by a highly conserved set of decapping activator proteins, including Pat1, Dhh1, Edc3 and the heptameric Lsm1-7 complex. The mechanisms regarding the interplay of mRNA decapping activators remains elusive owing to limited structural and biochemical understanding. My doctoral research was focused on elucidating the structural and functional roles of mRNA decapping activators involved in mRNA decay.

Pat1 has a modular domain architecture that allows it to interact with multiple decapping activators simultaneously. Pat1 acts as a bridging factor between the 3′-end and the 5′-end of the mRNA by interacting with multiple proteins involved in decapping. The interaction of *S. cerevisiae* Pat1 N-terminus with the DEAD-box protein Dhh1 was characterized by biochemical pull-down assays and binding affinities were determined quantitatively by isothermal titration calorimetery. Based on these experiments, the crystal structure of Dhh1 bound to Pat1 was determined at 2.8 Å resolution. The structure reveals that Pat1 wraps around RecA2 domain of Dhh1 via evolutionary conserved interactions. This conserved surface of Dhh1 is also implicated in interaction with another decapping activator, Edc3, rationalizing why Pat1 and Edc3 binding to Dhh1 is mutually exclusive. These interactions were supported by testing mutations in *in vitro* assays with the yeast proteins and in co-immunoprecipitation assays with the corresponding human orthologs. Furthermore, structural analysis combined with RNA pull-down assays and a crosslinking mass spectrometry based approach gave definitive evidence that Dhh1 engages with Pat1, Edc3 and RNA in a mutually exclusive manner.

The Lsm1-7 complex is another important activator of mRNA decapping. It protects the mRNA transcripts from 3′-end degradation and enhances the mRNA decapping. I determined the crystal structure of the Lsm1-7 complex at 2.3 Å resolution showing a hetero-heptameric complex of Lsm1-7 proteins that make a ring-like overall topology. Furthermore, an unusual helical structure of Lsm1 C-terminal extension and protrudes into the central channel of the heptameric ring, explaining how it is modulates the RNA binding properties of the complex.

The Lsm1-7 complex interacts with the C-terminal domain of Pat1. Structure determination of this octameric Lsm1-7-Pat1 complex at 3.7 Å gave insights into the interaction of Pat1 with Lsm1-7 complex. Unexpectedly, Pat1 binds to Lsm2 and Lsm3 but not with the cytoplasmic specific subunit Lsm1. The Pat1 C-terminus makes a super-helical structure consisting of HEAT-like repeats of anti-parallel helices similar to the structure of its human ortholog. Structure based mutagenesis analysis by i*n vitro* pull-downs showed that these interactions are conserved.

This doctoral thesis gives structural and mechanistic insight into the role of multi-domain protein Pat1 and how it engages at two distinct ends of mRNA by interacting with Dhh1 at 5′-end and with Lsm1-7 complex that at 3′-end. Combining these results present a model of dynamic interplay of these activators and gives a better understanding of protein-protein and protein-RNA interaction network in the decapping machinery.

1 Preface

This thesis is written in a cumulative style because my doctoral research work lead to two first author publications. Both the research papers are related and represent the work I did during the last three and a half years. The introduction chapter covers the broader field of research and its current status. Chapter three includes the full original manuscripts attached including detailed material and methods, results and discussion. Chapter four deals with the extended discussion of both the papers and puts forth the major advancement in the field contributed by this thesis. In the end, a brief outlook is presented.

Sharif, H., Ozgur, S., Sharma, K., Basquin, C., Urlaub, H., and Conti, E. (2013). Structural analysis of the yeast Dhh1-Pat1 complex reveals how Dhh1 engages Pat1, Edc3 and RNA in mutually exclusive interactions. ***Nucleic Acids Res.*** 41, 8377–8390 (2013).

Sharif, H and Conti, E. Architecture of the Lsm1-7-Pat1 complex: A conserved assembly in eukaryotic mRNA turnover. ***Cell Reports***. 5, 283–291 (2013).

2 Introduction

2.1 Mechanism of mRNA turnover

The control of post-transcriptional gene expression in eukaryotes includes regulation of every step involved in messenger RNA (mRNA) metabolism (Moore, 2005). From transcription and splicing in the nucleus to the cytoplasmic export, translation and degradation of the mRNAs, all aspects are stringently controlled by several cellular and non-cellular factors (Garneau et al., 2007; Moore, 2005).

Eukaryotic mRNAs actively involved in the translation pool in the cytoplasm can be distinguished from those which are destined for degradation by having a 5′-methylguanosine (m^7GpppN) cap structure and a polyadenlylated 3′ end (Cougot et al., 2004b; Garneau et al., 2007; Parker and Sheth, 2007). The m^7G cap structure protects the translating mRNAs from degradation and is protected by the cap-binding proteins complex eIF4F, which consists of eukaryotic initiation factors eIF4E, eIF4A, eIF4G (Sonenberg and Hinnebusch, 2009). Moreover, the mRNA poly(A) tail is protected by poly(A)-binding proteins (Pab1) which shield the mRNA from exonucleases and interact with eIF4G (Jackson et al., 2010; Sonenberg and Hinnebusch, 2009). The cooperative binding of eIF4F component eIF4G with Pab1 is believed to circularize the mRNA restricting the mRNA decay factors and promoting the faithful translation of the mRNA message (Topisirovic et al., 2011; Wells et al., 1998).

Two major pathways of mRNA degradation (Figure 2.1) start with the shortening of polyadenylated (poly(A)) tail (Chen and Shyu, 2011). Deadenylation is mainly mediated by the Pan2-Pan3 and Ccr4-Not deadenylase complexes (Wahle and Winkler, 2013). Following deadenylation, mRNAs are targeted for 5′-to-3′ decay, which is initiated by removal of m^7G cap from the target mRNAs, by a process called mRNA decapping and is followed by 5′ exonucleotic decay by Xrn1 (Decker and Parker, 1993; Dunckley and Parker, 1999; Hsu and Stevens, 1993). Moreover,

deadenylated mRNAs can be degraded by the exosome mediated 3′-to-5′ decay pathway (Franks and Lykke-Andersen, 2008; Januszyk and Lima, 2014; Mitchell et al., 1997) and the remaining cap structure is hydrolyzed by scavenger decapping enzyme DcpS (Liu et al., 2002) . The two-pathway conservation amongst all eukaryotes shows redundancy and can be attributed to tight control of mRNA degradation.

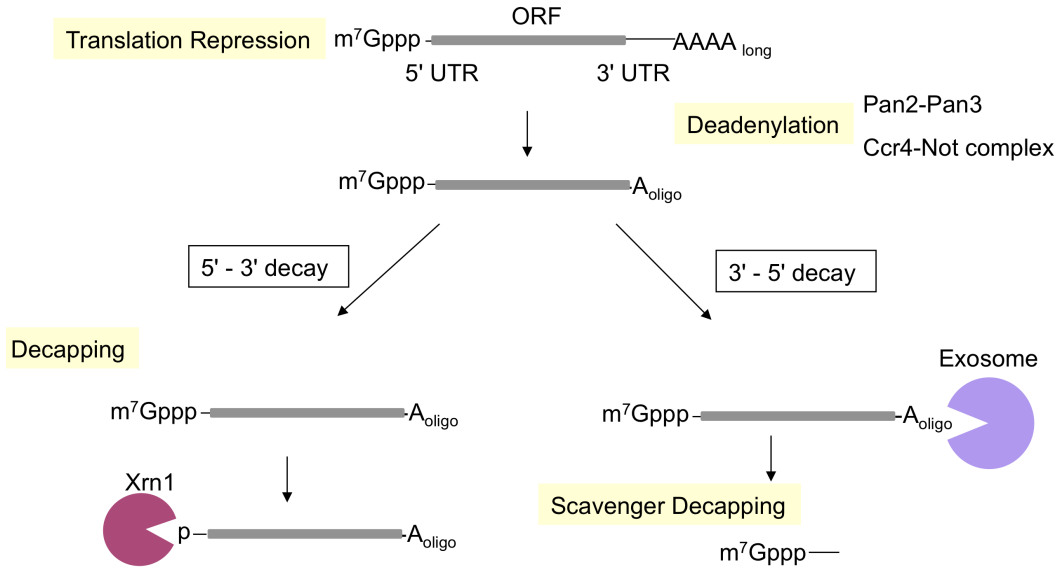

Figure 2.1: General mechanism of eukaryotic mRNA decay

Deadenylation dependent degradation is the major degradation mechanism in which mRNAs to be degraded are deadenylation of 3′-poly(A) tail of by Pan-Pan3 and Ccr4-Not complex. Following deadenylation the mRNA substrates can follow 5′-to-3′ decapping dependent decay pathway. In this pathway, the decapping enzymes Dcp1-Dcp2 hydrolyze the 5′-cap structure from the mRNAs with the help of decapping activator proteins. Following decapping, the exonuclease Xrn1 recognizes the decapped mRNAs and degrades them in 5′-to-3′ direction. Alternatively, mRNAs can follow 3′-to-5′ degradation pathway in which the exosome degrades the mRNAs from 3′ end and the remaining cap structure is then removed by scavenger of decapping (DcpS). For simplification, the mRNA is shown as linear line (adapted from (Garneau et al., 2007))

2.2 Deadenylation in eukaryotes: The first step to decay

The shortening of 3′-poly(A) tail signals the mRNA degradation. Two deadenylase complexes conserved from yeast to mammals have been studied extensively; the Ccr4-Not and Pan2-Pan3 complexes (Reviewed in (Chen and Shyu, 2011)). The major deadenylase complex in all eukaryotes is the Ccr4-Not complex (Tucker et al., 2001) that consists of two catalytic subunits Ccr4 and Caf1/Pop2 (Basquin et al., 2012) and Not proteins (Not1, Not2, Not3, Not4, Not5) (Bhaskar et al., 2013; Wahle and Winkler, 2013). The second type of deadenylase complex conserved amongst all eukaryotes contains the catalytic subunit Pan2 (catalytic subunit) and the regulatory subunit Pan3 (Boeck et al., 1996; Brown et al., 1996; Zuo and Deutscher, 2001).

Mature mRNA that is shuttled to the cytoplasm is bound by many accessory proteins for protection from exonuclueases and contain poly(A) tail bound by multiple copies of Pab1 (Mangus et al., 2004; Muhlrad et al., 1994). Deadenylation is a step-wise process in which the initial catalytic step is accomplished by the Pan2-Pan3 complex that starts shortening of the poly(A) tail (Brown and Sachs, 1998). The catalysis is eventually taken over by the Ccr4-Not complex which leaves an oligo(A) tail on mRNAs (Tucker et al., 2001; Yamashita et al., 2005; Zheng et al., 2008). Pab1 is currently believed to promote activity of Pan2 while restricts the activity Ccr4 (Boeck et al., 1996; Tucker et al., 2002), implying that for Ccr4 deadenylase activity Pab1 must be displaced from mRNAs to facilitate the deadenylation of remaining poly(A) tail to an oligo(A) tail (Tucker et al., 2002; Tucker et al., 2001). Moreover, Pan2 has been shown to interact with Caf1/Pop2 of the Ccr4-Not complex by co-immunoprecipitation studies (Zheng et al., 2008). These events lead to formation of an assembly of deadenylases that facilitate two-step deadenylation process in a coordinated manner (Zheng et al., 2008).

Once the 3′-end of mRNAs contain oligo(A) tail, they are either targets of the mRNA decapping activator Pat1-Lsm1-7 complex assembly at 3′-end, which in turn promotes 5′-to-3′ decay via decapping (He and Parker, 2001; Tharun and Parker, 2001). Deadenylated mRNAs can follow the 3′-to-5′ decay pathway mediated by the 3′ exonuclease complex, the exosome (Chlebowski et al., 2013).

2.3 Deadenylation dependent degradation pathways in eukaryotes

2.3.1 The Exosome mediated 3′-to-5′ mRNA decay pathway

The eukaryotic exosome is a multi-protein ribonuclease complex, which is essential for 3′-to-5′ mRNA degradation (Figure 2.1) and also for processing and degradation of many other kinds of RNAs (Allmang et al., 1999; Mitchell et al., 1997). The core of exosome (termed as Exo-9) is conserved in eukaryotes and is formed by six RNase PH-like proteins forming a central channel and three other RNA-binding proteins containing S1 and KH domains (Rrp4, Rrp40, Csl4) (reviewed in (Januszyk and Lima, 2014)). The eukaryotic exosome (Exo-9) is catalytically inactive and needs a catalytic subunit for its activity. In cytoplasm, Rrp44 that binds to distal end of S1 and KH ring provides this activity and this catalytically active 3′ exonuclease complex is termed Exo-10. However, in nucleus the exosome exists as Exo-11 complex containing two exonucleases Rrp44 and Rrp6 (Liu et al., 2006; Makino et al., 2013).
The eukaryotic exosome interacts with many co-factors. These co-factors modulate exosome activities by providing structural roles and also by interaction and processing of different RNA substrates. In cytoplasm, the exosome interacts with Ski protein complex (Ski2, Ski3, Ski8) via conserved Ski7 protein (Halbach et al., 2013; Halbach et al., 2012; Wang et al., 2005). Whereas in nucleus, exosome activity is modulated by its interaction with TRAMP complex containing Mtr4, Trf4 and Air2 proteins (Callahan and Butler, 2010; Weir et al., 2010). Following the 3′-to-5′ catalytic activity of the exosome, the short mRNAs with remaining cap structure are metabolized by the scavenger-decapping enzyme (DcpS) (Liu et al., 2002).

2.3.2 The Xrn1 dependent 5′-to-3′ decay pathway

The messenger ribonuleoprotein (mRNP) bound with decapping enzymes Dcp1-Dcp2 and decapping activator proteins, is destined to follow decapping mediated 5′-to-3′ decay pathway. The decapping of mRNA by Dcp2 with its co-activator Dcp1

generates 5′-monophosphorylated mRNAs. These are the substrates of 5′ exonucleases Xrn1 that readily degrades the mRNA transcripts (Reviewed in (Coller and Parker, 2004)).

Several factors play a crucial role for the decapping to occur. First the deadenylation of mRNA transcripts, secondly, the accessibility of the cap structure which includes the dissociation of the cytoplasmic cap-binding proteins and thirdly, the association of Dcp1-Dcp2 to the 5′ cap and assembly of mRNP including many activators of decapping Dhh1, Pat1, Edc3, Lsm1-7 complex (Chen and Shyu, 2011; Coller and Parker, 2004; Parker, 2012). Translationally repressed mRNAs associated with decapping proteins and with many other appear to assemble in distinctive cytoplasmic processing-bodies (P-bodies) (Decker and Parker, 2012) (Discussed in Section 2.3.1).

2.3.2.1 The decapping enzymes Dcp1-2: the duo that decaps the mRNA

In eukaryotes, mRNA is decapped by evolutionary conserved enzyme Dcp2 and its catalytic activity is dependent on its co-factor Dcp1 (Dunckley and Parker, 1999; Steiger et al., 2003; van Dijk et al., 2002; Wang et al., 2002).

Dcp2 catalyzes hydrolysis of 5′ 7-methylguanosine (m^7GpppN) cap from the mRNAs and releases m^7GDP and 5′ mono-phosphorylated mRNA which is substrate of rapid decay by Xrn1 (Figure 2.1) (Cohen et al., 2005; She et al., 2008; Steiger et al., 2003). Dcp2 primarily decaps the methylated mRNAs with either m^7G-capped or $m^{2,2,7}$G-capped mRNA and show poor catalytic activity towards the un-methylated G-capped mRNA transcripts (Cohen et al., 2005; Piccirillo et al., 2003; Steiger et al., 2003). Dcp2 belongs to Nudix family of pyrophosphatases and requires a divalent metal ion (Mg^{2+}) for its catalytic activity (Steiger et al., 2003; van Dijk et al., 2002). Dcp2 and its orthologs contain an N-terminus regulatory α-helical domain followed by Nudix domain and C-terminal highly divergent domain (She et al., 2004; She et al., 2008; Steiger et al., 2003; van Dijk et al., 2002). In yeast Dcp2, N-terminus and Nudix domains are enough to promote decapping (Dunckley and Parker, 1999; Harigaya et al., 2010).

Crystal structures of *Schizosaccharomyces pombe* Dcp2 (Figure 2.2) in different conformations revealed that its N-terminus and Nudix domain are linked with a flexible segment, making a bilobed structure that can adopt an active (closed) and inactive (open) conformation depending on the presence of cap-analog and its interaction with Dcp1 (EVH domain) (She et al., 2008). Dcp1 contains an EVH domain at N-terminus that interacts with Dcp2 and modulates its functions by stabilizing the closed conformation (She et al., 2004; She et al., 2008).

This interaction surface of Dcp1 is surprisingly not conserved and supports that in metazoans other activators or a mediator of this interaction may be needed to induce this active conformation. Indeed, additional factors, Edc4 and Hedls have been identified in higher eukaryotes (Chang et al., 2014; Fenger-Gron et al., 2005; Yu et al., 2005).

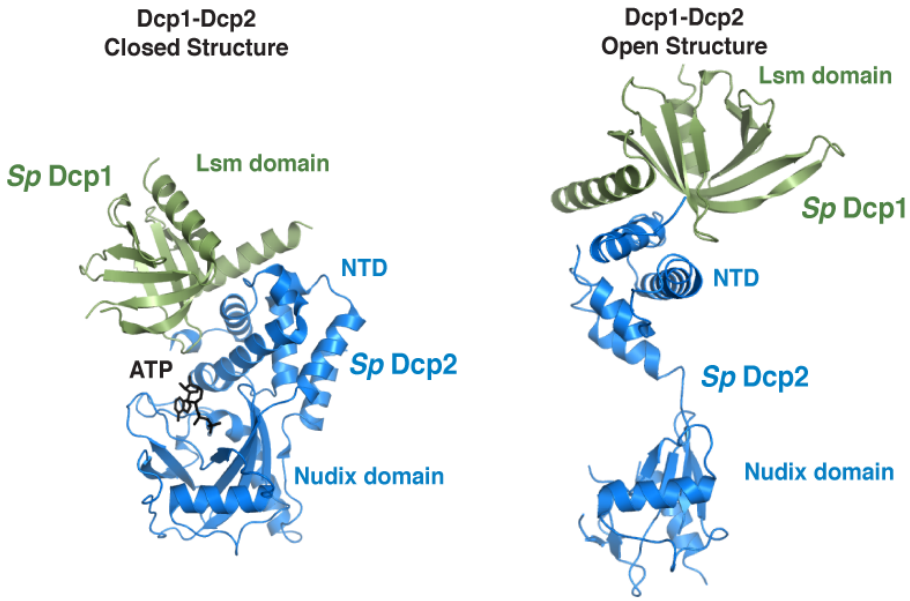

Figure 2.2: Crystal structures of S. pombe Dcp1-Dcp2

Dcp1 is depicted in green while Dcp2 N-terminal domain (NTD) and Nudix domain in blue, ATP analogue in black (PDB: 2qkm) (She et al., 2008).

2.3.2.2 Xrn1 is a highly conserved 5′ exoribonuclease

Xrn1 is a 5′ processive exoribonuclease involved in decapping induced mRNA decay pathway and is highly conserved from yeast to mammals (Jones et al., 2012). Degradation of mRNA by Xrn1 depends on nature of 5′-end of mRNA (Pellegrini et al., 2008). Following decapping by Dcp1-Dcp2 enzyme complex, 5′ monophosphorylated mRNAs are the targets of 5′ exoribonucleotic decay by Xrn1 (Coller and Parker, 2004; Stevens, 1980; Stevens and Poole, 1995). RNA hydrolysis by Xrn1 is predominant and specific to 5′ monophosphorylated substrates, whereas, Xrn1 shows poor hydrolysis of the substrates bearing 5′-cap structure, triphosphate or hydroxyl group (Stevens, 1980; Stevens and Poole, 1995).

Xrn1 physically interacts with the decapping enzyme Dcp1, with decapping activators Pat1-Lsm1-7 complex and co-localize to P-bodies with these proteins (Braun et al., 2012; Nissan et al., 2010; Parker and Sheth, 2007). *In vitro* analysis revealed that the Pat1 C-terminus interacts with Xrn1 (Nissan et al., 2010). Moreover, Dcp1 interacts with C-terminus of Xrn1 which is also supported by structural analysis (Braun et al., 2012) rationalizing the molecular basis of interaction between mRNA decapping and degradation (Braun et al., 2012). In addition, Xrn1 is also involved in mRNA degradation of endonucleotic products in mRNA surveillance pathways (Non-sense mediated decay and No-go decay) (Chen and Shyu, 2003; Orban and Izaurralde, 2005).

2.3.3 Processing (P) bodies: the foci for decapping and 5′-to-3′ degradation

In eukaryotic cells, translationaly inert mRNAs tend to cluster in two discrete cytoplasmic foci known as Processing bodies (P-bodies) and stress granules (reviewed in (Decker and Parker, 2012; Franks and Lykke-Andersen, 2008)). P-bodies are the cytoplasmic bodies known to contain all proteins involved in the mRNA decapping pathway. Studies in yeast and metazoans showed that P-bodies contain mRNA decapping proteins such as Dcp1/Dcp2, Dhh1, Pat1, Edc3, Lsm1-7,

exoribonuclease Xrn1 and also the deadenylase complex Ccr4-Not (Beckham et al., 2008; Fenger-Gron et al., 2005; Ingelfinger et al., 2002; Sheth and Parker, 2003). In addition to these general decay factors, P-bodies contain components from non-sense mediated decay (NMD) pathway (Durand et al., 2007; Unterholzner and Izaurralde, 2004). Additionally, in mammals they contain the miRNA repression machinery including GW182 (Eystathioy et al., 2003). This suggests the diverse roles of P-bodies and involvement of proteins from various decay pathways (Ding et al., 2005; Eulalio et al., 2008; Sheth and Parker, 2006; Unterholzner and Izaurralde, 2004).

Increase of mRNA localization into P-bodies has been shown in yeast upon translation repression, glucose deprivation or environmental stress (Teixeira et al., 2005). The repressed mRNAs can shuttle back to polysomes if the stress conditions are relieved (Brengues et al., 2005; Cougot et al., 2004a; Eulalio et al., 2007b; Teixeira et al., 2005). Formation of P-bodies is largely RNA dependent indicated by *in vitro* RNAse treatment of P-bodies and further biochemical and microscopic analysis (Teixeira et al., 2005).

In comparison with P-bodies, stress granules contain not only the decay machinery but also the translation initiation factors eIF4A, eIF4G, eIF4E, Pab1, ribosomal subunits (40S) and some factors from the decay pathway Ge-1/Hedls (in Metazoans) and Dhh1/DDX6/Rck (Buchan et al., 2008; Eulalio et al., 2007b; Kedersha et al., 2002; Liu et al., 2005b; Yu et al., 2005). They are extensively studied in mammalian cells and in yeast (Decker and Parker, 2012; Eulalio et al., 2007a).

2.4 Decapping activators and their mechanism of promoting decapping

The mRNA decapping is enhanced by many proteins known as mRNA decapping activators that are required for the faithful transition of actively translating mRNAs to the repressed and ready-for-decay state. This group of proteins is highly conserved amongst eukaryotes (Coller and Parker, 2004; Franks and Lykke-Andersen, 2008). The major set of proteins conserved in all eukaryotes includes Dhh1, Pat1, Edc3 and Lsm1-7 and many other proteins specific to some eukaryotes. Summary of functions of these highly conserved decapping activators is described in Table1 (Parker, 2012).

Activators of decapping affect or promote the decapping in different ways and at different steps of mRNA decapping. The factors, Dhh1 and Pat1, enhance decapping by promoting translation repression either by blocking the formation of pre-initiation 48S complex or by physically interacting with either the mRNA destined for decay or other activator proteins (Carroll et al., 2011; Coller and Parker, 2005; Nissan et al., 2010; Pilkington and Parker, 2008).

Another set of proteins consists of the enhancer of decapping Edc3 and Pat1 that promotes decapping by interacting with Dcp1-Dcp2 and stimulates Dcp2 catalytic activity (Coller and Parker, 2005; Nissan et al., 2010; Tritschler et al., 2007). Furthermore, Edc3 helps in recruitment of decapping enzyme complex to mRNAs (Decker et al., 2007; Kshirsagar and Parker, 2004; Tritschler et al., 2007).

Another conserved role of mRNA decapping activators is to rearrange the mRNP to enhance the decapping. The Pat1-Lsm1-7 complex not only interacts readily with the deadenylated mRNAs *in vivo* but also protects the dedadenylated 3′-end of mRNA from partial degradation by the exosome thus promoting the decapping pathway (He and Parker, 2001; Nissan et al., 2010; Tharun et al., 2000)

Promoting larger assemblies of mRNPs, to gather all the activators and decapping enzymes, is another feature in which Pat1 and Edc3 prove to be crucial by providing a scaffold for the assembly of these mRNPs which further promote the decapping (Figure 2.3) (Decker et al., 2007; Nissan et al., 2010; Tritschler et al., 2007).

Factors	Function
Dcp1/Dcp2	mRNA decapping enzyme, Dcp2: catalytic subunit member of Nudix family, hydrolyzes m^7GDP and 5′ p-RNA. Dcp1: stimulatory subunit, Evh1/WH1 family member, blocked by eIF4E bound to mRNA cap.
Xrn1	Major cytoplasmic 5′-to-3′ exonuclease, Processive and requires 5′ mono-phosphate
Pat1	Activates general mRNA decapping, serves as scaffolding protein for decapping complexes, represses translation initiation and stimulates Dcp2, interacts with Lsm1-7 complex and prefers to bind 3′ end of oligoadenylated mRNA, promotes P-body assembly, after deadenylation stabilizes 3′ ends against 3′ trimming.

Lsm1-7 complex	Required for efficient decapping, forms heptameric ring complex and binds to oligo or deadenylated mRNAs.
Dhh1	Required for efficient decapping of mRNAs, member of ATP dependent DEAD box RNA helicase family. Inhibits translation initiation *in vitro* upstream of 48S complex formation, accumulated in both stress granules and P-bodies, interacts with Dcp2, Pat1, Scd6, Edc3.
Edc3	RNA binding protein, binds and directly stimulates Dcp2, plays major role in aggregation of P-bodies and serves as a scaffold for decapping factors.
Scd6	RNA binding protein related to Edc3, genetic interaction with Edc3 and synthetic decapping defect in ΔEdc3 and ΔScd6, repress translation by binding eIF4G, interacts with Dhh1, Dcp2, Pat1.

Table1: mRNA decapping factors

General and highly conserved S. cerevisiae decapping activators with outlined functional details. Adapted from (Parker, 2012)

2.4.1 Assembly of mRNA decapping complex

Various studies including yeast two-hybrid screens and immunoprecipitation assays revealed mRNA decapping activators have a conserved extensive network of protein-protein and protein-RNA interactions (Reviewed in (Parker, 2012) (Coller and Parker, 2005; Nissan et al., 2010).

Two distinct complexes can be identified. First, a complex consisting of Pat1, Lsm1-7 and Xrn1 has been identified by tandem-affinity purifications (TAP) and co-immunoprecipitation that binds to 3′-end of deadenylated mRNAs (Bouveret et al., 2000; Nissan et al., 2010). Another complex containing the core-decapping enzymes Dcp1-Dcp2 together with Edc3, Dhh1, Scd6 assemble at the 5′-end of mRNAs. Edc3 provides the structural scaffold for the assembly of this sub-complex and enhances the Dcp1-Dcp2 activity (Fromm et al., 2012).

These two discrete complexes have been shown to interact via Pat1, the large scaffold protein that keeps both ends of the mRNA in a close proximity (Figure 2.3) (Nissan et al., 2010). Pat1 plays the central role of providing the scaffold for assembly of the whole decapping complex by interacting with Dhh1, Edc3, Dcp2, Lsm1-7 (Nissan et al., 2010).

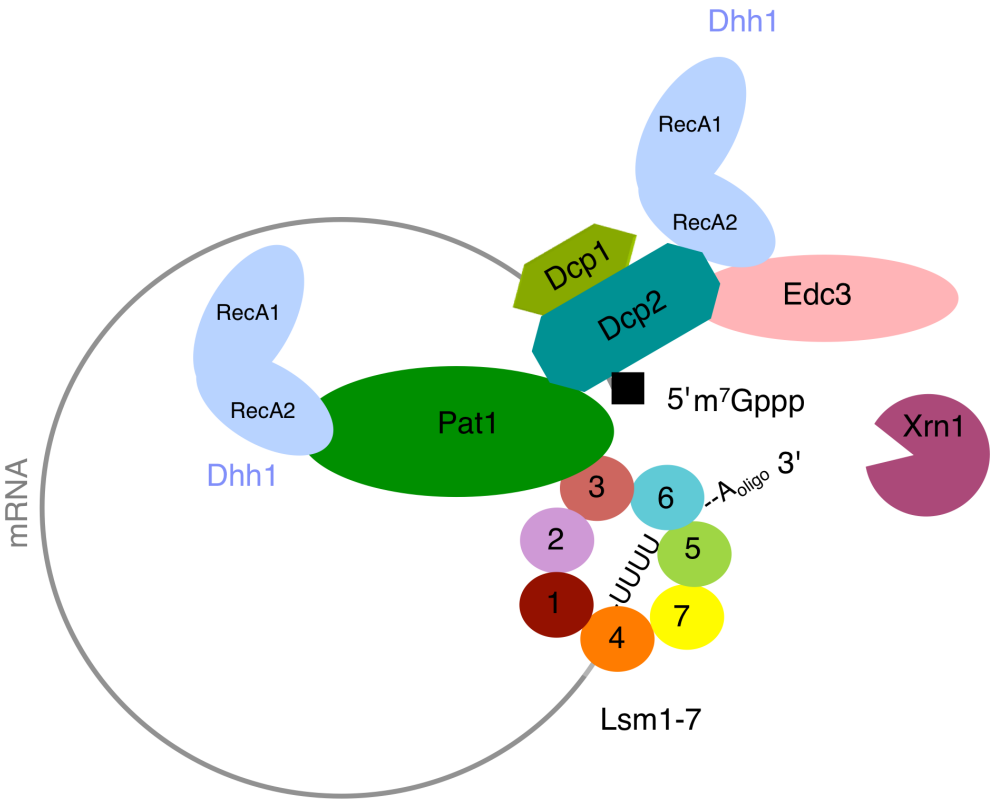

Figure 2.3: Model of *S.cerevisiae* mRNA decapping complex with circularized mRNA

Interactions shown are derived from in vivo and in vitro data (Braun et al., 2010; Coller and Parker, 2005; Haas et al., 2010; He and Parker, 2001; Nissan et al., 2010; Ozgur et al.; Pilkington and Parker, 2008; She et al., 2004; Tharun et al., 2000). Proteins are color coded as represented in Section 3.1 and Section 3.2.

2.4.2 General mRNA decapping activators

2.4.2.1 Pat1: a modular protein with diverse functions

Pat1 (protein associated with topoisomerase II) an 88-kDa protein was first identified as a protein associated with topoisomerase II (Wang et al., 1996). Yeast two-hybrid analysis and immuno-fluorescence based cellular localization experiments showed that Pat1 has the ability to localize into nucleus (Jensen et al., 2000; Marnef et al., 2012). However, most of the work in the past decade has been focused on its cytoplasmic functions, which are diverse and well studied with reference to mRNA decay.

Pat1 has multiple domains (Nissan et al., 2010) that are conserved amongst its othologs in human Pat1b (Ozgur et al., 2010) and in *Drosophila* HPat (Haas et al., 2010). In humans there are two Pat1 homologs termed Pat1a and Pat1b. By combining *in vitro* localization experiments with the YFP-tagged protein and immuno-fluorescence microscopy of endogenous Pat1 homologs it was observed that only Pat1b is localized to the P-bodies revealing its role in mRNA decay (Haas et al., 2010; Ozgur et al., 2010). Although the domain boundaries differ in different species but the functions of these domains are highly interrelated.

Pat1 serves as a scaffold for the mRNA decapping machinery and translation repression (Figure 2.3) (Coller and Parker, 2005; Nissan et al., 2010). Pat1 seems to be at the intersection of translational repression, mRNA decapping and exonuclease decay by Xrn1. *In vitro* Pat1 directly interacts with the decapping protein Dcp1-Dcp2 and stimulates the decapping activity (Nissan et al., 2010). Moreover, *in vitro* translation experiments show translation repression and inhibition of 48S complex formation upon addition of Pat1 in yeast (or its domains) (Nissan et al., 2010). *In vivo* over expression of Pat1 leads to accumulation of P-bodies and translation repression (Coller and Parker, 2005; Pilkington and Parker, 2008). Pat1 also interacts in an RNA-dependent manner with eIF4E, eIF4G and Pab1 thus validating its association with mRNA even before the deadenylation in the actively translating mRNAs (Bonnerot et al., 2000; Tharun and Parker, 2001). Furthermore, co-

immunoprecipitation assays of human and *Drosophila* Pat1 reveals its interaction with the components of Ccr4-Not complex and Xrn1 (Haas et al., 2010; Ozgur et al., 2010). These lines of information clearly explain Pat1 involvement in three very important and distinct steps for gene regulation.

Fold prediction and sequence alignment of Pat1 suggests that Pat1 N-terminal domain, Proline (P)-rich region and middle domain are not structured or they might make secondary structure upon binding to other proteins (Braun et al., 2010). The only structured domain of Pat1 is its C-terminal domain whose crystal structure from its human ortholog Pat1b has been solved (Figure 2.4) (Braun et al., 2010). The structure shows a α-α super-helical structure of Pat1 composed of 13-helices related to HEAT-repeats or ARM-repeat superfamily (Braun et al., 2010). These helices make a basic solvent exposed surface, which is involved in RNA and Dcp2, Edc4 and Lsm1-7 interactions (Braun et al., 2010).

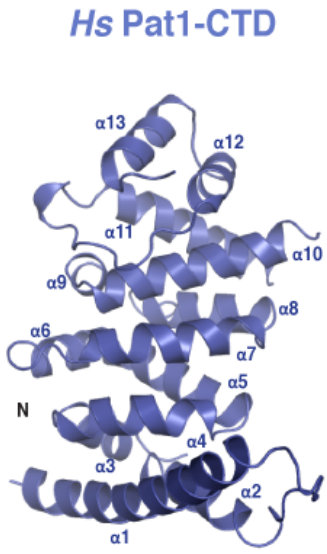

Figure 2.4: Crystal structure of human Pat C-terminal domain

Depicted in blue ribbon representation with 13 alpha helices labeled. (PDB: 2xer) (Braun et al., 2010).

Pat1 has been shown to co-immunoprecipitate with various yeast mRNAs (Tharun and Parker, 2001) and its middle and C-terminal domain binds to poly(U) RNA, both in human and yeast (Haas et al., 2010; Pilkington and Parker, 2008). This suggests

that Pat1 either directly interacts with RNA or indirectly by its RNA-interacting partners. Indeed, i*n vitro* analysis of human Pat1 C-terminus shows its interaction with RNA in size-exclusion chromatography experiments (Braun et al., 2010).

2.4.2.2 Dhh1 is a DEAD box protein

The DEAD-box proteins belong to super-family 2 (SF2) of RNA helicases that are involved in different cellular processes (Fairman-Williams et al., 2010). They not only possess unwinding RNA properties by utilizing ATP but also ATP-dependent clamping of RNA to regulate its function and to form RNA-protein complexes (RNPs) (Linder and Jankowsky, 2011). These proteins are characterized by having nine distinct motifs that are involved in RNA binding, ATP-binding and its hydrolysis (Linder and Jankowsky, 2011).

Yeast Dhh1 and its orthoglos in *Schizosaccharomyces pombe* (Ste1), *Xenopus laevis* (Xp54), *Drosophila melanogaster* (Me31B), *Caenorhabditis elegans* (CGH-1) and in mammals (DDX6/Rck) share a high sequence similarity in two RecA-like domains while C and N-terminal are not well conserved. The wealth of biochemical and structural data provided a glimpse of its involvement in wide variety of cellular processes (Presnyak and Coller, 2013). Sequence analysis reveals an N-terminus extension present in DDX6/Rck in human. Dhh1 is interesting in having Asn (N)-rich segment in N-terminus and Gln (Q)-rich region at C-terminus that might be involved in aggregation of the proteins leading to P-body formation (Cheng et al., 2005).

Dhh1 and its orthologs are versatile proteins and are shown to be involved in the interaction with mRNA decapping machinery, with deadenylation complexes and in promoting translation repression and P-body localization (Coller and Parker, 2005; Coller et al., 2001; Maillet and Collart, 2002; Teixeira et al., 2005)

The crystal structure of Dhh1 (Cheng et al., 2005) showed the protein with two RecA-like domains in an open conformation (Figure 2.5). Structural analysis showed a unique rearrangement of RecA domains because of the inter-domain interactions that might restrict or regulate its activities (Cheng et al., 2005). Indeed, these interactions play a crucial role in regulating the ATPase activity of the molecule (Dutta et al., 2011). Mutations leading to the disruption of these inter domain interactions

increased the overall ATPase activity and mRNA turnover, RNA binding and P-body accumulation *in vivo* (Dutta et al., 2011).

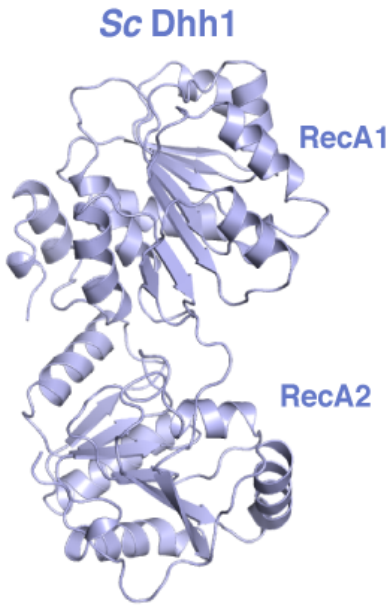

Figure 2.5: Crystal structure of S. cerevisiae Dhh1

The core helicase domains (RecA1 and RecA2) as depicted in two orientation in blue (PDB: 1s2m) (Cheng et al., 2005).

RNA fluorescence polarization experiments revealed Dhh1 binds most strongly to poly(U) 10-12 mer RNA (Dutta et al., 2011). Its affinity remained similar with upto U20-mer RNA but decreased many folds if the RNA was smaller than 10 nucleotides (Dutta et al., 2011). Although most of the DEAD-box proteins were shown to be RNA-dependent ATPases *in vitro* but most of them did not show any RNA-depedent helicase activity (Linder and Jankowsky, 2011). Consistent with this, Dhh1 helicase activity has not been shown except for its Xenopus ortholog Xp54 which can unwind 46 base pair duplex with 5′ overhangs ((Ladomery et al., 1997), reviewed in (Presnyak and Coller, 2013)).

2.4.2.3 Edc3: A scaffold for mRNA decapping enzymes

Enhancer of decapping 3 (Edc3) belongs to the Lsm family of proteins. It plays an important role in P-body formation and is one of the activators of decapping, which was first identified in *Saccharomyces cerevisiae* (Kshirsagar and Parker, 2004; Tritschler et al., 2007). Protein family Lsm16 contains three different functional domains: an N-terminal Lsm domain, FDF domain (containing a consensus Phe-Asp-Phe motif) and a C-terminal YjeF-N domain (Albrecht and Lengauer, 2004; Anantharaman and Aravind, 2004). These domains are evolutionary conserved and are involved in important cellular functions.

Several *in vivo* and *in vitro* studies including genome wide analysis, proteome analysis and yeast-two hybrid showed that Edc3 interacts with mRNA decay proteins (Fromont-Racine et al., 2000; Gavin et al., 2002; Ito et al., 2001; Uetz et al., 2000). In yeast, the deletion of Edc3 results in reduced P-body numbers and defective mRNA decay as compared to wild-type cells (Decker et al., 2007; Kshirsagar and Parker, 2004). Additionally, GFP-tagged Edc3 localizes to P-bodies showing that it is part of protein complexes involved in P-body assembly and stimulates the decapping activity of Dcp2 (Kshirsagar and Parker, 2004).

Individual domains of Edc3 are involved in important interactions. In yeast-two hybrid experiments complimented with *in vitro* pull-down assays Lsm domain of Edc3 interacts with catalytic domain of Dcp2 (Decker et al., 2007). While the co-imunoprecipitation of *Drosophila* Lsm domain shows interaction with Dcp1 only and none of the other decapping factors (Tritschler et al., 2007). Its interaction with Dcp1 or with DDX6/Me31B/Dhh1 is not sensitive to RNAse treatment showing that the interactions are RNA independent (Tritschler et al., 2007). In both orthologs, the N-terminal Lsm domains showed that it is important for Edc3 localization in P-bodies (Decker et al., 2007; Eulalio et al., 2007c; Tritschler et al., 2007). The crystal structure of Lsm domain of human Edc3 (Figure 6A) and solution structure of *Drosophila* Edc3 reveal that Edc3 Lsm domain has a divergent Sm-fold, which lacks the canonical N-terminal helix in the overall fold (Figure 2.6). On this basis it can also be classified in the Tudor domain family (Tritschler et al., 2007). This Lsm domain shows not only the differences at the structural level but also it lacks RNA binding properties (Tritschler et al., 2007).

Similarly, pull-down experiments of recombinant FDF domain of yeast Edc3 show interaction with RecA2 domain of Dhh1. These results are further supported by the crystal structure of human Edc3 FDF peptide bound to RecA2 domain of DDX6/Rck (Figure 2.6) (Tritschler et al., 2009). The structure shows a tight complex in which Edc3-FDF peptide adopts a helical conformation upon binding to DDX6. The structural analysis combined with mutational and competition studies shows that Dhh1/DDX6/Me31B has mutually exclusive interaction with Edc3, Pat1 and Tral/Scd6 that also has similar domain architecture (Tritschler et al., 2009; Tritschler et al., 2008).

The YjeF-N domain of yeast Edc3 interacts with itself thus helps in dimerization of Edc3 (Fromont-Racine et al., 2000; Marino-Ramirez and Hu, 2002). Furthermore, human Edc3 also forms a dimmer (Figure 2.6) and its Yjef-N domain is responsible for the dimerization as tested by gel filtration and ultra-centrifugation experiments (Ling et al., 2008). Overall crystal structure of human Edc3 YjeF-N domain revealed that it adopts a Rossmann-like topology (Figure 6B) (Ling et al., 2008). Dimerization of Edc3 is important for its ability to bind RNA as well as for P-body assembly which supports that YjeF-N domain is likely to be essential domain providing not only structural properties but also functional properties to dimeric Edc3 protein in mRNA degradation (Decker et al., 2007; Ling et al., 2008).

In the view of Edc3 functions, its direct interaction with decapping enzyme Dcp2 and modulation of its activity (Fromm et al., 2012) and in P-body formation (Eulalio et al., 2007a), it can be suggested that Edc3 provides the important scaffold for decapping enzyme complex Dcp1-Dcp2 to decap the mRNA transcripts and make them available for degradation by Xrn1.

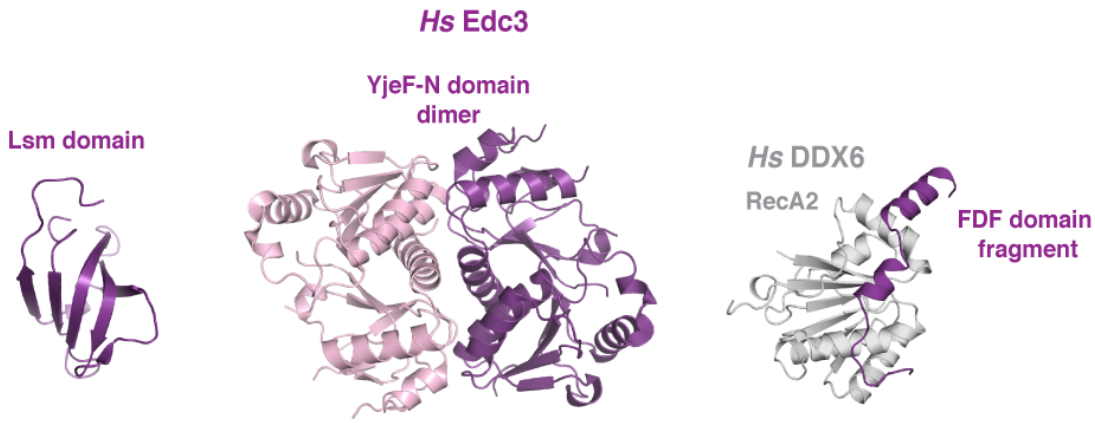

Figure 2.6: Crystal structures of human Edc3 domains

(Left): Crystal structure of human Lsm domain of Edc3 (PDB: 2vc8) (Tritschler et al., 2007). (Middle): Crystal structure of human YjeF-N domain of Edc3. Two molecules of dimer are shown in different colors for clarity (PDB: 3d3j) (Ling et al., 2008) . (Right): RecA2 domain of DDX6 is shown in gray and Edc3 peptide containing FDF motif in salmon color (PDB: 2wax) (Tritschler et al., 2009).

2.4.2.4 The Lsm1-7 complex: Ring that matters for protection of the 3′-end of mRNAs

Sm and Sm-like (Lsm) proteins are an important part of mRNPs involved in mRNA degradation and pre-mRNA splicing (Beggs, 2005; He and Parker, 2000). Several structural and biochemical studies provide evidence that Sm proteins assemble into heptameric complexes involved in pre-mRNA splicing through the interactions with different snRNA (U1, U2, U4, U5) and play important role in the biogenesis of associated snRNAs (Bouveret et al., 2000; Leung et al., 2011; Pomeranz Krummel et al., 2009; Weber et al., 2010). A similar hetero-heptameric complex, containing Sm-like (Lsm) proteins, is associated with U6 snRNA and *in vitro* analysis suggests that it binds to 3′ U-tract of U6 snRNA (Achsel et al., 1999; Kambach et al., 1999; Mayes et al., 1999; Salgado-Garrido et al., 1999; Zaric et al., 2005). In humans and yeast, Lsm2-8 protein complex co-immunoprecipitates with free U6 snRNA (Achsel et al., 1999; Salgado-Garrido et al., 1999). Sm proteins require RNA for their heptameric assembly where as Lsm proteins readily assemble into ring link complexes in the absence of RNA substrate (Achsel et al., 1999; Salgado-Garrido et al., 1999).

Several line of evidence on the yeast Lsm1-7 complex are provided by tandem-affinity purification (TAP), deletion mutants and in humans by co-expression of wild-type and mutant Lsm protein combined with fluorescence resonance energy transfer (FRET) analysis of Lsm1-7 complex revealed that it is vital for mRNA degradation (Bouveret et al., 2000; Ingelfinger et al., 2002; Tharun et al., 2000). First, it binds to Pat1 proteins and other decapping factors (Bouveret et al., 2000; Ingelfinger et al.,

2002; Tharun et al., 2000; Tharun and Parker, 2001). Second, Lsm1 does not co-immunoprecipitate with U6 snRNA (Mayes et al., 1999; Tharun et al., 2000). Third, the Lsm1-7 complex interacts with deadenylated mRNAs (Tharun and Parker, 2001). These evidences can be translated into that Lsm proteins exist in two distinct complexes, nuclear Lsm2-8 complex associated with U6 snRNA (Achsel et al., 1999; Mayes et al., 1999; Salgado-Garrido et al., 1999) while a cytoplasmic Lsm1-7 complex associated with Pat1 protein and implicated in mRNA degradation (Bouveret et al., 2000; Ingelfinger et al., 2002; Tharun et al., 2000).

Sm and Lsm proteins contain a common domain called the Sm-domain, which is followed by C-terminal extensions in some of the Sm proteins (Hermann et al., 1995; Seraphin, 1995). Crystal structures of Sm proteins revealed the conservation of the Sm domain that has an N-terminal α-helix followed by an anti-parallel 5-stranded (Figure) β-sheet (Kambach et al., 1999). Sm proteins are known to make hetero-oligomeric assemblies in which β4 strand of one protein interacts with β5 strand of another (Kambach et al., 1999). The loop between β4, β5 and between β2, β4 known as Sm1 and Sm2 motifs are highly conserved involved in protein-RNA interactions (Hermann et al., 1995; Kambach et al., 1999; Seraphin, 1995).

Figure 2.7: Crystal structures of Lsm proteins

(Left): Crystal structures of S. cerevisiae Lsm3 showing the conserved Sm fold having N-terminal α-helix followed by 5-stranded β-sheet (PDB: 3bw1) (Naidoo et al., 2008). (Right): Crystal structure of S. pombe Lsm6/5/7 depicted in cyan, green and yellow respectively (PDB: 3swn) (Mund et al., 2011).

2.4.3 Functional roles of mRNA decapping activators

2.4.3.1 P-body assembly and factors involved in it

Assembly of P-bodies is proposed to be a stepwise process of first accumulation of different proteins at 3′ and 5′-end of mRNA and then accumulation of these sub complexes into larger microscopic foci (Reviewed in (Decker and Parker, 2012; Franks and Lykke-Andersen, 2008)). In yeast at least two proteins have been identified as key factors in the assembly of these structures i.e. Edc3 and Lsm4 (Decker et al., 2007; Mazzoni et al., 2007; Reijns et al., 2008). YjeF-N domain of Edc3 and the Gln/Asn (Q/N) rich region (Prion-like) in Lsm4 C-terminus plays a central role in assembly of P-bodies (Decker et al., 2007; Mazzoni et al., 2007; Reijns et al., 2008). Participation of Edc3 in P-body formation appears to be conserved amongst higher organisms because the YjeF-N domain is evolutionary conserved (Ling et al., 2008). Moreover, the deletion of this domain does not greatly effect P-body formation in *Drosophila* S2 cells or in yeast (Decker et al., 2007; Eulalio et al., 2007b; Kshirsagar and Parker, 2004). Double deletion mutants of Edc3 and Lsm4 C-terminal domain show a dramatic decrease in P-body formation upon glucose deprivation (Decker et al., 2007; Mazzoni et al., 2007; Reijns et al., 2008). In contrast, the Lsm4 C-terminal Q/N region in not conserved in metazoans. Many other proteins containing Q/N region have been identified in metazoan P-bodies e.g. GW182 protein involved in miRNA mediated repression and Hedls/Ge-1 protein that is part of decapping complex in metazoans (Eulalio et al., 2007b; Liu et al., 2005a; Yu et al., 2005). Furthermore, the Q/N region of Lsm4 in metazoans is replaced by another Arg-Gly-Gly (RGG) domain, which plays a part in stress granule assembly (Tourriere et al., 2003).

Although yeast and metazoans P-body formation appears to be different in some aspects, the overall mechanism is conserved. Many other proteins also contain Q/N (Prion-like) regions including Dhh1, Pop2, Not1, Ccr4, Not4 that not only regulate decapping, but also are active components of deadenlyation machinery (Chen and Shyu, 2011). Interactions amongst the prion-like degradation prone domains can also play important role in assembly of these granules (Decker et al., 2007)

2.4.3.2 Translation repression and decapping activation mediated by Dhh1 and Pat1 require their interplay

Pat1 and Dhh1 are involved in mRNA degradation as well as in mRNA translation repression. Thus, these two decapping activators participate in two main events of post-transcriptional regulation (reviewed in (Marnef and Standart, 2010).

Pat1 interacts with multiple partners of the decapping. Out of them, one prominent is its interaction with Dhh1 that is RNA independent (Coller et al., 2001; Fischer and Weis, 2002). Co-immunoprecipitation assays of human and *Drosophila* orthologs of Pat1 showed that its conserved N-terminal domain has inherent capability to bind to Dhh1 while the rest of the Pat1 domains failed to interact (Haas et al., 2010; Ozgur et al., 2010).

Several studies show that Pat1 and Dhh1 have a critical role in controlling P-body formation and translation repression. While deletion of either Pat1 or Dhh1 in yeast repress the translation and induce P-body formation to some extent (Coller et al., 2001; Fischer and Weis, 2002), deletion mutants of both Pat1 and Dhh1 show an additive accumulation of deadenylated mRNAs and translation repression (Coller and Parker, 2005). Clustering of translationaly repressed mRNA in P-bodies, growth defects and decrease in polysomes depend on both Pat1 and Dhh1 because deletion of either of them does not effect P-body formation to the same extent as double deletion of these proteins does (Coller and Parker, 2005; Sheth and Parker, 2003). In human cells, studies of interaction deficient mutants of Dhh1 and Pat1 with knockdown and rescue strategies concluded that Dhh1 require Pat1 binding to promote P-body assembly (Ozgur and Stoecklin, 2013). Likewise, Pat1 upon losing interaction with Dhh1 suppresses expression of mRNAs (Ozgur and Stoecklin, 2013). These evidences show the importance of the Pat1 and Dhh1 complex that appears to have drastic effects on cell viability.

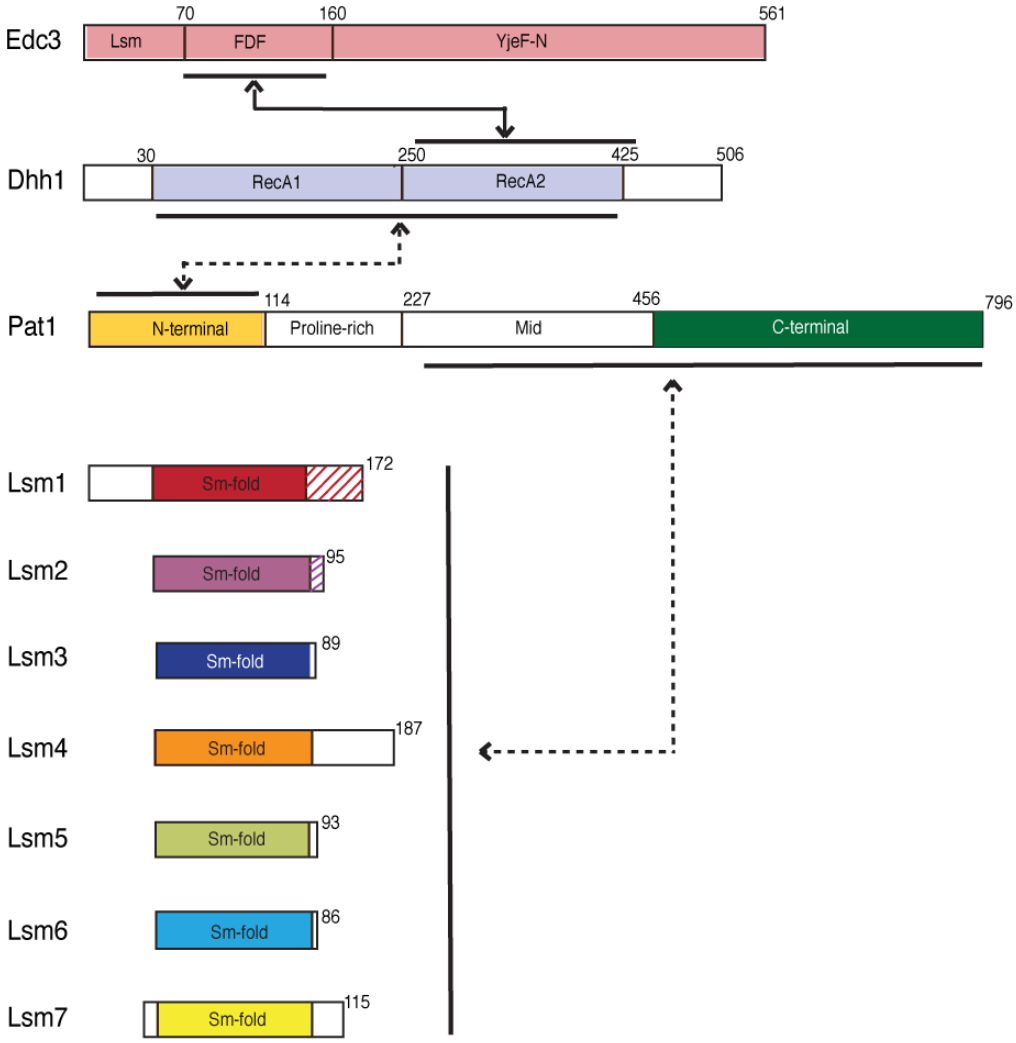

Figure 2.8: Domain architecture of S. cerevisiae decapping activators

Solid arrow lines represent the interaction of DDX6-RecA2 bound to Edc3-FDF fragment (Tritschler et al., 2009). Dashed arrow lines represent the interactions dealt mainly in this thesis. Colors are used as according to (Figure 2.1, Section 3.1, Section 3.2).

2.4.3.3 Pat1-Lsm1-7 complex: as part of mRNA destined for degradation

The interaction of Lsm1-7 complex with Pat1 is conserved in all eukaryotes and this complex promotes mRNA degradation by enhancing decapping (Reviewed in

(Tharun, 2009)). Pat1 is localized to P-bodies together with the Lsm1-7 complex. Furthermore, characterization of Pat1 domains showed that its middle and C-terminal domains are responsible for Lsm1-7 interaction (Braun et al., 2010; Haas et al., 2010; Nissan et al., 2010; Ozgur et al., 2010; Pilkington and Parker, 2008). The interaction of Lsm1-7 with the decapping machinery component i.e. Pat1, but not with the translation machinery indicates that this complex binds to mRNAs that are destined degradation (Tharun et al., 2000; Tharun and Parker, 2001). Furthermore, Pat1-Lsm1-7 can be co-immunoprecipitated more efficiently with oligoadenylated transcripts than with polyadenylated ones and mutations in any of the components stabilize the mRNA bearing cap structure (Chowdhury et al., 2007; Tharun and Parker, 2001). *In vitro* analysis of purified Pat1-Lsm1-7 complex from yeast showed preference in binding to oligoadenylated RNAs (Chowdhury et al., 2007). Moreover, *in vivo* analysis of unadenylated mRNAs generated by ribozyme cleavage at 3′-end shows no binding to Pat1-Lsm1-7 but rather quick degradation by exosome-mediated decay (He and Parker, 2001; Meaux and Van Hoof, 2006). Combining all these results reveal Pat1-Lsm1-7 complex acts as a decapping activator complex by protecting 3′-end of deadenylated mRNAs from the exosome and thus promote decapping pathway (He and Parker, 2001).

Interaction of Pat1-Lsm1-7 with oligo(A) tailed mRNAs is mediated by the presence of short poly(U) stretch at or near the 3′-end to which the Lsm1-7 complex binds (Chowdhury and Tharun, 2008). Multiple data suggest that a U-tract near the 3′-end facilitates binding of the Lsm1-7-Pat1 complex. First, Lsm proteins are shown to prefer binding to 3′ U-stretch in cell extracts (Song and Kiledjian, 2007) which is further supported by structural analysis of the U4 snRNP crystal structure bound to U4 snRNA at 3′ U-stretch (Leung et al., 2011). Second, the histone mRNAs which lack a poly(A) tail are oligouridylated first and then targeted for decapping via 5′-to-3′ decay pathway (Wilusz and Wilusz, 2008).

2.5 Scope of this Work

The importance of mRNA decapping activators has been demonstrated in literature and briefly described in the previous sections that how these factors involved in

faithful degradation of the mRNA. However, the mechanistic understanding of their assembly and the network of interactions amongst these activators remain elusive owing to limited structural details.

The work in this thesis aims at the overall understanding of how does decapping activator Pat1 plays a crucial role of providing a scaffold for the decapping machinery? How does Pat1 keep both ends of the mRNA in a close proximity by interacting with Dhh1 at the 5′-end and with the Lsm1-7 complex at the 3′-end of the mRNA? Furthermore, how does Dhh1 engage with multiple partners in a mutually exclusive manner? Structural and biochemical approaches were employed to elaborate on these imperative questions in the field.

3 Results

3.1 Dhh1 engages Pat1, Edc3 and RNA in a mutually exclusive interaction

This section deals with the original research article published in the journal Nucleic Acids Research (Vol. 42, No. 17, Pages 8377-8390, published online on July 12, 2013). In addition to main text, supplementary data including figures and methods are also added as they were published.

Published online 12 July 2013 *Nucleic Acids Research, 2013, Vol. 41, No. 17* ***8377–8390***
doi:10.1093/nar/gkt600

Structural analysis of the yeast Dhh1–Pat1 complex reveals how Dhh1 engages Pat1, Edc3 and RNA in mutually exclusive interactions

Humayun Sharif[1], Sevim Ozgur[1], Kundan Sharma[2], Claire Basquin[1], Henning Urlaub[2] and Elena Conti[1,*]

[1]Structural Cell Biology Department, Max Planck Institute of Biochemistry, Am Klopferspitz 18, Martinsried/Munich, D-82152 Germany and [2]Cellular Biochemistry Department, Max Planck Institute of Biophysical Chemistry, Am Faßberg 11, 37077 Göttingen, Germany

Received April 9, 2013; Revised June 7, 2013; Accepted June 12, 2013

ABSTRACT

Translational repression and deadenylation of eukaryotic mRNAs result either in the sequestration of the transcripts in a nontranslatable pool or in their degradation. Removal of the 5′ cap structure is a crucial step that commits deadenylated mRNAs to 5′-to-3′ degradation. Pat1, Edc3 and the DEAD-box protein Dhh1 are evolutionary conserved factors known to participate in both translational repression and decapping, but their interplay is currently unclear. We report the 2.8 Å resolution structure of yeast Dhh1 bound to the N-terminal domain of Pat1. The structure shows how Pat1 wraps around the C-terminal RecA domain of Dhh1, docking onto the Phe-Asp-Phe (FDF) binding site. The FDF-binding site of Dhh1 also recognizes Edc3, revealing why the binding of Pat1 and Edc3 on Dhh1 are mutually exclusive events. Using co-immunoprecipitation assays and structure-based mutants, we demonstrate that the mode of Dhh1-Pat1 recognition is conserved in humans. Pat1 and Edc3 also interfere and compete with the RNA-binding properties of Dhh1. Mapping the RNA-binding sites on Dhh1 with a crosslinking–mass spectrometry approach shows a large RNA-binding surface around the C-terminal RecA domain, including the FDF-binding pocket. The results suggest a model for how Dhh1-containing messenger ribonucleoprotein particles might be remodeled upon Pat1 and Edc3 binding.

INTRODUCTION

The fate of eukaryotic mRNAs is linked to the complement of proteins with which they associate to form messenger ribonucleoprotein particles (mRNPs) (1). The 5′ cap structure and the 3′ poly(A) tail are general hallmarks of mRNPs that are targeted, either directly or indirectly, by translation factors as well as mRNA decay factors. Translation and decay are mutually dependent and antagonistic processes. The presence of the m^7G cap structure at the 5′ end, for example, is crucial for eIF4E binding and for translation initiation [reviewed in (2)]. Conversely, its removal by the decapping complex is a prerequisite for 5′–3′ degradation by the exoribonuclease Xrn1 [reviewed in (3)]. Shortening of the poly(A)-tail is also linked to the shift of mRNA from active translation to a translationally repressed state in which the transcript can either be temporarily stored or can be decapped and degraded [reviewed in (4)].

Although the exact sequence of events and interplay of the factors involved in translational repression, deadenylation and decay is currently debated, it is clear that removal of the cap structure is an irreversible step that commits the mRNA to 5′–3′ degradation [reviewed in (3)]. Studies originally in yeast have shown that decapping is catalyzed by Dcp1-Dcp2 (5,6) and is activated *in vivo* by a cohort of regulators, including Pat1, Edc3, Scd6, Dhh1 and the heptameric Lsm 1–7 complex (7–12). These core components of the decapping machinery are conserved from yeast to humans, suggesting the presence of common basic mechanisms (13). Additional components as well as detailed intermolecular interactions can, however, vary across species. All components of the decapping/5′–3′ decay pathway co-localize in P-bodies together with factors involved in translational repression [reviewed in (14–17)]. Two P-body components in particular, Dhh1 and Pat1 (18–24), appear to be at the intersection of translational repression and mRNA turnover [reviewed in (25,26)].

Pat1 is a conserved multidomain protein that forms a scaffold for protein–protein interactions: the N-terminal domain (NTD) binds Dhh1, the downstream region is important for P-body formation and the middle and C-terminal domains recruit a plethora of factors, including

*To whom correspondence should be addressed. Tel: +49 89 85783602; Fax: +49 89 85783605; Email: conti@biochem.mpg.de

8378 *Nucleic Acids Research, 2013, Vol. 41, No. 17*

the decapping complex Dcp1–Dcp2, the Ccr4–Not complex, the Lsm1–7 complex and Xrn1 (22–24,27). The Ccr4–Not complex is a major deadenylase: it trims the mRNA 3′ end to a short oligoadenylated tail that forms the platform for the Lsm1–7 complex [reviewed in (28)]. Mechanistically, Pat1 is thus believed to link the deadenylated 3′ end with the decapping factors at the 5′ end. Indeed, Pat1 triggers deadenylation when tethered to mRNAs in human and *Drosophila* cells (22,24) and leads to a strong effect in decapping upon deletion in yeast (8,9). In addition to its prevalent role in mRNA degradation, in yeast Pat1 acts as a translational repressor together with Dhh1 (18).

Dhh1 (also known as RCK/p54/DDX6 in humans, Me31b in *Drosophila melanogaster* and CGH-1 in *Caenorhabditis elegans*) has been known as a decapping activator since the finding 10 years ago that its deletion in *Saccharomyces cerevisiae* stabilizes mRNA transcripts and inhibits decapping *in vivo* (10,11). However, Dhh1 does not appear to function like Pat1 and Edc3/Sdc6 by directly binding and activating the Dcp1–Dcp2 decapping complex (27,29). Evidence is instead accumulating pointing to a prevalent role of Dhh1 in translational repression in yeast (18,30) as well as in higher eukaryotes (21,31–35). Dhh1 is highly abundant in all species examined to date [yeast (36), Trypanosoma (37), Xenopus oocytes (38) and mammalian cells (39)] and is present in large excess over the expected mRNA substrates (39,40–42). Dhh1 belongs to the DEAD-box protein family of RNA-dependent ATPases, but has several unusual features. While other DEAD-box proteins bind RNA and ATP in a cooperative manner (43), Dhh1 binds RNA even in the absence of ATP (39,44). In addition, the two RecA-like domains of Dhh1 are not flexible as in most other DEAD-box proteins, but are engaged in intramolecular interactions (45). This conformational rigidity restricts the ATPase activity of Dhh1 *in vitro* (44,45). *In vivo*, the ATPase activity of yeast Dhh1 is nonetheless critical for the dissociation from P-bodies (44,46).

Dhh1 and Pat1 are emerging as crucial players in guiding the mRNPs from a translationally repressed state to a decapping state. The C-terminal RecA-like domain (RecA2) of Dhh1 is sufficient for translational repression and accumulation in P-bodies in human cells (21). Studies with the *Drosophila* orthologues have shown that this domain of Dhh1 binds in a mutually exclusive manner Edc3 and Scd6 (known as TraI in flies) (47), two partially redundant proteins with a similar domain organization (12). The C-terminal RecA-like domain is also required to bind Pat1 (22). In this work, we have elucidated the evolutionary conserved molecular mechanisms of the interaction between Dhh1 and Pat1, showing how Pat1 and Edc3 compete for the same surface of Dhh1 and how they impact on RNA binding. These results suggest that Dhh1 might switch protein and RNA-binding partners in the transition from translational repression to decapping.

MATERIALS AND METHODS

Protein expression and purification

S. cerevisiae $Dhh1_{30–425}$ and $Dhh1_{46–422}$ were cloned as Tobacco etc virus (TEV)-cleavable His_6-GST-tag fusion proteins. They were expressed in BL21-Gold (DE3) pLysS (Stratagene) in Terrific Broth medium. Cells were resuspended in lysis buffer (20 mM Tris, pH 7.4, 200 mM NaCl) supplemented with 10 mM imidazole, DNase, lysozyme and phenylmethylsulfonyl fluoride, and lysed by sonication. Proteins (wild type and mutants) were purified using Nickel-based affinity chromatography. Point mutations were introduced by QuickChange site–directed mutagenesis according to the manufacturer's instruction (Stratagene). The His_6-GST tag was either kept or cleaved by overnight incubation with TEV. Proteins were further purified by ion exchange chromatography at pH 7.4 (Heparin, GE healthcare) followed by size-exclusion chromatography (Superdex 75, GE Healthcare).

S. cerevisiae $Pat1_{1–30}$, $Pat1_{1–56}$, $Pat1_{1–114}$ and $Pat1_{5–79}$ proteins were expressed as TEV-cleavable GST-His-tagged proteins in BL21-Gold (DE3) pLysS cells. The cells were resuspended in lysis buffer and disrupted by sonication. The proteins were purified by Nickel-based affinity chromatography and then subjected (either tagged or untagged following the addition of TEV protease) to ion exchange chromatography at pH 8.0 (MonoQ 5/50, GE healthcare) and to size exclusion chromatography (Superdex 75). For isothermal titration calorimetry (ITC), Pat1 proteins were subcloned with a His_6-SUMO tag. *S. cerevisiae* $Edc3_{77–158}$ was subcloned with His_6-GST tag, while $Edc3_{77–158}$ and $Edc3_{77–116}$ were subcloned as cleavable His_6-SUMO proteins. All proteins were expressed and purified following similar protocols as the ones described above. For crystallization, the His_6-SUMO tag was cleaved using the SUMO protease Senp2.

The complexes of yeast Dhh1 with Pat1 or Edc3 were reconstituted by incubating the individually purified proteins in a 1:1.5 molar ratio for 1 h at 4°C. Dhh1–Pat1 and Dhh1–Edc3 were further purified by size exclusion chromatography (Superdex 75) in a buffer containing 20 mM Tris, pH 7.4, 150 mM NaCl, 1 mM DTT.

Crystallization and structure determination

Crystallization was carried out at 18°C using the vapor diffusion method by mixing equal volumes of protein complex at 27 mg/ml and of crystallization buffer. The best diffracting crystals of $Dhh1_{46–422}$ K234D, V238D $Pat1_{5–79}$ complex were obtained in 50 mM Tris, pH 8.0, 4% MPD, 200 mM NaCl, 25% PEG 400 after 10 days. Crystals were flash-frozen in liquid nitrogen directly from the crystallization drop. Crystals of $Dhh1_{46–422}$ K234D, V238D $Edc3_{77–158}$ were obtained with 50 mM MES, pH 6.5, 5% PEG 400, 0.1 M KCl, 10 mM $MgCl_2$. The crystals were cryoprotected by adding glycerol and diffracted to 3.5 Å resolution (data not shown). Crystals of $Dhh1_{46–422}$ K234D, V238D and $Edc3_{77–116}$ were obtained at 19 mg/ml concentration of the complex and 50 mM MES, pH 6.0, 10% MPD within 5 days. Crystals were flash-frozen by adding 25% glycerol in the crystallization buffer and diffracted to 3.25 Å resolution.

All diffraction data were collected at 100 K at the beamline PXII of the Swiss Light Source synchrotron and processed using XDS. The structures were determined

by molecular replacement with the program Phaser (48) using the two RecA domains from the apo Dhh1 structure (45) as search models. The atomic model was built with the program Coot (49) and refined with PHENIX (50). The data collection and refinement statistics are summarized in Table 1.

In vitro pull-down assays

Experiments were performed by mixing 3 µg of GST-tagged (bait) protein with equal molar amounts of untagged (prey) protein. Binding buffer (20 mM Hepes, pH 7.5, 250 mM NaCl, 2 mM $MgAc_2$, 10% glycerol, 2 mM imidazole, 1 mM DTT, 0.1 % Nonidet 40) was added to a final volume of 60 µl. The reaction mixtures were incubated on ice for 1–2 h. Fifteen microliters of 50% (v/v) suspension of GSH–Sepharose beads in 200 µl of binding buffer was added to each reaction mixture and incubated at 4°C for 1 h. Beads were washed three times with 500 µl binding buffer. Bound proteins were eluted with 20 mM reduced glutathione. Samples were separated on sodium dodecyl sulphate-polyacrylamide gel electrophoresis (SDS-PAGE) and visualized by Coomassie blue stain.

In vitro RNA-binding assays

The experiments were carried out essentially as previously described (52). Single-stranded 5′ biotinylated U_{20} RNA (Dharmacon) was mixed with 3 µg of a given protein and/or nucleotide in binding buffer (20 mM Hepes, pH 7.5, 50 mM NaCl, 10 mM $MgCl_2$, 1 mM DTT, 10% glycerol, 0.1% Nonidet 40) to a final volume of 60 µl and was kept at 4°C overnight. Each reaction was then supplemented with 200 µl of binding buffer and 50 µg of preblocked magnetic streptavidin beads (Dynal) for 2 h, rocking at 4°C. Beads were washed three times with 500 µl of binding buffer. Proteins were eluted from the beads with 17 µl SDS loading buffer. Eluted samples were boiled for 5 min and analyzed on SDS-PAGE.

Isothermal titration calorimetry

$Dhh1_{30–425}$ and His_6-SUMO tagged $Pat1_{5–56}$, $Pat1_{5–79}$ or $Pat1_{5–114}$ proteins were dialyzed overnight in the same buffer (20 mM Hepes, pH 7.5, 150 mM NaCl, 1 mM TCEP). ITC experiments were carried out at 25°C with a VP-ITC Microcal calorimeter (Microcal, GE healthcare). The MicroCal cell was filled with $Dhh1_{30–425}$ at 17 µM concentration. For each titration, Pat1 was injected into the cell 45 times in 10 µl volumes per injection at the same intervals of time (5 min). The concentration of Pat1 in the syringe was ~10 times the concentration of the protein sample in the cell. The released heat was obtained by integrating the calorimetric output curves and was corrected for the effect of dilution by carrying out a control experiment, titrating Pat1 against the buffer in the cell. The Kd values and binding ratios were calculated with the Origin (V7) software supplied with the calorimeter. We used a similar protocol to measure the Kd of $Dhh1_{30–425}$ and $Edc3_{77–158}$.

Co-immunoprecipitation assays

HEK293T cells were cultured in Dulbecco's modified Eagle medium containing 10% fetal bovine serum (Gibco), 100 U/ml penicillin and 0.1 mg/ml streptomycin (Gibco) at 37°C/5% CO_2. Plasmids were transfected with

Table 1. Data collection and refinement statistics. The Ramachandran plot was calculated using the program Molprobity (59)

Data set	$Dhh1_{46–422}$ K234D, V238D and $Pat_{5–79}$	$Dhh1_{46–422}$ K234D, V238D $Edc3_{77–116}$
Space group	$P4_122$	$P4_122$
Cell dimensions		
a, *b*, *c* (Å)	105.6, 105.6, 122.1	105.8, 105.8, 124.6
Data collection		
Wavelength (Å)	0.9714	0.9796
Resolution (Å)	48.47–2.80 (2.90–2.80)	80.68–3.25 (3.36–3.25)
R_{merge} (%)	7.6 (75.8)	9.2 (120.4)
$I / \sigma(I)$	18.3 (2.8)	23.5 (2.4)
Completeness (%)	99.6 (96.17)	99.7 (97.47)
Multiplicity	6.8	17.3
Refinement		
Resolution (Å)	53.11–2.80	53.70–3.25
No. of unique reflections	17 636	11 712
R_{work} / R_{free} (%)	20.42/24.71	20.85/24.57
Average *B*-factors (Å^2)	48.30	105.60
No. of atoms		
Proteins	3185	3115
Water	4	
Stereochemistry		
R.m.s.d. bond lengths (Å)	0.003	0.003
R.m.s.d. bond angles (°)	0.743	0.790
Ramachandran outliers (%)	0.00	0.25
Ramachandran favored (%)	97.51	98.25

Values in parentheses are for the highest-resolution shell.

8380 Nucleic Acids Research, 2013, Vol. 41, No. 17

polyethyleneimine (Polysciences Inc., 1 mg/ml) for protein interaction studies. HEK293T cells were collected from confluent 6-cm dish after 24 h of transient transfection. Cells were lysed in 300 µl of lysis buffer containing 10 mM Tris, pH 7.5, 10 mM NaCl, 10 mM EDTA, 0.5% Triton X-100 and protease inhibitors (Roche). Lysate was centrifuged at 1000*g* for 5 min at 4°C. Thirty microliters of GFP binder protein sepharose beads were added to supernatant for 1 h at 4°C. Beads were washed five times with 1 ml of NET2 buffer (50 mM Tris, pH 7.5, 150 mM NaCl, 0.05% Triton X-100) and proteins were eluted with 40 µl SDS sample buffer containing 5% β-mercaptoethanol. Eluted proteins were run on 12% polyacrylamide gels and transferred onto nitrocellulose membrane (0.45 µm pore size) (Whatman Protran BA85) for western blotting. Mouse monoclonal anti-GFP (Santa Cruz biotechnology, sc-9996) and anti-HA (Covance, MMS-101 R) antibodies and horseradish peroxidase–coupled goat anti-mouse (Millipore, AQ502A) secondary antibody were used in combination with ECL prime western blotting detection reagent (GE healthcare) for detection of HA- and GFP-tagged proteins via western blotting.

Crosslinking–mass spectrometry analysis

The protein–RNA contacts site on Dhh1 were investigated with mass spectrometry after UV-induced protein–RNA crosslinking as described in (53). The purified crosslinks were analyzed using Top10HCD method on an Orbitrap Velos instrument and the data were analyzed using OpenMS and OMSSA as a search engine (see Supplementary Methods).

RESULTS AND DISCUSSION

Biochemical and biophysical characterization of the yeast Dhh1–Pat1 interaction

S. cerevisiae Pat1 is an 88 kDa protein containing an NTD followed by a proline-rich region, a middle domain and a C-terminal domain (20,22) (Figure 1A). Dhh1 contains two RecA-like domains (RecA1 and RecA2) flanked by N-terminal and C-terminal low-complexity regions (45) (Figure 1A). The NTD of Pat1 is conserved from yeast to humans and has been shown in the case of the *D. melanogaster* and human proteins to mediate the interaction with the corresponding Dhh1 orthologues using co-immunoprecipitation assays (22,23). This domain is also part of a larger region found to strongly bind Dhh1 in the case of the yeast proteins (27).

To investigate the *S. cerevisiae* Dhh1–Pat1 complex, we first narrowed down the interacting domains using pull-down assays with recombinant Dhh1 and GST-tagged Pat1 proteins. The NTD of yeast Pat1 (residues 1–114) efficiently precipitated the DEAD-box core of Dhh1 (residues 30–425, including RecA1 and RecA2) (Figure 1B, lane 9). A segment of the Pat1 NTD that we engineered based on evolutionary conservation (residues 1–56) was also able to precipitate $Dhh1_{30–425}$ (Figure 1B, lane 8), while no binding was observed when using a fragment of Pat1 encompassing residues 1–30 (Figure 1B, lane 7). To experimentally identify a Pat1 segment suitable for structural studies, we purified the complex of $Dhh1_{30–425}$ and $Pat1_{1–114}$ and subjected it to limited proteolysis. Treatment with the protease chymotrypsin resulted in the accumulation of a fragment that we characterized using mass spectrometry analysis and N-terminal sequencing as corresponding to Pat1 residues 5–79 (Figure 1C).

Next, we assessed binding affinities quantitatively using ITC. In the presence of 150 mM salt, yeast $Dhh1_{30–425}$ and $Pat1_{5–79}$ interacted with a Kd of ~50 nM (Figure 1D, left panel). A similar dissociation constant was obtained when using $Pat1_{5–114}$ or $Pat1_{5–56}$ (Supplementary Figure S1), indicating that most of the binding determinants reside in the evolutionary conserved segment of the Pat1 NTD. $Pat1_{5–79}$ and the RecA2 domain of Dhh1 interacted with a Kd of 32 nM (Figure 1D, central panel), while no binding was detected with the RecA1 domain (Figure 1D, right panel). We concluded that the Dhh1–Pat1 interaction is confined to the RecA2 domain of the DEAD-box protein.

Crystal structure determination of a yeast Dhh1–Pat1 complex

Attempts to crystallize yeast $Pat1_{5–79}$ or $Pat1_{5–56}$ with the RecA2 domain of Dhh1 failed, as the complexes appeared to be too soluble to achieve the supersaturated conditions required for nucleation. Complexes of Pat1 with $Dhh1_{30–425}$ yielded the same crystal form that was previously reported for apo-Dhh1 (45), and indeed contained only Dhh1. Inspection of this crystal form revealed that the RecA2 domain of a Dhh1 molecule contacts the RecA1 domain of a neighboring Dhh1 molecule in the lattice (Supplementary Figure S2A). The surface of RecA2 mediating crystal contacts is conserved and has been shown in the case of the human orthologue DDX6 to bind the Phe-Asp-Phe (FDF) motif of Edc3 (35).

We reasoned that lattice contacts might promote the dissociation of Pat1 from RecA2 during crystallization. We therefore mutated the corresponding interacting surface of the RecA1 domain (Supplementary Figure S2), which did not contribute to Pat1 binding as assessed by quantitative binding affinity measurements (Figure 1D). For crystallization purposes, we introduced the Lys234Asp, Val238Asp substitutions in $Dhh1_{46–422}$, a construct that includes only the ordered polypeptide region observed in the structure of apo $Dhh1_{30–425}$ (45). $Dhh1_{46–422}$ K234D, V238D and $Pat1_{5–79}$ crystallized as a complex and yielded crystals that diffracted to 2.8 Å resolution. The structure was determined by molecular replacement and refined to an R_{free} of 24.7%, R_{work} of 20.6% and good stereochemistry (Table 1). The final model consists of residues 46–421 of Dhh1 and residues 25–54 of Pat1 (hereafter referred to as $Pat1_N$). No ordered electron density was present for residues 5–24 and 55–79 of Pat1, consistent with the results from the binding assays (Figure 1B, D and Supplementary Figure S1).

Overall structure of the yeast Dhh1–Pat1 core complex

In the complex we crystallized, Dhh1 adopts an open conformation (Figure 2). The relative orientation of the two RecA domains is different from that observed in the

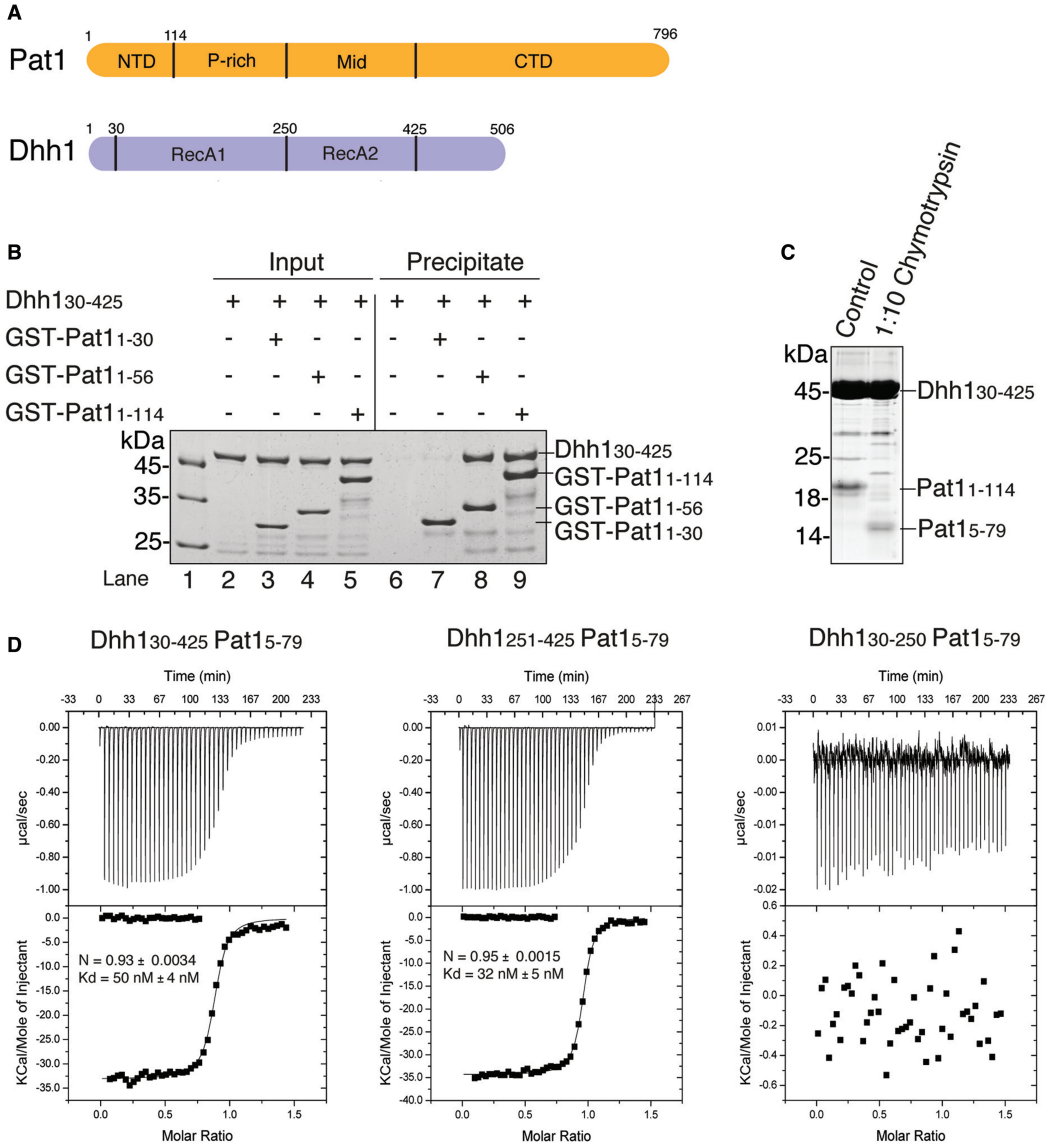

Figure 1. Identification of the interacting regions of yeast Dhh1 and Pat1. (**A**) Schematic representation of the domain architecture of yeast Pat1 (in orange) and Dhh1 (in blue). The domain boundaries are derived from previous studies (45, 27, 22, 23) and from computational analysis. The NTD of Pat1 refers to the segment upstream of the proline-rich (P-rich) segment. (**B**) Qualitative analysis of Dhh1-Pat1 interaction by GST pull-down assays. $Dhh1_{30–425}$ was incubated with purified GST-tagged fragments of the Pat1 NTD ($Pat1_{1–114}$, $Pat1_{1–56}$, $Pat1_{1–30}$). One-sixth of the reaction mixture was used as input and the bound fractions (precipitate) were analyzed on 4–20% SDS-NuPAGE Bis-Tris gels (Invitrogen). The longest fragment of Pat1 NTD ($Pat1_{1–114}$) as well as $Pat1_{1–56}$ were precipitated $Dhh1_{30–425}$, while the shorter fragment $Pat1_{1–30}$ was unable to do so. (**C**) Limited proteolysis experiment. The complex of $Dhh1_{30–425}$ and $Pat1_{1–114}$ was incubated at 0.6 mg/ml with chymotrypsin (Roche) in a 1:10 (wt/wt) enzyme:protein ratio for 30 min at 4°C. The products of the proteolysis were resolved on 17% SDS-PAGE gel. (**D**) Quantitative analysis of Dhh1–Pat1 interaction by ITC. The MicroCal cell was filled with Dhh1 proteins at 17 µM and His_6-SUMO-tagged $Pat1_{5–79}$ was injected at 150 µM concentration consecutively in 10 µl volumes. The three panels correspond to the ITC experiments with $Dhh1_{30–425}$ (RecA1-RecA2, left), with $Dhh1_{251–425}$ (RecA2, central) and with $Dhh1_{30–250}$ (RecA1, right). Shown in the insets are the number of calculated binding sites (N), and the dissociation constant (K_d), as calculated with the program Origin.

8382 Nucleic Acids Research, 2013, Vol. 41, No. 17

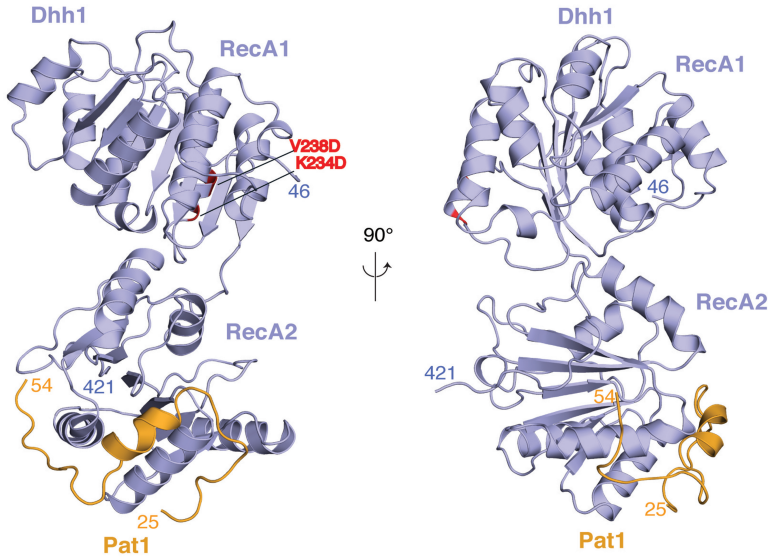

Figure 2. Structure of the yeast Dhh1–Pat1 core complex. The two RecA domains of Dhh1 are in blue. The Dhh1-binding domain of Pat1 spans residues 24–54 (in orange). The structure is shown in two views related by a 90° rotation around a vertical axis. The N- and C-terminal residues ordered in the structure are indicated. The two residues of RecA1 mutated for crystallization (K234D and V238D, shown in red) are far from the RecA2 domain, where Pat1 binds.

structure of wild-type apo Dhh1 (45) (Supplementary Figure S2B). The difference probably arises from the mutations we had introduced: an intramolecular interaction between the two RecA domains observed in the structure of the wild-type protein (a salt bridge between Lys234 and Glu251) is impaired by the K234D mutation (Supplementary Figure S2B). In either conformation, the residues mutated on RecA1 are at >40 Å distance from the residues that bind $Pat1_N$ (Figure 2 and Supplementary Figure S2B). $Pat1_N$ wraps around the RecA2 domain of Dhh1, burying ~10% (9118 $Å^2$) of the solvent accessible surface. $Pat1_N$ folds into an α-helical segment (residues 25–42) and an extended segment (residues 43–54) (Figure 2).

An extended segment of yeast Pat1 docks onto the FDF-binding site of Dhh1

The extended segment of yeast $Pat1_N$ contains a FDF sequence motif (residues 51–53). The FDF motif binds at a shallow surface pocket on the RecA2 domain of yeast Dhh1 (that we refer to as the patch 1 surface) formed by Ala263, Val265, Cys273, Leu277 and Ile409 (Figure 3A, central panel). The motif is recognized at the same pocket and with the same conformation as the DDX6-bound FDF motif of human Edc3 (patch 1, Figure 3A, left panel) (35). Mutation of four residues surrounding the FDF-binding site in *D. melanogaster* Me31b has been previously shown by co-immunoprecipitation studies to abolish Edc3 binding (35). We mutated the equivalent residues at the patch 1 surface of yeast Dhh1 (Mut-1: Asn269Ala, His272Ala, Thr276Ala, Lys280Ala). In pull-down assays with purified GST-tagged $Pat1_{5–79}$ and $Dhh1_{46–422}$ proteins, the binding of Pat1 to Mut-1 was decreased as compared with wild-type Dhh1 (Figure 3B, compare lanes 3 and 7).

In the case of human Edc3, the FDF motif is followed by two helices that contain a conserved Phe-Asp-Lys FDK motif and bind at a second surface patch (35) (patch 2, Figure 3A, left panel). In the structure of yeast $Pat1_N$, there is no ordered extension C-terminal to the FDF motif (Figure 3A, central panel), although this part of the molecule is in principle present in the construct we crystallized. We engineered a yeast Dhh1 mutant with substitutions at patch 2 (Mut-2: Phe393Ala, Tyr396Ala, Glu399Ala, Gln400Ala) corresponding to the Me31b mutant shown to abolish Edc3 binding in the case of the *D. melanogaster* proteins (35). Consistently with the structure, yeast $Pat1_{5–79}$ was able to precipitate Mut-2 Dhh1 (Figure 3B, lane 6). As a control, we tested the Dhh1 mutants with yeast $Edc3_{77–158}$. This ~80-residue long segment of yeast Edc3 includes the equivalent ~30-residue long segment of human Edc3 that is ordered in the structure with DDX6 (35) (Figure 4A). The Mut-1 and Mut-2 Dhh1 proteins failed to interact with yeast $Edc3_{77–158}$ (Figure 3C, compare lane 3 with lanes 7 and 6). These results indicated that yeast Pat1 and Edc3 compete for the same FDF-binding site on Dhh1 (patch 1). Yeast $Pat1_N$, however, lacks the additional Dhh1-binding segment at the C-terminus of the FDF motif (patch 2) that is present in human and *Drosophila* Edc3 (while absent in TraI) (35).

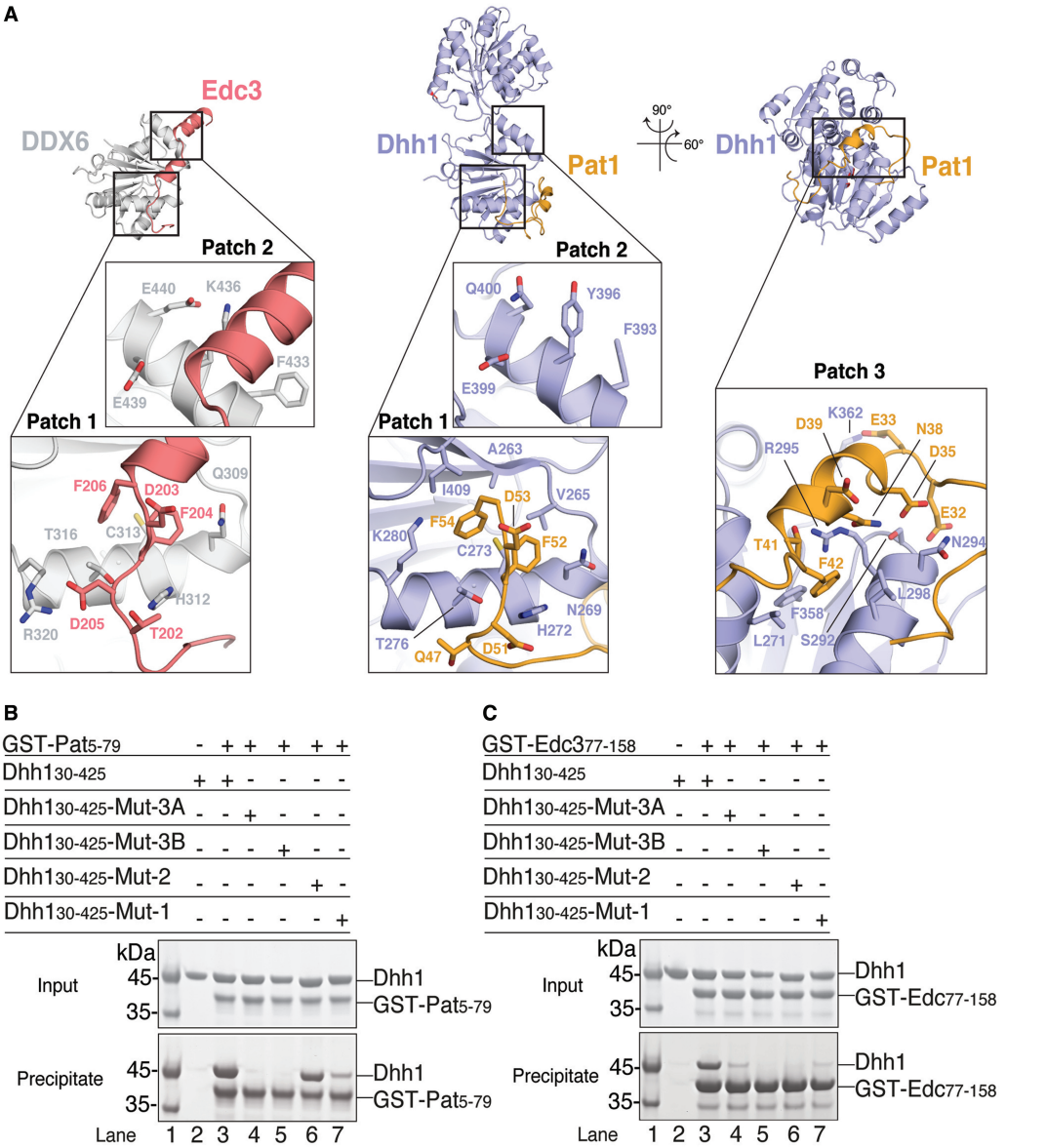

Figure 3. Hotspots of interactions on Dhh1. (**A**) The structure of Dhh1–Pat1 (central and right panel) is shown in comparison with the previously determined structure of the RecA2 domain of human orthologue DDX6 (in gray) bound to another regulator, Edc3 (in salmon) (35) (left panel). The structures in the central and left panels are in the same orientation relative to the RecA2 domain. The orientation of the Dhh1–Pat1 structure in the right panel is related by rotations around a vertical and horizontal axis, as indicated. The close-up views show three hotspots of interactions on Dhh1 discussed in the text (patch 1, patch 2 and patch 3). Conserved residues involved in the interactions are shown in a ball-and-stick representation (at patch 1 and patch 3 for Dhh1–Pat1, and at patch 1 and patch 2 for DDX6–Edc3). Patch 1 binds FDF motifs of yeast Pat1 and human Edc3. Patch 2 binds the FDK motif of human Edc3 (35). Patch 3 binds an acidic segment of yeast Pat1. (**B**) Protein co-precipitations by GST pull-down assays. The experiments were performed as described in Figure 1B after incubating yeast GST-tagged $Pat1_{5–79}$ with $Dhh1_{30–425}$ wild type or mutants. Mut-1 corresponds to the N269A, H272A, T276A, K280A substitutions at Dhh1 patch1. Mut-2 corresponds to the F393A, Y396A, E399A, Q400A at patch 2. Mut-3A corresponds to S292D, N294D and Mut3-B to R295D at patch 3. The Mut-1, Mut-3A and Mut-3B mutants of yeast Dhh1 decreased the interaction with Pat1 while Mut-2 did not, consistently with the structural analysis (Figure 3A, central and right panels). (**C**) Similar pull-down experiments were performed with yeast GST-tagged $Edc3_{77–158}$ and $Dhh1_{30–425}$ wild type or mutants. The Mut-1, Mut-2, Mut-3A and Mut-3B mutants of yeast Dhh1 all decreased the interaction with Edc3.

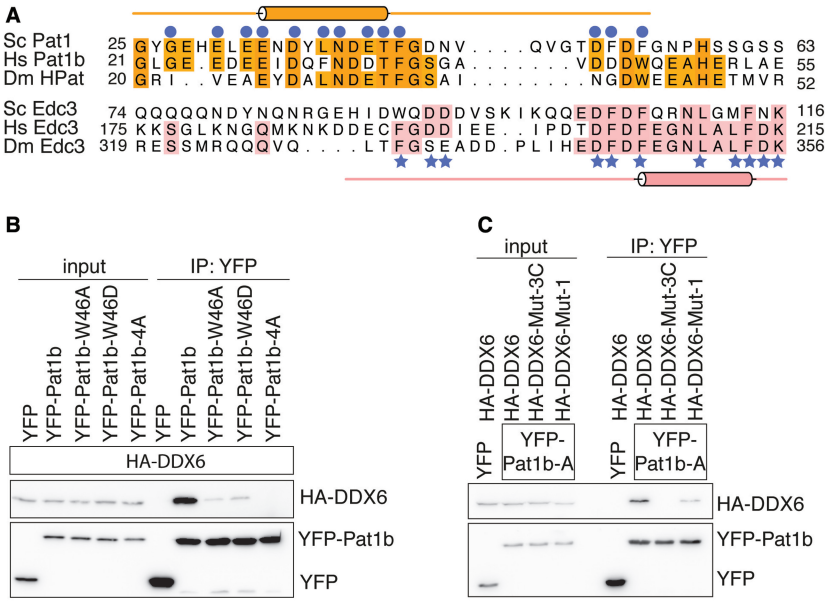

Figure 4. Pat1 binds Dhh1 via evolutionary conserved residues. (**A**) Structure-based sequence alignment of Pat1 and Edc3 orthologues from *S. cerevisiae* (Sc), *Homo sapiens* (Hs), *D. melanogaster* (Dm). Conserved residues are highlighted in orange for Pat1 and in salmon for Edc3. The secondary structures (helices indicated as cylinders) are shown above and below the Pat1 and Edc3 sequences and correspond to the structures of the yeast complexes reported in this manuscript. Conserved residues of yeast Pat1 and Edc3 that directly interact with Dhh1 are indicated with blue circles and stars, respectively. (**B**) Co-immunoprecipitation assays of *H. sapiens* HA-tagged DDX6 with YFP-labeled Pat1b (residues 1–84). Wild type and mutants (W46A, W46D and 4A) were transiently transfected in HEK293T cells. Trp46 of human Pat1b is predicted to reside at the corresponding FDF motif of yeast Pat1 (panel A). The human 4A mutant corresponds to the D34, D35, T36 and F37 substitutions (53). Cell lysates (input) were immunoprecipitated with GFP binder. HA-tagged and YFP-tagged proteins were detected by western blots. The Pat1b mutants (W46A, W46D and 4A) impaired the interaction with wild-type DDX6. (**C**) Immunoprecipitation (IP) of wild-type YFP-tagged Pat1b (residues 1–84) with HA-tagged DDX6 wild type, Mut-1 and Mut-3C. Mut-3C corresponds to the combined Mut-3A and Mut-3B substitutions (S343D, Q345D, R346D in human DDX6). The IP was done as described above. The DDX6 mutants (Mut-1 and Mut-3C) impaired the interaction with wild-type Pat1b.

The interaction at the FDF-binding site is conserved in the human Pat1–DDX6 complex

Human and *Drosophila* Pat1 proteins do not contain a FDF sequence motif. Structure-based sequence alignments, however, suggested the presence of an Asp-Trp (DW) motif in metazoan Pat1 proteins at the corresponding position of the yeast Pat1 FDF motif (Figure 4A). We therefore tested whether the hydrophobic residue in the DW motif of human Pat1b might dock on the FDF-binding pocket of DDX6. We transiently co-expressed full-length HA-tagged DDX6 and YFP-tagged Pat1b residues 1–84 (hereby referred to as YFP-Pat1b) in HEK293T cells and carried out co-immunoprecipitation assays with GFP-binder beads. We found that a Trp46Ala or a Trp46Asp substitution in YFP-Pat1b strongly decreased the interaction with full-length HA-tagged DDX6 (Figure 4B). The effect was similar to a Pat1-4A mutant that has been recently shown to impair Dhh1 binding (54). In this assay, mutation of the FDF-binding site in human HA-tagged DDX6 (Mut-1) significantly decreased the interaction with YFP-Pat1b (Figure 4C). We concluded that the interaction of Pat1 at the FDF-binding site of Dhh1 is evolutionary conserved in yeast and humans. Drosophila HPat is also expected to dock at the FDF-binding site of Me31b (Figure 4A), but it is possible that in this case the FDF-binding site contributes less to the overall interaction, explaining previous co-immunoprecipitation data (35).

An acidic helical segment of Pat1 docks onto a positively charged surface of Dhh1

N-terminal to the FDF motif, $Pat1_N$ features a helical segment that binds with extensive interactions at a third surface patch on Dhh1 (patch 3, Figure 3A, right panel). The helical segment of Pat1 is highly negatively charged (Figure 4A) and binds to a positively charged surface of Dhh1. Pat1 Asn34, Asn38, Thr41 and Asp45 make polar contacts with Dhh1 Ser292, Asn294 and Arg295 (Figure 3A, right panel). In addition, Pat1 Glu33 forms a salt bridge with Dhh1 Lys362 and Pat1 Phe42 makes hydrophobic contacts with Dhh1 Leu298, Phe358 and Arg295. The human Pat1b-4A mutant shown to disrupt the interaction with DDX6 (54) (Figure 4B) maps to the helical segment of Pat1 (alanine substitutions at Asp34, Asp35, Thr36, Phe37, Figure 4A). We engineered mutations in Dhh1 to disrupt patch 3. Substitutions of

Ser292Asp, Asn294Asp (Mut-3A) or of Arg295Asp (Mut-3B) abolished binding to $Pat1_{5–79}$ in GST pull-down assays (Figure 3B, lanes 4 and 5). The interacting residues are conserved in the human orthologues. Indeed a combined mutation of the Mut-3A and Mut-3B substitutions in human DDX6 (Ser343Asp, Gln345Asp, Arg346Asp or Mut-3C) impaired the interaction with human Pat1 in co-immunoprecipitation assays (Figure 4C).

Comparison of the structure of Dhh1–Pat1 with that of the DEAD-box protein eIF4AIII in the exon junction complex (EJC) (55,56) reveals that the patch 3 surface is used in both DEAD-box proteins to recruit binding partners (Supplementary Figure S3). The EJC is an assembly formed by four proteins (eIF4AIII, Btz, Mago and Y14), RNA and ATP (57). In the EJC, eIF4AIII binds RNA with the two RecA domains in the typical closed conformation observed in all known structures of DEAD-box proteins in the active (RNA-ATP-bound) state (55,56). Btz wraps around eIF4AIII and contributes to RNA binding. The N-terminal segment of Btz contacts RNA directly (via Phe188). In addition, Btz features several positively charged residues (Arg176, Arg184 and Arg185) that form a favorable electrostatic environment for an incoming nucleic acid (Supplementary Figure S3). The helical segment of $Pat1_N$ also approaches the RNA-binding site expected for the ATP-bound conformation, but features several surface-exposed negatively charged residues (Glu28, Glu30, Glu32, Asp35, Asp39 and Glu40) that are predicted to electrostatically disfavor binding of Dhh1 to nucleic acids (Supplementary Figure S3).

Yeast Edc3 contains an acidic segment similar to Pat1

Originally as a control, we tested the Dhh1 patch 3 mutants with yeast $Edc3_{77–158}$ (Figure 3C). In the human DDX6-Edc3 structure (35), there is no ordered segment N-terminal to the FDF motif of Edc3 and therefore there is no binding to the corresponding patch 3 surface of DDX6. In pull-down assays, however, yeast $Edc3_{77–158}$ failed to interact with the Mut-3A and Mut-3B Dhh1 proteins (Figure 3C, lanes 4 and 5). As we could not rationalize these biochemical results based on the available structural information, we set out to determine the crystal structure of yeast Dhh1-Edc3. Yeast $Dhh1_{30–425}$ interacted with $Edc3_{77–158}$ with a Kd of 200 nM (Supplementary Figure S1B). The $Edc3_{77–158}$ construct is considerably longer than the boundaries (residues 98–127) expected from the structure of human Edc3 (35). Initial crystals of the complex of yeast $Dhh1_{46–422}$ K234D, V238D and $Edc3_{77–158}$ diffracted to 3.5 Å resolution. The electron density map was of sufficient quality to show binding of yeast Edc3 to patch 3 and to narrow down the domain boundaries (i.e. no ordered electron density beyond residue 116 of Edc3) (data not shown). We proceeded to crystallize yeast $Dhh1_{46–422}$ K234D, V238D and $Edc3_{77–116}$. The structure was determined at 3.25 Å resolution with an R_{free} of 24.6% and Rfactor of 21.0%. The final model includes residues 46–420 of Dhh1 and residues 88–116 of yeast Edc3 (Figure 5A).

Comparison of the yeast Dhh1-Edc3 structure with that of human DDX6-Edc3 shows a similar binding of the FDF motif at the patch 1 surface. There is no equivalent binding of a C-terminal helix to patch 2 (Figure 5A). However, this is likely an artifact of crystallization, due to a crystal contact that blocks Edc3 from accessing patch 2 of Dhh1. Indeed, binding of Dhh1 to yeast $Edc3_{77–158}$ was abolished by the patch 2 mutations (Figure 3C, lane 6). More importantly, yeast Edc3 features an ordered segment (residues 88–104) N-terminal to the FDF motif (Figure 5A). In this segment, Trp91 of yeast Edc3 binds in the same pocket of patch 3 as Phe42 of yeast Pat1, explaining the results of the pull-down assays with the patch 3 mutants (Figure 3C). Also similarly to yeast Pat1, this segment of Edc3 is rich in negatively charged residues (Figure 5B). While the N-terminal segment of $Pat1_N$ is evolutionary conserved, the N-terminal segment of yeast Edc3 is apparently not present in the human and *Drosophila* orthologues. Indeed, the Mut-3C substitutions in human DDX6 did not impair the interaction with human Edc3 in co-immunoprecipitation assays (Figure 5C). We concluded that these differences in the structures of the orthologous complexes reflect genuine differences in the interactions.

Pat1 and Edc3 disrupt RNA binding of Dhh1

We tested the effect of yeast Pat1 and Edc3 on the RNA-binding properties of Dhh1 using a biotin-RNA pull-down assay. In agreement with previous findings, $Dhh1_{30–425}$ was precipitated by biotinylated RNA immobilized on streptavidin beads even in the absence of nucleotide analogs (Figure 6A, lanes 4 and 5) (44). On measuring the affinity of $Dhh1_{30–425}$ for a U_{15} RNA by fluorescence anisotropy, we found a Kd in the low micromolar range (Supplementary Figure S4A), lower than that previously reported for a full-length Dhh1 fusion protein (44), and lower than that measured for Pat1 and Edc3 using ITC (Figure 1D and Supplementary Figure S1). In the presence of either $Pat1_{5–79}$, or $Edc3_{77–158}$, $Dhh1_{30–425}$ failed to bind to RNA in the pull-down assay (Figure 6A, lanes 6,7 and lanes 8,9, respectively), suggesting that they interfere with RNA binding.

Intrigued by the observation that there was no significant difference in the RNA pull-down assays in the presence or absence of ATP, we analyzed the nucleotide-binding properties of Dhh1. First, inspection of the crystal structure of apo Dhh1 (45) indicated that its closed conformation is incompatible with ATP binding (Supplementary Figure S4B). $Dhh1_{30–425}$ indeed did not bind ATP in ITC experiments (Supplementary Figure S4C) and appeared to be essentially inactive in RNA-dependent ATPase assays (Supplementary Figure S4D), suggesting that Dhh1 is in an enzymatically inactive conformation.

To map how this unusual DEAD-box protein can bind RNA in the absence of ATP, we crosslinked $Dhh1_{30–425}$ to a U_{15} RNA by subjecting the complex to UV irradiation at 254 nm. We then used LC-MS/MS mass spectrometry to detect and sequence peptides conjugated to the mass of an RNA nucleotide [reviewed in (53)]. Using this approach, we identified 6 tryptic peptides mapping to the RecA2 domain

8386 Nucleic Acids Research, 2013, Vol. 41, No. 17

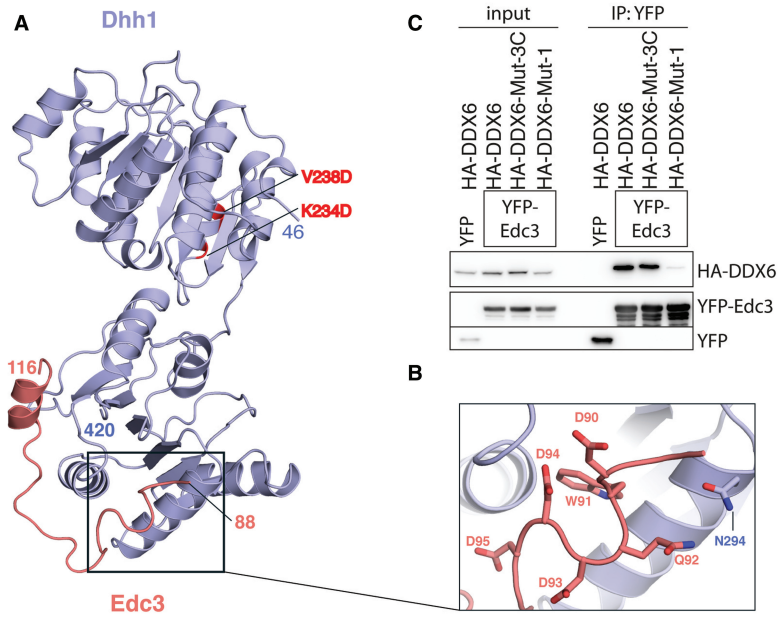

Figure 5. The interaction of Dhh1 and Edc3. (**A**) The structure of the yeast Dhh1–Edc3 core complex is shown in a similar orientation as in Figure 3A. The two RecA domains of yeast Dhh1 are in blue and Edc3 residues 88–116 are in salmon. The two residues on RecA1 mutated for crystallization purposes are highlighted in red. (**B**) Close-up view of the negatively charged residues of yeast Edc3 lining the patch 3 surface of Dhh1. (**C**) Co-immunoprecipitation assays of human YFP-tagged Edc3 and HA-tagged DDX6 wild type, Mut-1 or Mut-3C were carried out as described in Figure 4C. With the human proteins, mutations at patch 3 (Mut-3C) do not abrogate binding.

of Dhh1 (Figure 6B and Supplementary Figure S5). No peptide was detected in the RecA1 domain, suggesting that this domain is not able to bind RNA when Dhh1 is in the enzymatically inactive conformation. However, the flexible N-terminal region that precedes RecA1 might contribute to RNA binding, as we detected an additional peptide encompassing residues 32–44 (Supplementary Figure S5). Within RecA2, two peptides mapped to the canonical RNA-binding surface expected for the active state of the DEAD-box protein (red and magenta patches in Figure 6B). Others mapped to the outer surface of RecA2 (green and yellow patches in Figure 6B), corresponding to the patch 1 and patch 3 sites. The mass spectrometry analysis identified a direct crosslink between a uridine nucleotide and Cys273 (Figure 6C), a residue in a central position at the FDF-binding site on patch 1 (Figure 3A, central panel). Consistently, the electrostatic properties of the RecA2 surface show patches of positive charges along the RNA-binding surface mapped by mass-spectrometry (Figure 6D). These data indicate that Dhh1 binds Pat1, Edc3 and RNA with mutually exclusive interactions at patch 1 and patch 3.

CONCLUSIONS

Dhh1 has a prominent pocket on the C-terminal RecA2 domain that recognizes short FDF linear motifs present in both yeast Pat1 and Edc3. In the case of the human orthologues, this pocket recognizes either the FDF motif of Edc3 (35) or a DW motif in Pat1b. It is possible that Dhh1 might bind other factors at this pocket, not necessarily with a FDF motif in their sequence. A hydrophobic pocket is present at the corresponding position in human eIF4AIII, where it is used to bind a Tyr-containing short linear motif of Upf3b (58). An analogous pocket is also present in yeast eIF4A and is used to bind a Trp-containing short linear motif of eIF4G (59). Other DEAD-box proteins might have evolved this structural feature to recruit short motifs present in their binding factors. While such hydrophobic pocket probably contributes binding affinity, specificity is likely provided by binding to additional surfaces. We note that binding of Pat1 or Edc3 leaves a considerable surface area of Dhh1 unoccupied and potentially available to other binding partners.

Because of their overlapping binding sites, Pat1 and Edc3 cannot bind simultaneously on Dhh1. In addition, they interfere with the RNA-binding properties of Dhh1. Mapping the RNA-binding surfaces of Dhh1 by a crosslinking–mass spectrometry approach suggests that RNA wraps around the RecA2 domain, docking also at the FDF-binding site of Dhh1 (at patch 1). In this conformation, in the absence of ATP, Dhh1 is in an enzymatically inactive state. The presence of both ATP and RNA appears to be insufficient to release the inactive conformation of Dhh1 that arises from the stabilization of an unproductive conformation of the two RecA

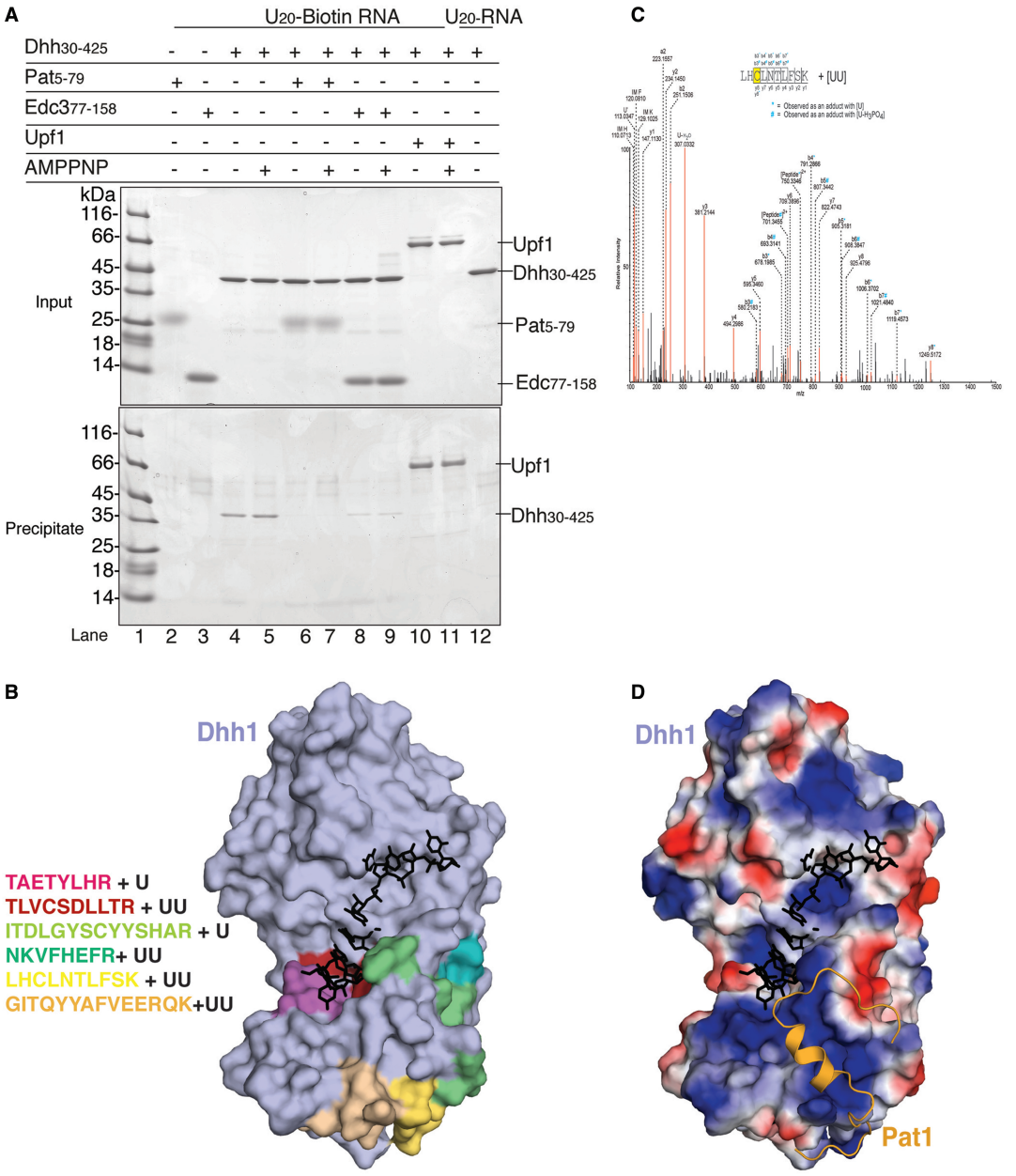

Figure 6. Pat1 and Edc3 compete with RNA for binding to Dhh1. **(A)** Co-precipitation of 5′ biotinylated single-stranded poly-U_{20} RNA with yeast Dhh1 alone or in complex with $Pat1_{5–79}$ or $Edc3_{77–158}$. The pull-down experiments were performed with streptavidin beads [essentially as described in (51)] and analyzed on 4–20% NuPAGE Bis-Tris gels (Invitrogen) using 20% of the total as input and bound samples. Dhh1 bound to RNA in presence or absence of nucleotides, as previously reported (44,39). In the presence of either $Pat1_{5–79}$ or $Edc3_{77–158}$, Dhh1 binding to RNA was impaired. **(B)** On the left are the peptides of RecA2 identified by mass spectrometry analysis to be crosslinked to RNA (Supplementary Figure S5). On the right, surface representation of apo Dhh1 (45) (in light blue) with the RNA-crosslinked peptides shown in the same colors as on the right. Shown in black is the RNA modeled after superposition with eIF4AIII-AMPNP-RNA in EJC structure upon superposition of the RecA2 domains (54,55). Notice that, in this conformation of Dhh1, an RNA bound in the typical ATP-dependent conformation would sterically clash against the

(continued)

domains by an extensive network of intramolecular interactions (44,45). Pat1 and in yeast Edc3 are expected also to approach the canonical ATP-dependent RNA-binding surface (at patch 3) with a negatively charged segment, and thus to interfere with it.

The results predict that Pat1, Edc3 and RNA bind Dhh1 as separate steps in the pathway, pointing to the presence of transitions in the architecture of an mRNP as it gets targeted to decay. A working model for the sequence and coordination of these structural rearrangements is outlined below. In the cytoplasm, Dhh1 is present in large excess and binds mRNAs in a constitutive, ATP-independent manner (39,44,45). We envision that upon triggering translational repression and deadenylation, Pat1 and Edc3 binding to Dhh1 would release it from the nonproductive ATP-independent mode of RNA binding. This displacement would allow Dhh1 to bind RNA in a productive ATP-dependent manner, triggering ATP hydrolysis and dissociation from the mRNP. This step is likely to require the binding of an activator to release Dhh1 from the enzymatically inhibited conformation. Besides the Dhh1-binding domain, Pat1 and Edc3 bridge to the Lsm complex and to the decapping complex, respectively. Discovering the precise sequel of events that lead to the swap between Pat1-containing and Edc3-containing complexes on Dhh1 as well as the identity of the Dhh1 activator are quests for future studies.

ACCESSION NUMBERS

Atomic coordinates and structure factors have been deposited in the Protein data Bank with accession codes 4brw for the yeast Dhh1–Pat1 complex and 4bru for the yeast Dhh1–Edc3 complex.

SUPPLEMENTARY DATA

Supplementary Data are available at NAR Online, including [60–66].

ACKNOWLEDGEMENTS

We would like to thank the Max Planck Institute of Biochemistry Core Facility and Crystallization Facility; the staff members at the beamlines PXII and PXIII of the Swiss Light Source. We also thank members of our lab for useful discussions and critical reading of the manuscript. H.S. performed the biochemical, ITC and crystallography experiments; S.O. performed the coIP experiments; C.B. performed the fluorescence anisotropy experiments; K.S. and H.U. carried out the crosslinking/mass spectroscopy analysis; E.C. and H. U. supervised the project; E.C. and H.S. wrote the manuscript.

FUNDING

Max Planck Gesellschaft, the EU [ERC Advanced Investigator Grant 294371 and Marie Curie Initial Training Network RNPnet 289007]; Deutsche Forschungsgemeinschaft [SFB646, SFB1035, GRK1721, FOR1680 and CIPSM to E.C.]. Funding for open access charge: MPG internal funding.

Conflict of interest statement. None declared.

REFERENCES

1. Moore,M.J. (2005) From birth to death: the complex lives of eukaryotic mRNAs. *Science*, **309**, 1514–1518.
2. Sonenberg,N. and Dever,T.E. (2003) Eukaryotic translation initiation factors and regulators. *Curr. Opin. Struct. Biol.*, **13**, 56–63.
3. Garneau,N.L., Wilusz,J. and Wilusz,C.J. (2007) The highways and byways of mRNA decay. *Nat. Rev. Mol. Cell. Biol.*, **8**, 113–126.
4. Wickens,M. and Goldstrohm,A. (2003) Molecular biology. A place to die, a place to sleep. *Science*, **300**, 753–755.
5. van Dijk,E., Cougot,N., Meyer,S., Babajko,S., Wahle,E. and Seraphin,B. (2002) Human Dcp2: a catalytically active mRNA decapping enzyme located in specific cytoplasmic structures. *EMBO J.*, **21**, 6915–6924.
6. Steiger,M., Carr-Schmid,A., Schwartz,D.C., Kiledjian,M. and Parker,R. (2003) Analysis of recombinant yeast decapping enzyme. *RNA*, **9**, 231–238.
7. Tharun,S., He,W., Mayes,A.E., Lennertz,P., Beggs,J.D. and Parker,R. (2000) Yeast Sm-like proteins function in mRNA decapping and decay. *Nature*, **404**, 515–518.
8. Bouveret,E., Rigaut,G., Shevchenko,A., Wilm,M. and Séraphin,B. (2000) A Sm-like protein complex that participates in mRNA degradation. *EMBO J.*, **19**, 1661–1671.
9. Bonnerot,C., Boeck,R. and Lapeyre,B. (2000) The two proteins Pat1p (Mrt1p) and Spb8p interact in vivo, are required for mRNA decay, and are functionally linked to Pab1p. *Mol. Cell. Biol.*, **20**, 5939–5946.
10. Coller,J.M., Tucker,M., Sheth,U., Valencia-Sanchez,M.A. and Parker,R. (2001) The DEAD box helicase, Dhh1p, functions in mRNA decapping and interacts with both the decapping and deadenylase complexes. *RNA*, **7**, 1717–1727.
11. Fischer,N. and Weis,K. (2002) The DEAD box protein Dhh1 stimulates the decapping enzyme Dcp1. *EMBO J.*, **21**, 2788–2797.
12. Decourty,L., Saveanu,C., Zemam,K., Hantraye,F., Frachon,E., Rousselle,J.-C., Fromont-Racine,M. and Jacquier,A. (2008) Linking functionally related genes by sensitive and quantitative characterization of genetic interaction profiles. *Proc. Natl Acad. Sci. USA*, **105**, 5821–5826.
13. Decker,C.J. and Parker,R. (2002) mRNA decay enzymes: decappers conserved between yeast and mammals. *Proc. Natl Acad. Sci. USA*, **99**, 12512–12514.
14. Parker,R. and Sheth,U. (2007) P bodies and the control of mRNA translation and degradation. *Mol. Cell*, **25**, 635–646.

Figure 6. Continued
surface of Dhh1. (**C**) MS/MS mass spectrum of Dhh1 residues 271–280 identifies an additional mass that corresponds to two uracil nucleotides associated to a cysteine. Peptide sequence and the fragment ions are indicated on the top. The peptide fragmentation occurs with the cleavage of amide bonds resulting in b-ions and y-ions when the charge is retained by the amino-terminal and carboxy-terminal fragments, respectively. Asterisk (*) and hash (#) indicate the b-ions that were observed with a mass shift corresponding to U and U-H_3PO_4, respectively. IM: Immonium ions. U': U marker ion of 113.03 Da. (**D**) Surface representation of apo Dhh1 (45) in the same orientation as in panel B, colored by electrostatic potential, with positively charged residues in blue and negatively charged residues in red. The binding paths of RNA (in the ATP-dependent state) and of Pat1 are shown modeled in black and in orange.

15. Eulalio,A., Behm-Ansmant,I. and Izaurralde,E. (2007) P bodies: at the crossroads of post-transcriptional pathways. *Nat. Rev. Mol. Cell. Biol.*, **8**, 9–22.
16. Franks,T.M. and Lykke-Andersen,J. (2008) The control of mRNA decapping and P-body formation. *Mol. Cell*, **32**, 605–615.
17. Kulkarni,M., Ozgur,S. and Stoecklin,G. (2010) On track with P-bodies. *Biochem. Soc. Trans.*, **38**, 242–251.
18. Coller,J. and Parker,R. (2005) General translational repression by activators of mRNA decapping. *Cell*, **122**, 875–886.
19. Teixeira,D. and Parker,R. (2007) Analysis of P-body assembly in Saccharomyces cerevisiae. *Mol. Biol. Cell*, **18**, 2274–2287.
20. Pilkington,G.R. and Parker,R. (2008) Pat1 contains distinct functional domains that promote P-body assembly and activation of decapping. *Mol. Cell. Biol.*, **28**, 1298–1312.
21. Minshall,N., Kress,M., Weil,D. and Standart,N. (2009) Role of p54 RNA helicase activity and its C-terminal domain in translational repression, P-body localization and assembly. *Mol. Biol. Cell*, **20**, 2464–2472.
22. Haas,G., Braun,J.E., Igreja,C., Tritschler,F., Nishihara,T. and Izaurralde,E. (2010) HPat provides a link between deadenylation and decapping in metazoa. *J. Cell Biol.*, **189**, 289–302.
23. Ozgur,S., Chekulaeva,M. and Stoecklin,G. (2010) Human Pat1b connects deadenylation with mRNA decapping and controls the assembly of processing bodies. *Mol. Cell. Biol.*, **30**, 4308–4323.
24. Totaro,A., Renzi,F., La Fata,G., Mattioli,C., Raabe,M., Urlaub,H. and Achsel,T. (2010) The human Pat1b protein: a novel mRNA deadenylation factor identified by a new immunoprecipitation technique. *Nucleic Acids Res.*, **39**, 635–647.
25. Weston,A. and Sommerville,J. (2006) Xp54 and related (DDX6-like) RNA helicases: roles in messenger RNP assembly, translation regulation and RNA degradation. *Nucleic Acids Res.*, **34**, 3082–3094.
26. Marnef,A. and Standart,N. (2010) Pat1 proteins: a life in translation, translation repression and mRNA decay. *Biochem. Soc. Trans.*, **38**, 1602–1607.
27. Nissan,T., Rajyaguru,P., She,M., Song,H. and Parker,R. (2010) Decapping Activators in Saccharomyces cerevisiae Act by Multiple Mechanisms. *Mol. Cell*, **39**, 773–783.
28. Tharun,S. (2009) Lsm1-7-Pat1 complex: a link between 3′ and 5′-ends in mRNA decay? *RNA Biol.*, **6**, 228–232.
29. Fromm,S.A., Truffault,V., Kamenz,J., Braun,J.E., Hoffmann,N.A., Izaurralde,E. and Sprangers,R. (2011) The structural basis of Edc3- and Scd6-mediated activation of the Dcp1:Dcp2 mRNA decapping complex. *EMBO J.*, **31**, 279–290.
30. Sweet,T., Kovalak,C. and Coller,J. (2012) The DEAD-box protein Dhh1 promotes decapping by slowing ribosome movement. *PLoS Biol.*, **10**, e1001342.
31. Nakamura,A., Amikura,R., Hanyu,K. and Kobayashi,S. (2001) Me31B silences translation of oocyte-localizing RNAs through the formation of cytoplasmic RNP complex during Drosophila oogenesis. *Development*, **128**, 3233–3242.
32. Navarro,R.E., Shim,E.Y., Kohara,Y., Singson,A. and Blackwell,T.K. (2001) cgh-1, a conserved predicted RNA helicase required for gametogenesis and protection from physiological germline apoptosis in C. elegans. *Development*, **128**, 3221–3232.
33. Minshall,N. and Standart,N. (2004) The active form of Xp54 RNA helicase in translational repression is an RNA-mediated oligomer. *Nucleic Acids Res.*, **32**, 1325–1334.
34. Chu,C.Y. and Rana,T.M. (2006) Translation repression in human cells by microRNA-induced gene silencing requires RCK/p54. *PLoS Biol.*, **4**, e210.
35. Tritschler,F., Braun,J.E., Eulalio,A., Truffault,V., Izaurralde,E. and Weichenrieder,O. (2009) Structural basis for the mutually exclusive anchoring of P body components EDC3 and Tral to the DEAD box protein DDX6/Me31B. *Mol. Cell*, **33**, 661–668.
36. Ghaemmaghami,S., Huh,W.-K., Bower,K., Howson,R.W., Belle,A., Dephoure,N., O'Shea,E.K. and Weissman,J.S. (2003) Global analysis of protein expression in yeast. *Nature*, **425**, 737–741.
37. Kramer,S., Queiroz,R., Ellis,L., Hoheisel,J.D., Clayton,C. and Carrington,M. (2010) The RNA helicase DHH1 is central to the correct expression of many developmentally regulated mRNAs in trypanosomes. *J. Cell Sci.*, **123**, 699–711.
38. Minshall,N., Reiter,M.H., Weil,D. and Standart,N. (2007) CPEB interacts with an ovary-specific eIF4E and 4E-T in early Xenopus oocytes. *J. Biochem.*, **282**, 37389–37401.
39. Ernoult-Lange,M., Baconnais,S., Harper,M., Minshall,N., Souquere,S., Boudier,T., Bénard,M., Andrey,P., Pierron,G., Kress,M. *et al.* (2012) Multiple binding of repressed mRNAs by the P-body protein Rck/p54. *RNA*, **18**, 1702–1715.
40. Gygi,S.P., Rochon,Y., Franza,B.R. and Aebersold,R. (1999) Correlation between protein and mRNA abundance in yeast. *Mol. Cell Biol.*, **19**, 1720–1730.
41. Smillie,D.A. and Sommerville,J. (2002) RNA helicase p54 (DDX6) is a shuttling protein involved in nuclear assembly of stored mRNP particles. *J. Cell Sci.*, **115**, 395–407.
42. Haanstra,J.R., Stewart,M., Luu,V.D., van Tuijl,A., Westerhoff,H.V., Clayton,C. and Bakker,B.M. (2008) Control and regulation of gene expression: quantitative analysis of the expression of phosphoglycerate kinase in bloodstream form Trypanosoma brucei. *J. Biochem.*, **283**, 2495–2507.
43. Cordin,O., Banroques,J., Tanner,N.K. and Linder,P. (2006) The DEAD-box protein family of RNA helicases. *Gene*, **367**, 17–37.
44. Dutta,A., Zheng,S., Jain,D., Cameron,C.E. and Reese,J.C. (2011) Intermolecular interactions within the abundant DEAD-box protein Dhh1 regulate its activity *in vivo*. *J. Biol. Chem.*, **286**, 27454–27470.
45. Cheng,Z., Coller,J., Parker,R. and Song,H. (2005) Crystal structure and functional analysis of DEAD-box protein Dhh1p. *RNA*, **11**, 1258–1270.
46. Carroll,J.S., Munchel,S.E. and Weis,K. (2011) The DExD/H box ATPase Dhh1 functions in translational repression, mRNA decay, and processing body dynamics. *J. Cell Biol.*, **194**, 527–537.
47. Tritschler,F., Eulalio,A., Helms,S., Schmidt,S., Coles,M., Weichenrieder,O., Izaurralde,E. and Truffault,V. (2008) A similar mode of interaction enables Trailer Hitch and EDC3 to associate with DCP1 and Me31B in distinct protein complexes. *Mol. Cell. Biol.*, **28**, 6695–6708.
48. McCoy,A.J. (2007) Solving structures of protein complexes by molecular replacement with Phaser. *Acta Crystallogr. D Biol. Crystallogr.*, **63**, 32–41.
49. Emsley,P., Lohkamp,B., Scott,W.G. and Cowtan,K. (2010) Features and development of Coot. *Acta Crystallogr. D Biol. Crystallogr.*, **66**, 486–501.
50. Adams,P.D., Afonine,P.V., Bunkóczi,G., Chen,V.B., Davis,I.W., Echols,N., Headd,J.J., Hung,L.-W., Kapral,G.J., Grosse-Kunstleve,R.W. *et al.* (2010) PHENIX: a comprehensive Python-based system for macromolecular structure solution. *Acta Crystallogr. D Biol. Crystallogr.*, **66**, 213–221.
51. Davis,I.W., Murray,L.W., Richardson,J.S. and Richardson,D.C. (2004) MOLPROBITY: structure validation and all-atom contact analysis for nucleic acids and their complexes. *Nucleic Acids Res.*, **32**, W615–W619.
52. von Moeller,H., Basquin,C. and Conti,E. (2009) The mRNA export protein DBP5 binds RNA and the cytoplasmic nucleoporin NUP214 in a mutually exclusive manner. *Nat. Struct. Mol. Biol.*, **16**, 247–254.
53. Schmidt,C., Kramer,K. and Urlaub,H. (2012) Investigation of protein-RNA interactions by mass spectrometry.Techniques and applications. *J. Proteomics*, **75**, 3478–3494.
54. Ozgur,S. and Stoecklin,G. (2013) Role of Rck-Pat1b binding in assembly of processing-bodies. *RNA Biol.*, **10**, 1–12.
55. Bono,F., Ebert,J., Lorentzen,E. and Conti,E. (2006) The crystal structure of the exon junction complex reveals how it maintains a stable grip on mRNA. *Cell*, **126**, 713–725.
56. Andersen,C.B.F., Ballut,L., Johansen,J.S., Chamieh,H., Nielsen,K.H., Oliveira,C.L.P., Pedersen,J.S., Seraphin,B., Le Hir,H. and Andersen,G.R. (2006) Structure of the exon junction core complex with a trapped DEAD-box ATPase bound to RNA. *Science*, **313**, 1968–1972.
57. Ballut,L., Marchadier,B., Baguet,A., Tomasetto,C., Seraphin,B. and Le Hir,H. (2005) The exon junction core complex is locked onto RNA by inhibition of eIF4AIII ATPase activity. *Nat. Struct. Mol. Biol.*, **12**, 861–869.
58. Buchwald,G., Ebert,J., Basquin,C., Saulière,J., Jayachandran,U., Bono,F., Le Hir,H. and Conti,E. (2010) Insights into the

recruitment of the NMD machinery from the crystal structure of a core EJC-UPF3b complex. *Proc. Natl Acad. Sci. USA*, **107**, 10050–10055.
59. Schütz,P., Bumann,M., Oberholzer,A.E., Bieniossek,C., Trachsel,H., Altmann,M. and Baumann,U. (2008) Crystal structure of the yeast eIF4A-eIF4G complex: an RNA-helicase controlled by protein-protein interactions. *Proc. Natl Acad. Sci. USA*, **105**, 9564–9569.
60. Halbach,F., Rode,M. and Conti,E. (2012) The crystal structure of S. cerevisiae Ski2, a DExH helicase associated with the cytoplasmic functions of the exosome. *RNA*, **18**, 124–134.
61. Kramer,K., Hummel,P., Hsiao,H., Luo,X., Wahl,M. and Urlaub,H. (2011) Mass-spectrometric analysis of proteins cross-linked to 4-thio-uracil- and 5-bromo-uracil-substituted RNA. *Int. J. Mass Spectrom.*, **304**, 184–194.
62. Kessner,D., Chambers,M., Burke,R., Agus,D. and Mallick,P. (2008) ProteoWizard: open source software for rapid proteomics tools development. *Bioinformatics*, **24**, 2534–2536.
63. Sturm,M., Bertsch,A., Gropl,C., Hidebrandt,A., Hussong,R., Lange,E., Pfeifer,N., Shulz-Trieglaff,O., Zerck,A., Reinert,K. *et al.* (2011) OpenMS - an open-source software framework for mass spectrometry. *BMC Bioinformatics*, **9**, 163.
64. Bertsch,A., Gröpl,C., Reinert,K. and Kohlbacher,O. (2011) OpenMS and TOPP: open source software for LC-MS data analysis. *Methods Mol. Biol.*, **696**, 353–367.
65. Geer,L.Y., Merkey,S.P., Kowalak,J.A., Wagner,L., Xu,M., Maynard,D.M., Yang,X., Shi,W. and Bryant,S.H. (2004) Open mass spectrometry search algorithm. *J. Proteome Res.*, **3**, 958–964.

Supplementary Information

Structural analysis of the yeast Dhh1-Pat1 complex reveals how Dhh1 engages Pat1, Edc3 and RNA in mutually exclusive interactions

Humayun Sharif[1], Sevim Ozgur[1], Kundan Sharma[2], Claire Basquin[1], Henning Urlaub[2] and Elena Conti[1]*

[1]Structural Cell Biology Department, Max Planck Institute of Biochemistry, Munich, D-82152 Germany
[2]Max Planck Institute of Biophysical Chemistry, Am Faßberg 11, 37077 Göttingen, Germany

Supplementary Figures

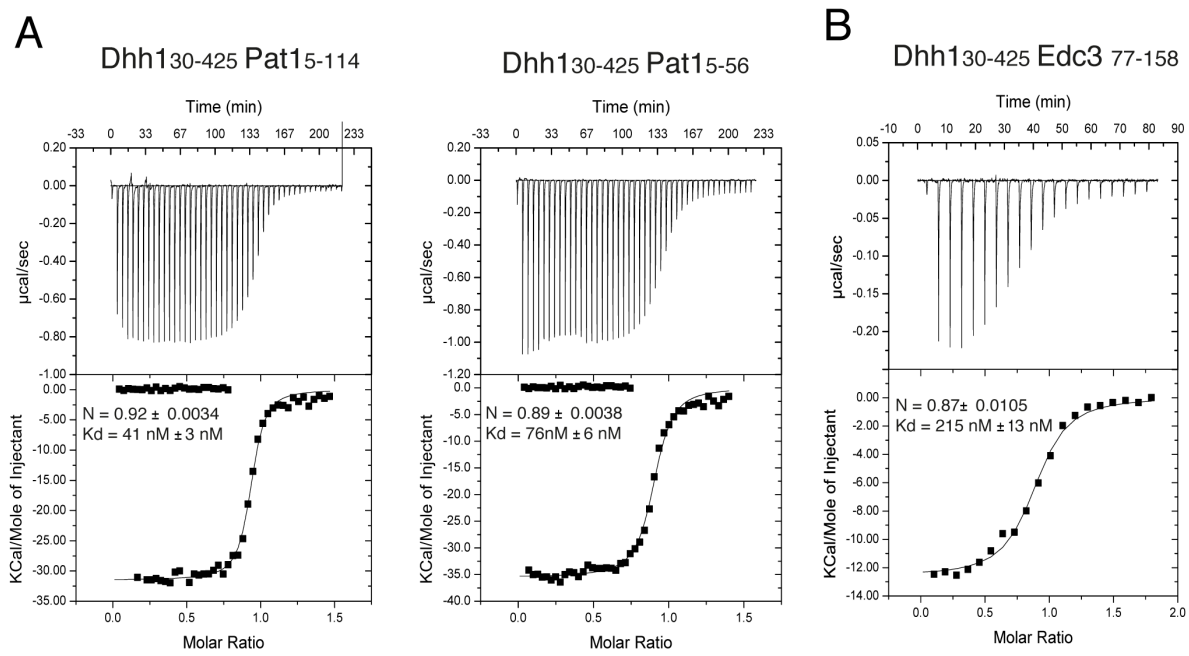

Figure S1

Quantitative analysis of yeast Dhh1-Pat1 and Dhh1-Edc3 interaction

(**A**) Isothermal titration calorimetry (ITC) of $Dhh1_{30-425}$ with His-SUMO-$Pat1_{5-56}$ and $Pat1_{5-114}$. Experiments were performed as described for Figure 1D.

(**B**) ITC of $Dhh1_{30-425}$ with His-SUMO-$Edc3_{77-158}$. Experiments were performed as described for Figure 1D.

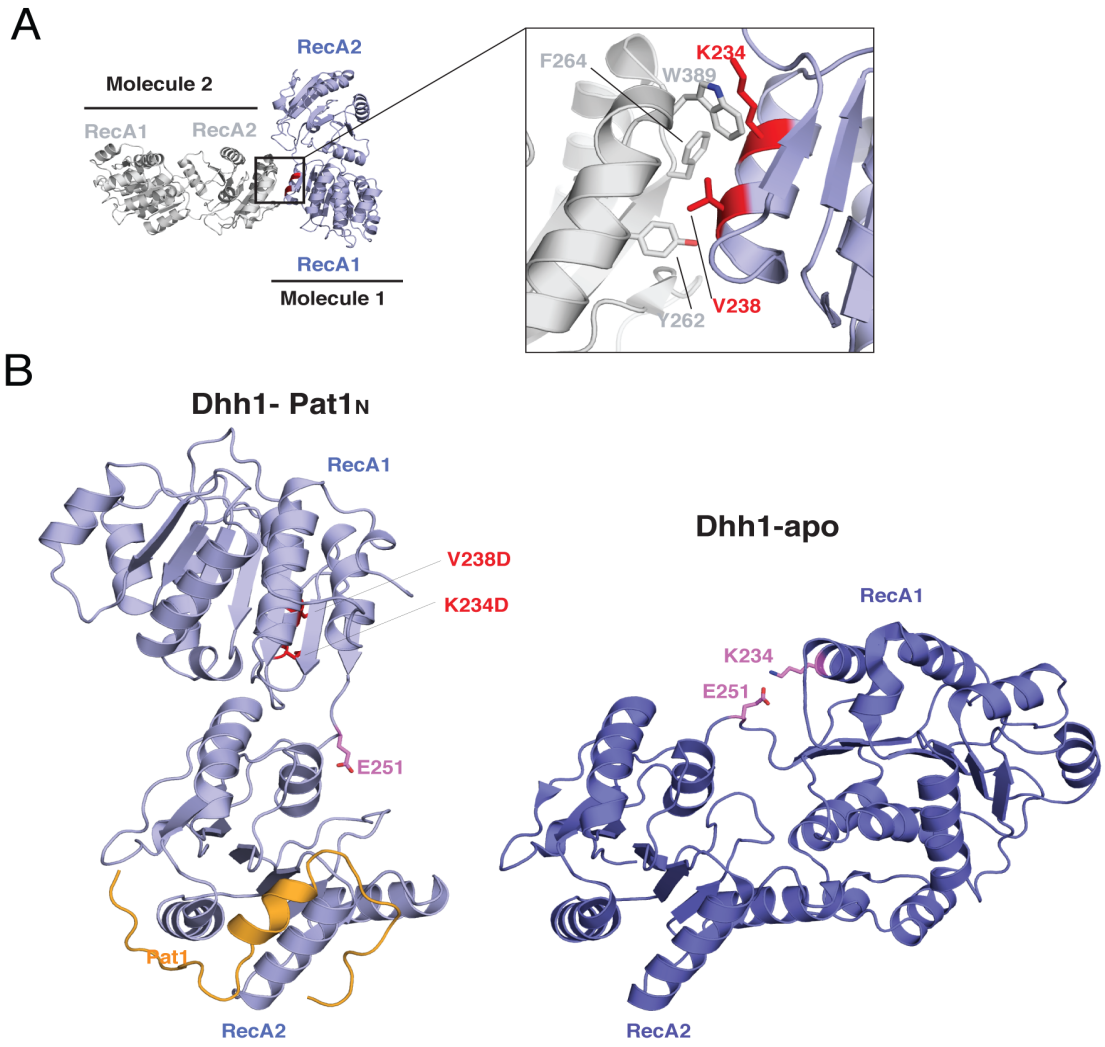

Figure S2

Intermolecular and intramolecular Dhh1 interactions in the crystals

(**A**) The close-up view shows the crystal lattice contacts of yeast Dhh1 wild-type crystals (45). The RecA2 domain of one Dhh1 molecule (in blue) interacts with the RecA1 domain of a neighbouring one (in gray), at the so-called FDF-binding site (patch1). The residues of RecA1 mutated for crystallization of the yeast Dhh1-Pat1 and Dhh1-Edc3 complexes are highlighted in red.

(**B**) The crystal structure of wild-type Dhh1 in the unbound state (45) is shown on the right, in the same orientation as the structure of the yeast Dhh1 K234D, V238D mutant in complex with Pat1 (on the left) after superposition of the RecA2 domains.

On the right, the intramolecular interaction of K234 (on RecA1) and E251 (on RecA2) is highlighted. This interaction is impaired in the mutant we have used for crystallizing the complexes.

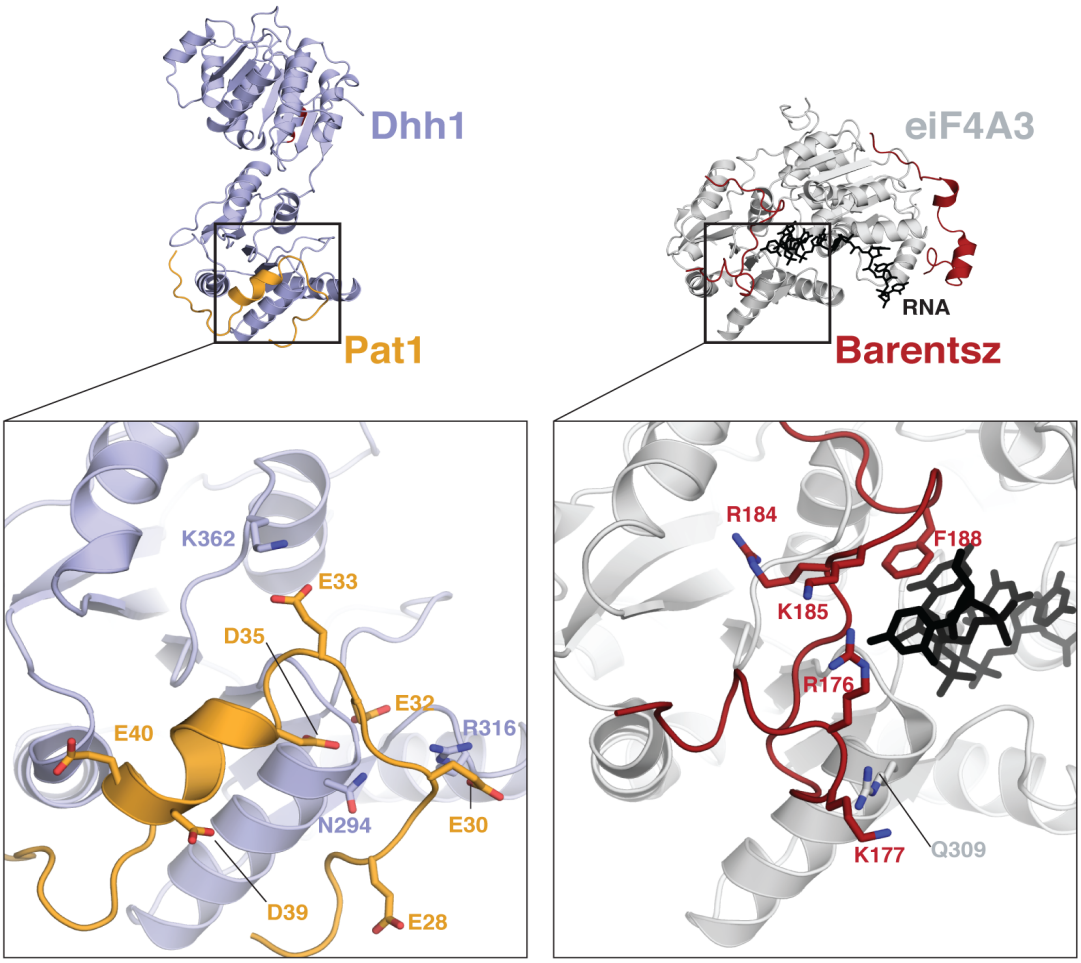

Figure S3

Different DEAD-box proteins use the patch 3 surface to bind regulators

Close-up views of the negatively-charged residues of yeast Pat1 lining the patch 3 surface of Dhh1 (left panel). The right panel shows the structure of human eIF4AIII (gray), Btz (red) and RNA (in black) extracted from the structure of the EJC (54, 55) and viewed in the same orientation as the structure in the left panel, after superposition of the RecA2 domains. Positively-charged residues of Btz line the corresponding patch 3 surface of eIF4AIII and approach the RNA-binding site.

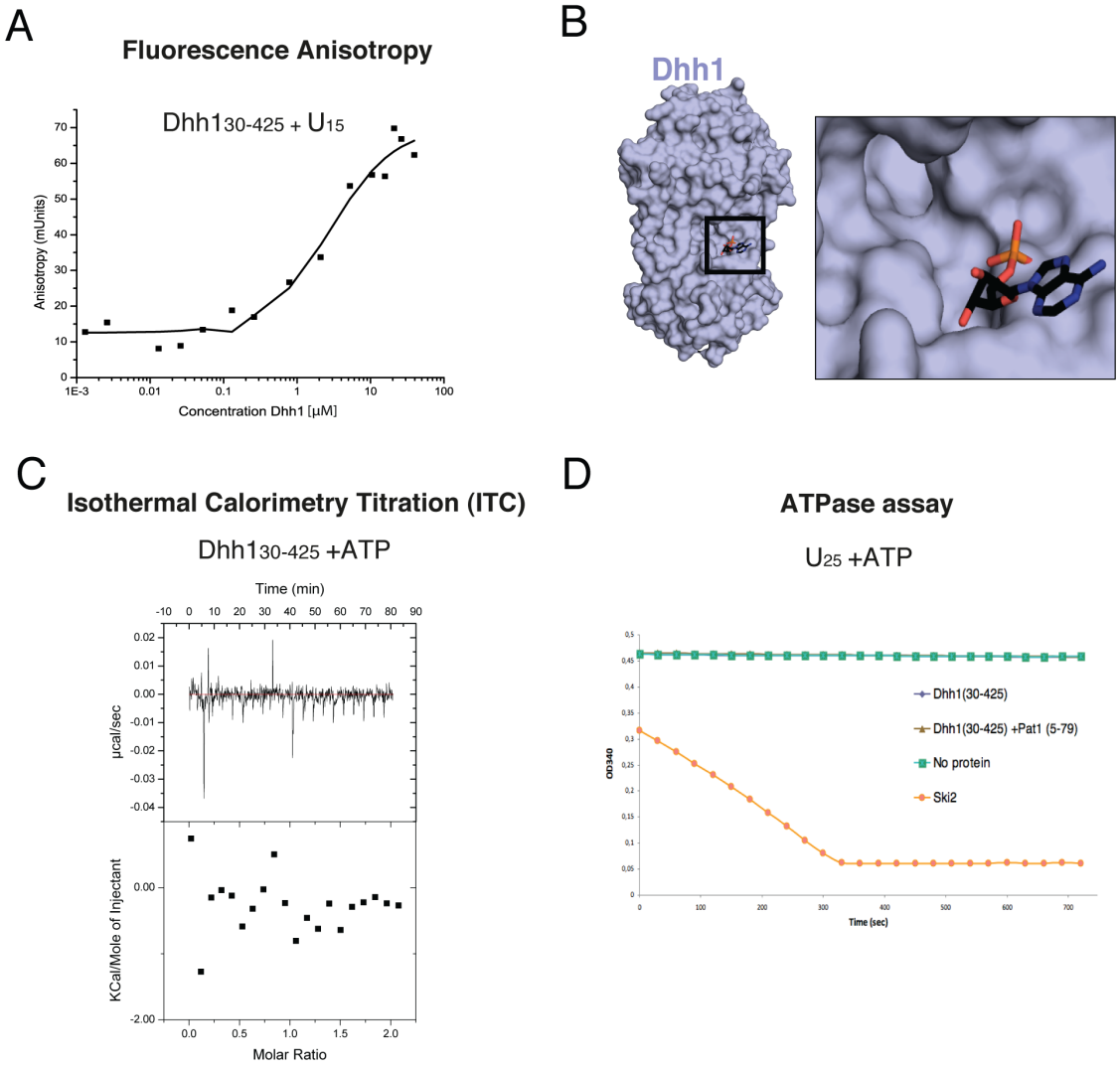

Supplementary Figure S4

RNA-binding and nucleotide-binding properties of the Dhh1 DEAD-box core

(**A**) Quantitative analysis of $Dhh1_{30-425}$ binding to a U_{15} RNA by fluorescence anisotropy (FA). FA measurements were performed with a 5'-6-carboxy-fluorescein (6-FAM)-labeled U_{15} RNA at 20°C on a Genios Pro (Tecan) using 50µl-reactions. The RNA was dissolved to a concentration of 9.6 nM and incubated with $Dhh1_{30-425}$ at different concentrations in 25mM MOPS pH 7.0, 150 mM NaCl, 10mM MgCl2 and 2mM β-mercaptoethanol. The excitation and emission wavelengths were 485nm and 535 nm, respectively. Each titration point was measured three times using ten reads

with an integration time of 40 µs. The data were analyzed using nonlinear regression fitting using the Origin software.

(**B**) Surface representation of apo Dhh1 with an ATP analogue modeled from the Dbp5-AMPPNP-RNA structure (60) after superposition of the RecA2 domains. Only the α-phosphate of ATP (in red) is in principle accessible in this closed conformation of Dhh1.

(**C**) ITC of $Dhh1_{30-425}$ with ATP. Experiments were performed as described as for Figure 1D.

(**D**) ATPase assays performed in the presence of a U_{25} RNA with $Dhh1_{30-425}$ either alone (blue diamonds) or in complex with $Pat1_{5-79}$ (brown triangles). The activity of Ski2 (61) is shown as a control (orange circles). The data represent mean values and standard deviations from three independent experiments. The measurements were carried out as reported in (61).

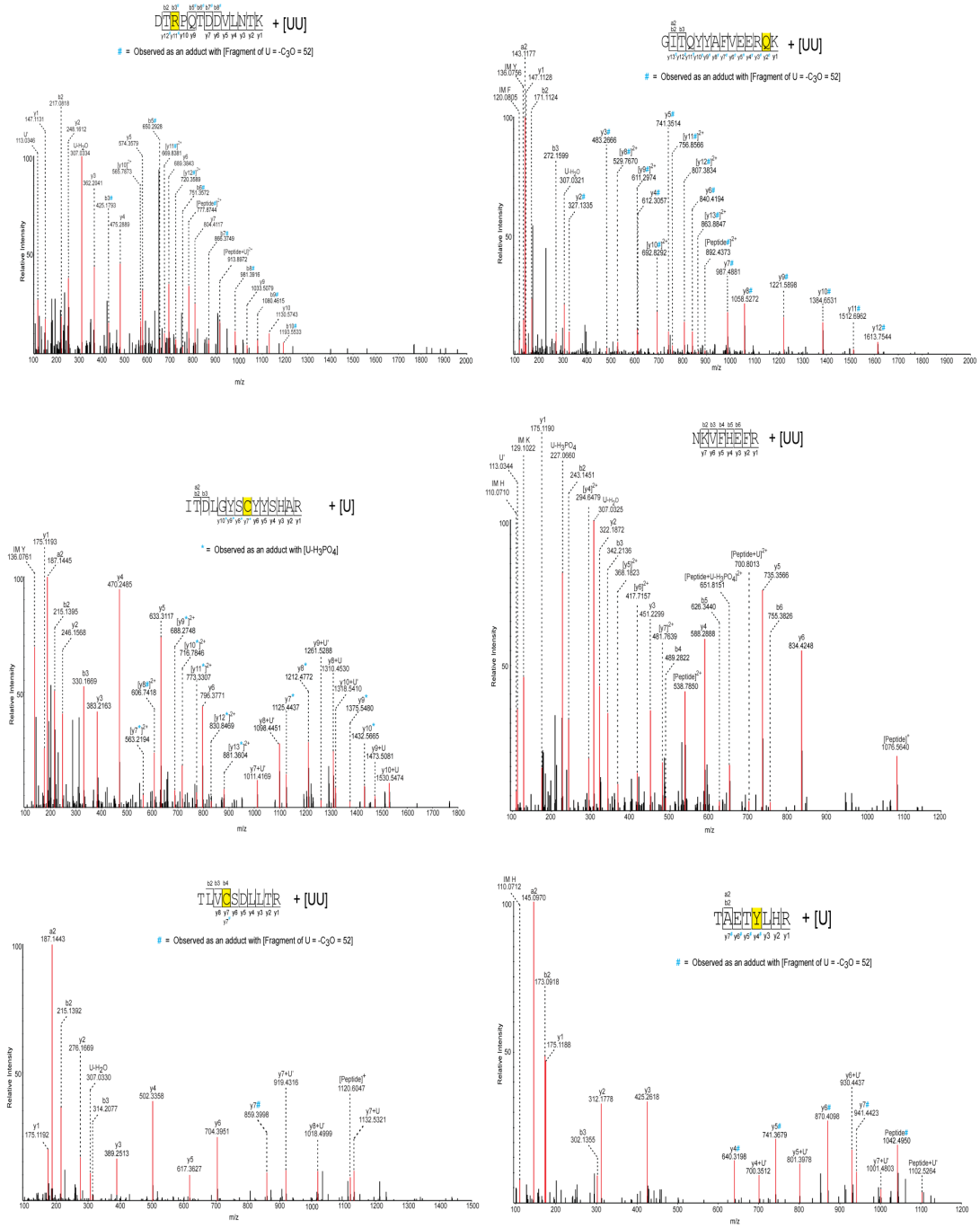

Figure S5

Dhh1-RNA crosslinking and mass spectrometry analysis

MS/MS spectra of Dhh1 peptides with an additional mass that corresponds to uracil nucleotides. Peptide sequence and the fragment ions are indicated on the top. The crosslinked residues are highlighted in yellow. The peptide fragmentation occurs with

the cleavage of amide bonds resulting in b-ions and y-ions when the charge is retained by the amino-terminal and carboxy-terminal fragments, respectively. Asterisk (*) and hash (#) indicate the ions that were observed with a mass shift corresponding to U-H_3PO_4 and $–C_3O$ (a 52 Da fragment of Uracil), respectively. IM: Immonium ions. U': U marker ion of 113.03 Da.

Supplementary Methods

UV induced Protein-RNA crosslinking and enrichment of cross-linked peptides

UV cross-linking and enrichment of cross-linked peptides was performed according to the established protocols described in (62). Briefly, 1 nmol of the single stranded U_{15} RNA oligonucleotide and 1 nmole of $Dhh1_{30-425}$ were mixed in a 1:1 molar ratio and the total reaction volume was made up to 100 µl in 20 mM HEPES pH 7.5, 50 mM NaCl, 2 mM DTT and 5 mM EDTA. The mixture was incubated on ice overnight. The samples were then transferred to black polypropylene microplates (Greiner Bio-One) and irradiated at 254 nm for 10 minutes. After ethanol precipitation the samples were denatured in 4M Urea, 50 mM Tris-HCl pH 7.9 and digested for 2 hours at 52°C with 1 µg RNase A (Ambion, Applied Biosystems). Following RNA digestion, proteolysis with trypsin (Promega) was performed overnight at 37°C. The sample was desalted on an in-house prepared C18 (Dr. Maisch GmbH) column and the cross-linked peptides were enriched on an in-house prepared TiO_2 (GL Sciences) column using the protocol described in (62). The samples were dried and then resuspended in 10 µl sample solvent (5% v/v ACN, 1% v/v FA) for mass spectrometry analysis.

Nano-liquid chromatography and MS analysis

5 µL of the above sample was injected onto a nano-liquid chromatography system (Agilent 1100 series, Agilent Technologies) including a C18 trapping column of length ~2 cm and inner diameter 150 µm, in-line with a C18 analytical column of length ~15 cm and inner diameter 75 µm (both packed in-house, C18 AQ 120 Å 5 µm, Dr. Maisch GmbH). Analytes were loaded on the trapping column at a flow rate of 10 µL/min in buffer A (0.1% v/v FA) and subsequently eluted and separated on the analytical column with a gradient of 7–38% buffer B (95% v/v acetonitrile, 0.1% v/v FA) with an elution time of 33 min (0.87%/min) and a flow rate of 300 nL/min. Online ESI-MS was performed with an LTQ-Orbitrap Velos instrument (Thermo Scientific), operated in data-dependent mode using a TOP10 method. MS scans were recorded in the m/z range of 350-1600 and for subsequent MS/MS top 10 most intense ions were selected. Both Precursor ions as well as fragment ions were scanned in the Orbitrap. Fragment ions were generated by HCD activation (higher energy collision dissociation, normalized collision energy=40), and recorded from m/z=100.

As precursor ions as well as fragment ions were scanned in the Orbitrap, the resulting spectra were measured with high accuracy (< 5 ppm) both in the MS and MSMS level.

Data analysis

The MS .raw files were converted into the .mzML format with msconvert (63). Protein-RNA cross-links were analyzed using OpenMS (64, 65) and OMSSA (66) as search engine. Data analysis workflows were assembled based on (66). The high scoring cross-linked peptides were manually annotated for confirmation. Protein RNA interactions between the N1T25LP complex and polyU RNA was analyzed with UV induced protein-RNA crosslinking followed by mass spectrometry. Seven peptides of Dhh1 protein were observed carrying an additional mass corresponding to Uracil nucleotides.

Supplementary References

45. Cheng,Z., Coller,J., Parker,R. and Song,H. (2005) Crystal structure and functional analysis of DEAD-box protein Dhh1p. *RNA*, **11**, 1258–1270.

54. Bono,F., Ebert,J., Lorentzen,E. and Conti,E. (2006) The crystal structure of the exon junction complex reveals how it maintains a stable grip on mRNA. *Cell*, **126**, 713–725.

55. Andersen,C.B.F., Ballut,L., Johansen,J.S., Chamieh,H., Nielsen,K.H., Oliveira,C.L.P., Pedersen,J.S., Seraphin,B., Le Hir,H. and Andersen,G.R. (2006) Structure of the exon junction core complex with a trapped DEAD-box ATPase bound to RNA. *Science*, **313**, 1968–1972.

60. Moeller,von,H., Basquin,C. and Conti,E. (2009) The mRNA export protein DBP5 binds RNA and the cytoplasmic nucleoporin NUP214 in a mutually exclusive manner. *Nat Struct Mol Biol*, **16**, 247-254.

61. Halbach,F., Rode,M. and Conti,E. (2012) The crystal structure of S. cerevisiae Ski2, a DExH helicase associated with the cytoplasmic functions of the exosome. *RNA*, **18**, 124–134.

62. Kramer,K., Hummel,P., Hsiao,H., Luo,X., Wahl,M. and Urlaub,H. (2011) Mass-spectrometric analysis of proteins cross-linked to 4-thio-uracil- and 5-bromo-uracil-substituted RNA. *Int J Mass Spectrometry*, **304**, 184–194.

63. Kessner, D., Chambers, M., Burke, R., Agus, D. & Mallick, P. (2008) ProteoWizard: open source software for rapid proteomics tools development. *Bioinformatics* **24**, 2534–2536.

64. Sturm,M., Bertsch,A., Gropl,C., Hidebrandt,A., Hussong,R., Lange,E., Pfeifer,N., Shulz-Trieglaff,O., Zerck,A., Reinert,K. and Kohlbacher O. (2011) . OpenMS - an open-source software framework for mass spectrometry. *BMC Bioinformatics* **9**, 163.

65. Bertsch,A., Gröpl,C., Reinert,K. and Kohlbacher,O. OpenMS and TOPP: open source software for LC-MS data analysis. *Methods Mol Biol* **696**, 353–367 (2011).

66. Geer, L.Y., Merkey,S.P., Kowalak, J.A., Wagner,L, Xu,M., Maynard,D.M., Yang,X., Shi,W. and Bryant,S.H. (2004) Open mass spectrometry search algorithm. *J Proteome Res* **3**, 958–964.

3.2 Architecture of the Lsm1-7-Pat1 complex

In this section, the research article published in the journal Cell Reports (Volume 5, Issue 2, Pages 283-291, published on October 31, 2013) is presented as it was published. In addition to the main text, supplementary data is also attached.

Cell Reports
Report

Architecture of the Lsm1-7-Pat1 Complex: A Conserved Assembly in Eukaryotic mRNA Turnover

Humayun Sharif[1] and Elena Conti[1,*]
[1]Department of Structural Cell Biology, Max Planck Institute of Biochemistry, Am Klopferspitz 18, 82152 Martinsried, Germany
*Correspondence: conti@biochem.mpg.de
http://dx.doi.org/10.1016/j.celrep.2013.10.004

SUMMARY

The decay of mRNAs is a key step in eukaryotic gene expression. The cytoplasmic Lsm1-7-Pat1 complex is a conserved component of the 5′-to-3′ mRNA decay pathway, linking deadenylation to decapping. Lsm1-7 is similar to the nuclear Sm complexes that bind oligo-uridine tracts in snRNAs. The 2.3 Å resolution structure of *S. cerevisiae* Lsm1-7 shows the presence of a heptameric ring with Lsm1-2-3-6-5-7-4 topology. A distinct structural feature of the cytoplasmic Lsm ring is the C-terminal extension of Lsm1, which plugs the exit site of the central channel and approaches the RNA binding pockets. The 3.7 Å resolution structure of Lsm1-7 bound to the C-terminal domain of Pat1 reveals that Pat1 recognition is not mediated by the distinguishing cytoplasmic subunit, Lsm1, but by Lsm2 and Lsm3. These results show how the auxiliary domains and the canonical Sm folds of the Lsm1-7 complex are organized in order to mediate and modulate macromolecular interactions.

INTRODUCTION

RNA degradation modulates the steady-state levels of cellular transcripts and has emerged as a powerful mechanism for altering the abundance of proteins in response to changes in physiological conditions (reviewed in Schoenberg and Maquat, 2012). In eukaryotes, cytoplasmic mRNA turnover generally starts with the shortening of the poly(A) tail at the 3′ end of the message (reviewed in Chen and Shyu, 2011). The short stretch of adenosines that is left by the action of the deadenylases (Ccr4-Not and Pan2-Pan3) is the foothold for initiating two alternative decay pathways: the degradation of the RNA body in the 3′-to-5′ direction (via the exosome-Ski complex) or the removal of the 5′ cap structure and degradation in the 5′-to-3′ direction (via the decapping factors and Xrn1) (reviewed in Garneau et al., 2007). Genetic, biochemical, and structural data have shown that the core enzymes and regulators in mRNA turnover are evolutionarily conserved and have revealed the presence of intricate interaction networks (see the reviews above).

The conserved Lsm1-7-Pat1 complex plays an important role in coupling deadenylation and decapping in the 5′-to-3′ decay pathway (Bouveret et al., 2000; Tharun et al., 2000, Tharun, 2009; Haas et al., 2010; Ozgur et al., 2010; Totaro et al., 2011). Lsm1-7-Pat1 preferentially associates with the 3′ end of oligoadenylated mRNAs in vivo (Tharun et al., 2000; Tharun and Parker, 2001), protecting the last 20–30 nucleotides of the message (He and Parker, 2001). Lsm1-7-Pat1 subunits are required for normal rates of decapping in vivo (Bouveret et al., 2000; Tharun et al., 2000) and colocalize to discrete cytoplasmic foci known as P bodies along with all other 5′-to-3′ decay factors (Tharun et al., 2000; Pilkington and Parker, 2008; Haas et al., 2010; Ozgur et al., 2010). Lsm1-7 is composed of seven Sm-like proteins (numbered 1–7) and is related to the nuclear Sm complexes involved in binding small nuclear RNAs (snRNAs) (reviewed in Wilusz and Wilusz, 2005). Pat1 is a multifunctional protein. It binds the decapping complex Dcp1-Dcp2 (Pilkington and Parker, 2008; Braun et al., 2010; Nissan et al., 2010; Ozgur et al., 2010) as well as another decapping activator, Dhh1 (DDX6) (Braun et al., 2010; Haas et al., 2010; Nissan et al., 2010; Ozgur et al., 2010; Sharif et al., 2013). Pat1 has also been shown to interact with the Xrn1 exoribonuclease in yeast (Bouveret et al., 2000; Nissan et al., 2010) and with the Ccr4-Not deadenylase in *Drosophila* (Haas et al., 2010). Although many of these interactions are likely to be transient, the association of Pat1 with Lsm1-7 is sufficiently stable to allow the purification of the endogenous octameric complex from yeast (Bouveret et al., 2000; Chowdhury et al., 2007). In vitro, Lsm1-7-Pat1 binds directly polyuridine oligonucleotides with enhanced affinity when flanked by a short oligo-adenosine tail (Chowdhury et al., 2007). In yeast, Lsm1-7-Pat1 preferentially binds short oligo-uridine stretches located close to the 3′ end of endogenous mRNAs (Chowdhury et al., 2007; Mitchell et al., 2013).

Sm folds are uridine-specific RNA binding domains (Achsel et al., 2001). Structural studies have revealed how nuclear Sm complexes assemble into heteroheptameric rings around specific U-rich sequences of the U1 and U4 snRNAs (Pomeranz Krummel et al., 2009; Weber et al., 2010; Leung et al., 2011). In contrast to the spliceosomal Sm proteins, the two canonical Lsm complexes (Lsm1-7 and Lsm2-8) form rings spontaneously in the absence of RNA (Achsel et al., 1999; Salgado-Garrido et al., 1999). The cytoplasmic Lsm1-7 and the nuclear Lsm2-8 complexes share six of their seven subunits (reviewed in Wilusz and Wilusz, 2005). The distinguishing cytoplasmic subunit Lsm1 harbors critical determinants for the RNA binding properties of the complex not only in the canonical Sm domain but also in the distinctive C-terminal domain (Tharun et al.,

Cell PRESS
Open ACCESS

A

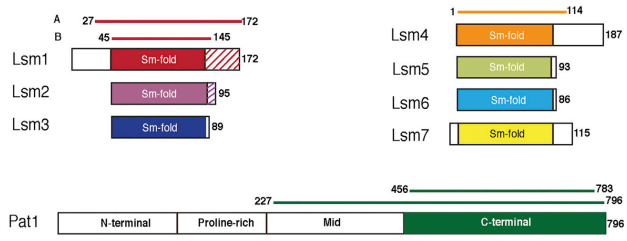

Figure 1. Structural Analysis of Lsm1-7 and Lsm1-7-Pat1 Complexes

(A) A schematic representation of the domain arrangements of the yeast Lsm1-7 and Pat1 proteins. Color-filled rectangles highlight the Sm folds of the Lsm proteins and the folded domain of Pat1. Dashed rectangles highlight the C-terminal extensions of Lsm1 and Lsm2. The residue numbers indicate the constructs used in this study.

(B) A table with data collection and refinement statistics. Values for the highest-resolution shell are given in parenthesis. Structure validation was carried out with Molprobity (Chen et al., 2010).

B

Dataset	**Lsm1-7$_A$**	**Lsm1$_B$-7-Pat1$_C$**
Space group	$P2_1$	$P6_3$
Cell dimensions		
a , *b*, *c* (Å)	61.80, 90.57, 68.46	258.69, 258.69, 47.10
α , β, γ (°)	90.0, 100.8, 90.0	90.0, 90.0, 120.0
Data Collection		
Wavelength (Å)	0.9980	0.8729
Resolution (Å)	90.53-2.30 (2.42-2.30)	84.68-3.70 (3.90-3.70)
R_{merge}	4.9 (41.2)	7.0 (68.9)
$I / \sigma I$	13.5 (3.1)	11.3 (1.4)
Completeness	99.3 (96.5)	99.4 (97.6)
Multiplicity	2.1 (2.0)	1.8 (1.6)
Refinement		
Resolution (Å)	53.99 (2.3)	43.40 (3.70)
No. of unique reflections	62641	36400
R_{work} / R_{free} (%)	21.1 / 25.8	24.9 / 29.5
B-factors	45.5	129.3
No. of atoms		
Proteins	4889	6277
Water	108	
Stereochemistry		
R.m.s.d. bond lengths (Å)	0.0080	0.0060
R.m.s.d. bond angles (°)	1.223	1.533
Ramachandran favored (%)	98.38	94.51
Ramachandran outliers (%)	0.00	0.24

2005; Chowdhury and Tharun, 2008; Chowdhury et al., 2012). The expectation is that Lsm1 might also specify other cytoplasmic-specific interactions. In this work, we address how the Sm folds and the distinct auxiliary domains of Lsm1-7 are structured and how they mediate the interaction with Pat1.

RESULTS AND DISCUSSION

Reconstitution of a Recombinant Lsm1-7-Pat1 Core Complex

The Lsm1–Lsm7 proteins contain a central Sm-like domain flanked by N-terminal and C-terminal extensions (Figure 1A). The Lsm1-7 complex is expected to be formed by hetero-oligomeric building blocks similar to those of the nuclear Sm complex, and Lsm2-3 corresponds to SmD1-D2, Lsm6-5-7 to SmF-E-G, and Lsm4-1 to SmD3/B (Kambach et al., 1999; Raker et al., 1999; Salgado-Garrido et al., 1999; Bouveret et al., 2000; Zaric et al., 2005; Mund et al., 2011). We obtained recombinant *S. cerevisiae* Lsm2-3 and Lsm5-6-7 from coexpression constructs (a gift of K. Nagai and Y. Kondo). *S. cerevisiae* Lsm1 and Lsm4 were expressed individually. In the latter case, the polypeptide (residues 1–114, hereby referred to as Lsm4) lacked the long Q- and N-rich C-terminal extension (Figure 1A). This region of Lsm4 is proteolytically sensitive in vitro (K. Nagai and Y. Kondo, personal communication) and is not required for normal mRNA decay rates in vivo (Decker et al., 2007). Reconstitution of the Lsm1-7 complex included a mild denaturing step (Zaric et al., 2005) that most likely overcomes the tendency of these proteins to oligomerize unspecifically when at high concentrations in vitro.

S. cerevisiae Pat1 (796 residues) is a multidomain protein with N-terminal, proline-rich, Mid, and C-terminal domains (Figure 1A) (Haas et al., 2010; Nissan et al., 2010). The C-terminal domain is required and sufficient to bind Lsm1-7 in both yeast (Nissan et al., 2010) and humans (Braun et al., 2010). The Mid domain has also been shown to contribute to Lsm1-7 binding (Pilkington and Parker, 2008; Braun et al., 2010) and, in the case of the *Drosophila* ortholog, provides a major interaction site (Haas et al., 2010). We expressed and purified a portion of *S. cerevisiae* Pat1 including both the Mid and C-terminal domains (residues 220–796), formed a complex with the reconstituted Lsm1-7, and subjected the octameric assembly to limited proteolysis (Figure S1A). Treatment with the protease elastase resulted in the accumulation of truncated Pat1 and

Lsm1 proteins, whereas all other subunits of the complex remained stable (Figure S1A). N-terminal sequencing and mass spectrometry analysis mapped the proteolytic fragment of Pat1 to the C-terminal domain (residues 450–796, hereby referred to as $Pat1_C$). Full-length Lsm1 (172 residues) was proteolyzed into different fragments that started at residues 27 or 45 and ended at residues 145 or 159. Previous studies have shown that the N-terminal extension of Lsm1 is functionally dispensable in yeast (Tharun et al., 2005). In contrast, the conserved C-terminal extension (also known as C-terminal domain or CTD) is required for RNA binding in vitro and for Lsm1 function in vivo (Tharun et al., 2005; Chowdhury et al., 2012). Therefore, we engineered a construct of Lsm1 containing residues 27–172 (referred to as $Lsm1_A$) and purified the corresponding $Lsm1_A$-7 and $Lsm1_A$-7-$Pat1_C$ complexes for structural analysis.

Lsm1-7 Is an Sm-like Heptameric Ring

We obtained crystals of yeast $Lsm1_A$-7 diffracting at 2.3 Å resolution and solved the structure by molecular replacement with the coordinates of known Sm-like rings (Leung et al., 2011; Mund et al., 2011). The final model is refined to an R_{free} of 25.8% and an R_{work} of 21.1% with good stereochemistry (Figures 1B and S1B). The model includes most of the polypeptide chains (see the Supplemental Information) and, in addition, includes ten residues of the tag engineered in Lsm2 for purification purposes (Figure 2A). Each of the seven Lsm proteins contains the characteristic Sm fold, a β barrel of five antiparallel and highly bent β strands with an N-terminal α helix (helix α1) on top. The seven Sm domains pack side by side in a ring-like architecture with a flat surface on top (the so-called proximal face, where the α helix is positioned) and the so-called tapered or distal surface at the bottom (Figure 2A). The overall oligomeric structure of the Lsm1-7 ring is generally similar to that of the nuclear U4 snRNP core (Leung et al., 2011). The oligomerization is based on the same repeating principle, namely the β4 strand of one subunit packing against the β5 strand of the neighboring subunit (Figure 2A, left). This results in an intermolecular β sheet that scaffolds the ring via extensive hydrophobic contacts.

The order of the subunits in the ring is Lsm1-2-3-6-5-7-4, as predicted previously (Kambach et al., 1999; Raker et al., 1999; Salgado-Garrido et al., 1999; Bouveret et al., 2000; Zaric et al., 2005; Mund et al., 2011) (Figure 2A, left). Specificity in the hetero-oligomerization is dictated by subunit-specific interactions, typically electrostatic contacts along the outer and inner circumferences of the ring. Several conserved electrostatic pairs are observed within the Lsm2-3 and Lsm6-5-7 building blocks (for example, $Glu18^{Lsm2}$-$Arg61^{Lsm3}$, $Asp22^{Lsm2}$-$Arg24^{Lsm3}$, and $Glu29^{Lsm5}$-$Arg87^{Lsm7}$) (Figures 2B and S2). In addition, conserved electrostatic pairs also occur between building blocks (for example, $Lys19^{Lsm3}$-$Glu54^{Lsm6}$, $Lys41^{Lsm7}$-$Glu23^{Lsm4}$, and $Arg62^{Lsm1}$-$Glu48^{Lsm4}$) (Figures 2B and S2) and most likely contribute to the ability of the Lsm subunits to assemble in a preformed ring without the need of an RNA molecule to nucleate hetero-oligomerization (Achsel et al., 1999; Salgado-Garrido et al., 1999). We note that the corresponding Sm building blocks lack some of the charged pairs at the equivalent positions, suggesting why mixed assemblies of Sm and Lsm proteins might not be favored.

The Lsm1-7 Ring Is Complemented by the Distinct C-Terminal Extensions of Lsm1 and Lsm2

The Lsm1-7 ring has distinct structural features in comparison to known Sm rings. First, the C-terminal extension of Lsm2 (residues 72–94) forms a short α helix (α2) that lies on the proximal face of the ring between the α1 helices of Lsm2 and Lsm3 (Figure 2A, right). The second and most striking feature is the C-terminal extension of Lsm1 (residues 115–172). This domain starts at the proximal face of the ring, wraps around the outer surface of the Lsm1 β barrel with a short α helix (α2), and reaches the distal face (Figure 2A, right). Here, it forms a long α helix (α3) that traverses the diameter of the ring, interacting with Lsm1 and Lsm4 on one side and with Lsm3 and Lsm6 on the other (Figure 2A, left). Then, the polypeptide makes a sharp bend (at the conserved Gly162) and stretches in an antiparallel fashion on top of helix α3 (Figure 3, left). Several evolutionarily conserved interactions hook the very C terminus of Lsm1 inside the ring; $Tyr172^{Lsm1}$ fits in a pocket created between Lsm1 and Lsm4, whereas $Asp170^{Lsm1}$ interacts electrostatically with $Arg59^{Lsm1}$. The extensive interactions we observe in the structure rationalize why the C-terminal extension of Lsm1 is able to function even when in trans (Chowdhury et al., 2012).

Deletion of the C-terminal extension of Lsm1 has been shown to decrease the RNA binding affinity of the complex but not to prevent the specific recognition of U tracts (Chowdhury et al., 2012). Superposition of the $Lsm1_A$-7 structure with that of the U4 snRNP core (Leung et al., 2011) allowed us to examine the putative RNA binding path (Figure 3). In the nuclear Sm complex, RNA binds at the consecutive uridine binding pockets that line the inner circumference of the ring and then threads through the entire central channel to exit with the 3′ end at the distal surface (Leung et al., 2011) (Figure 3, right). The uridine-binding pockets are created by the so-called Sm1 and Sm2 sequence motifs and are also present in Lsm1-7 (Figure 2B). Therefore, the Lsm proteins are expected to engage U bases with stacking and hydrogen-bonding interactions similar to those observed in the nuclear Sm complex (Leung et al., 2011). In contrast, RNA cannot exit the Lsm1-7 ring with the same path observed in the U4 snRNP structure because it would clash against the C-terminal extension of Lsm1 (Figures 3 and S3). It is possible that, although it poses considerable steric hindrance at the exit site of the channel, the Lsm1 extension might still allow the RNA 3′ end to thread through a narrow hole leading to the distal face of the ring. However, it is also possible that the C-terminal extension prevents the RNA from threading through the entire channel. In this case, we note that the unhindered part of the channel would be able to fit two to three additional nucleotides after the last uridine expected from the U4 snRNP structure (U836) (Figure 3).

The Pat1 C-Terminal Domain Protrudes on the Side of the Lsm1-7 Ring

Next, we addressed how Lsm1-7 binds Pat1. The $Lsm1_A$-7-$Pat1_C$ complex yielded diffracting crystals, but we found that only $Lsm1_A$-7 was present in the asymmetric unit. Inspection of the lattice suggested the presence of a possibly unfavorable crystal contact involving the C-terminal extension of Lsm1. Given that the Lsm1 C-terminal extension is not required for

Cell PRESS
Open ACCESS

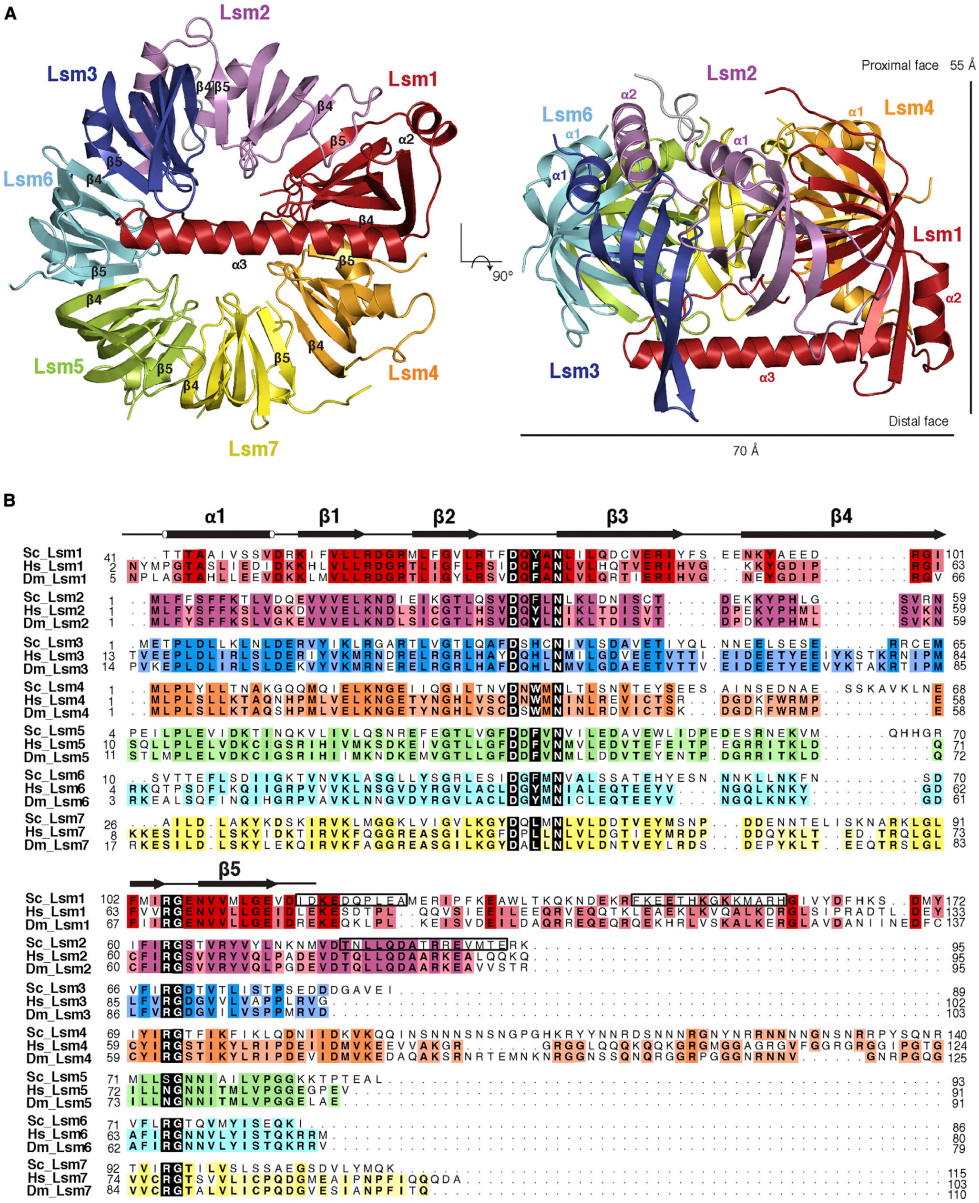

(legend on next page)

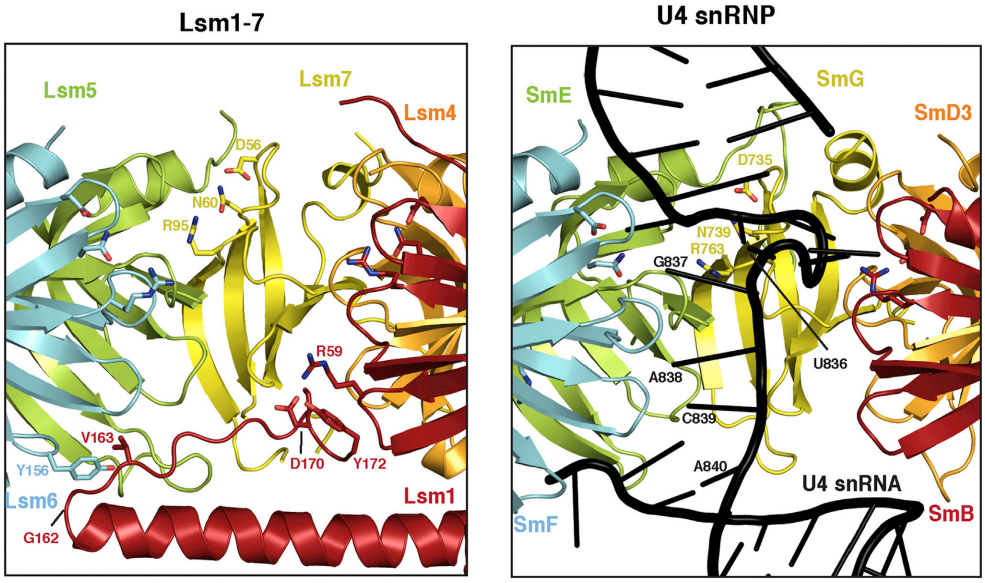

Figure 3. The C-Terminal Extension of Lsm1 Obstructs the RNA Exit Site

The C-terminal extension of Lsm1 binds in the central channel. On the left, a zoom-in of the $Lsm1_A$-7 structure is shown in the same orientation as in the left panel of Figure 2A. On the right is the corresponding zoom-in view of the U4 snRNP core structure (Leung et al., 2011) after optimal superposition of the Sm subunits, and RNA is shown in black. The Asp and Asn residues of the Sm1 motif and the Arg residue of the Sm2 motif indicate the position of the uridine-binding pocket of Lsm7 (left) and SmG (right). Lsm2-3 and SmD1-D2 have been removed for clarity. The Lsm1 C-terminal extension is 12–15 Å away from the corresponding position of U836 in the U4 snRNP structure and would clash against a nucleotide at the corresponding position of A840.

the assembly of the Lsm ring or Pat1 binding (Chowdhury et al., 2012), we generated an Lsm1 construct encompassing residues 45–145 (referred to as $Lsm1_B$), which corresponds to its smallest proteolytic fragment (Figure S1A). The $Lsm1_B$-7-$Pat1_C$ complex yielded crystals diffracting to 3.7 Å resolution. We solved the structure by molecular replacement using $Lsm1_A$-7 and a homology model of $Pat1_C$ based on the crystal structure of the human ortholog previously crystallized in isolation (Braun et al., 2010). The structure is refined to an R_{free} of 29.5% and an R_{work} of 24.9% with good stereochemistry (Figures 1B and S1B). The final model includes essentially all the residues of $Lsm1_B$-7 and residues 471–783 of Pat1.

S. cerevisiae $Pat1_C$ is an elongated domain formed by helical hairpins related to the ARM repeat and HEAT repeat family of proteins (Figures 4A and S4A). Each hairpin is composed of two antiparallel α helices (termed A and B) connected by loops or additional helical segments (Andrade et al., 2001). The hairpins pack side by side with a right-handed twist, forming a superhelix with a layer of six A helices on one side and a layer of five B helices on the other. However, the hairpins of Pat_C are rather irregular in both length and curvature. A comparison of the structure of yeast $Pat1_C$ with that of the human ortholog (Braun et al., 2010) shows that the first four hairpins are very similar, whereas the last two differ substantially in the position and orientation of the individual helices (Figure S4B). The $Pat1_C$ superhelix binds with the N-terminal repeats to the outer surface of Lsm1-7 and projects into solvent, the last hairpin being positioned more than 40 Å away from Lsm1-7 (Figure 4A).

Figure 2. Canonical and Idiosyncratic Features of the Lsm1-7 Ring

(A) The crystal structure of *S. cerevisiae* $Lsm1_A$-7 is shown in two orientations related by a 90° rotation around a horizontal axis. In the left panel, the complex is viewed on the distal face. The β4 and β5 strands of each subunit are labeled. The right panel is a side view of the complex. The N-terminal helices (α1 and α2) in the C-terminal extension of Lsm2 are labeled as well as the helices in the C-terminal extension of Lsm1 (α2 and α3). The additional residues of the Lsm2 tag are highlighted in gray in the right panel.

(B) Structure-based sequence alignment of Lsm1-7 orthologs from *S. cerevisiae* (Sc), *H. sapiens* (Hs), and *D. melanogaster* (Dm). Conserved residues are in colored boxes. In black are the central residues of the Sm1 motif (the D-x-Φ-x-N sequence, Φ being a hydrophobic residue) and the Sm2 motif (the R-G sequence). The canonical secondary structures of the Sm cores are above the sequences. The additional helices in the extensions of Lsm1 and Lsm2 are boxed around the corresponding sequences.

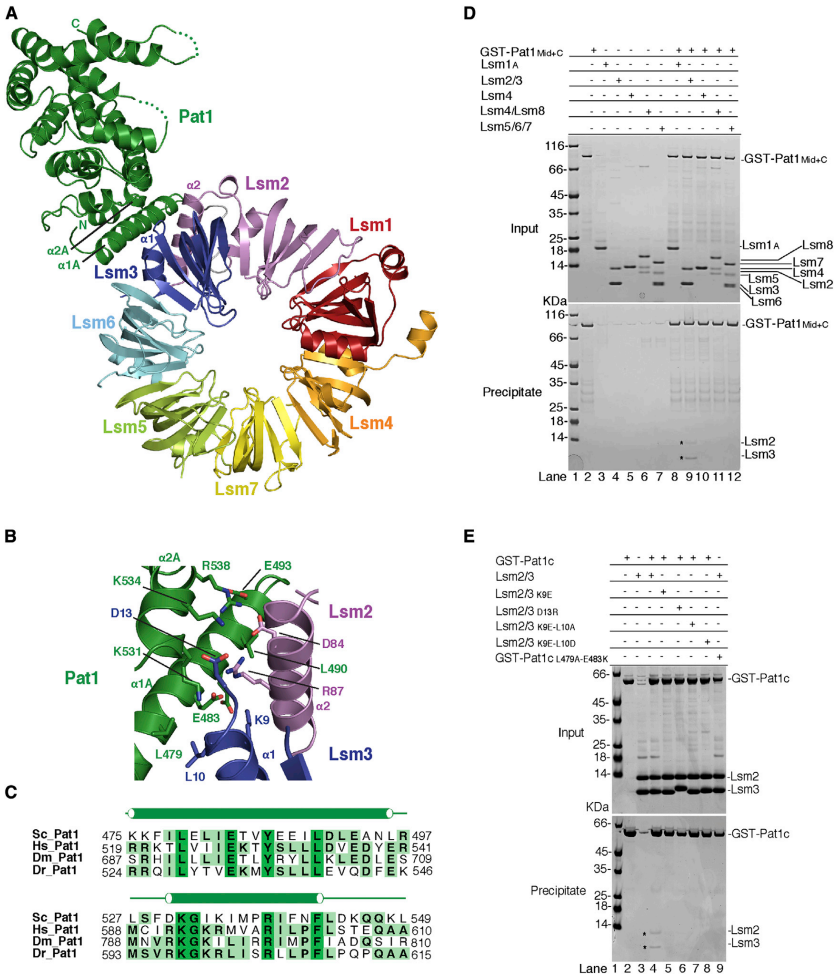

Figure 4. Pat1$_C$ Binds the Lsm1-7 Ring at Lsm2 and Lsm3

(A) Structure of Lsm1$_B$-7-Pat1$_C$ viewed with the ring in the same orientation and colors as in Figure 2A, left. Pat1 is shown in green, and the interacting helices of the HEAT-repeat-like superhelix is indicated.

(B) A zoom-in view of the interaction interface between Pat1, Lsm2, and Lsm3 with conserved interacting residues highlighted and indicated.

(C) Evolutionary conservation of the Lsm2-3 binding region of Pat1$_C$ (helices 1A and 2A).

(D) Pull-down experiments of GST-tagged Pat1 residues (Mid + C-terminal domains) with untagged Lsm2-3, Lsm5-6-7, Lsm4, and Lsm1. Input samples (top) and samples precipitated on glutathione-agarose beads (bottom) were analyzed on 4%–12% Bis-Tris NuPage gel with 2-(N-morpholino)ethanesulfonic acid running buffer. The proteins corresponding to the bands are indicated on the right side of both panels. Asterisks indicate the precipitated bands.

(E) Pull-down experiments of GST-tagged Lsm2-3 (WT and mutants) with WT Pat1$_C$ and of GST-tagged Pat1$_C$ WT and mutants with WT Lsm2-3. The experiments were carried out and are shown as described in (C).

Conserved Interactions of Pat1 with Lsm2 and Lsm3

$Pat1_C$ binds Lsm1-7 at the Lsm2 and Lsm3 subunits (Figure 4A). Helices 1A and 2A of $Pat1_C$ dock onto the C-terminal extension of Lsm2 (helix α2) and onto the canonical helix of the Lsm3 core (α1) (Figure 4B). A comparison of the yeast $Lsm1_B$-7-$Pat1_C$ structure with that of human $Pat1_C$ and of yeast $Lsm1_A$-7 in isolation shows that the interacting regions do not undergo significant conformational changes upon binding. Pat1, Lsm2, and Lsm3 are involved in an intricate set of electrostatic interactions. $Glu483^{Pat1}$ interacts with $Arg87^{Lsm2}$ and $Lys9^{Lsm3}$. Salt bridges also occur between $Arg538^{Pat1}$-$Asp84^{Lsm2}$ and $Lys534^{Pat1}$-$Asp13^{Lsm3}$. In addition, hydrophobic contacts engage $Leu479^{Pat1}$, $Tyr486^{Pat1}$, and $Leu490^{Pat1}$ with $Arg87^{Lsm2}$ and $Leu10^{Lsm3}$. All these residues are evolutionarily conserved (Figures 2B and 4C), suggesting that the metazoan orthologs share a similar recognition mechanism. Indeed, substitution of some of the equivalent residues in quadruple mutations of human Pat1 have been shown to impair Lsm1 binding in coimmunoprecipitation assays (Braun et al., 2010).

The structural analysis predicts that the Lsm2-Lsm3 subcomplex is sufficient for $Pat1_C$ binding. We tested this hypothesis in GST pull-down assays. A GST-Pat1 polypeptide encompassing both the Mid and C-terminal domains was indeed able to precipitate Lsm2-3 and not Lsm1, Lsm4, or Lsm5-6-7 (Figure 4D). Next, we engineered specific mutations. Consistent with the structure, GST-$Pat1_C$ was unable to precipitate Lsm2-3 upon mutation of Lsm2 Lys9Glu, Leu10Asp. Furthermore, mutation of Leu479Ala, Glu483Lys in GST-$Pat1_C$ impaired the interaction with wild-type (WT) Lsm2-3 (Figure 4E). The structural analysis also suggests a possible mechanism for the recognition of the Mid domain of Pat1. In both Lsm1-7 structures, part of the tag of Lsm2 is well ordered and wedges between the α1 and α2 helices of Lsm2 (Figures 2A, 4A, and S1B). The Asn-Leu-Tyr-Phe-Gln sequence of the tag interacts with evolutionarily conserved residues of Lsm2 (Leu2, Lys8, and Thr9 on α1 and Leu82 and Ala85 on α2). Interestingly, the Mid domain of Pat1 contains a similar stretch of amino acids (Asp-Phe-Tyr-Phe-Gln, residues 304–308 in *S. cerevisiae* Pat1) that are highly conserved and embedded in a predicted unstructured region, both of which are typical features of short linear motifs (Davey et al., 2012). Thus, it is possible that the tag serendipitously mimics a short linear motif in the Mid domain of Pat1.

Concluding Remarks

The Lsm1-7 complex contains an Sm ring with auxiliary structural features. The C-terminal extension that is characteristic of Lsm1 partially occupies the internal channel of the Sm-like ring. This extension approaches the RNA binding pockets of Lsm1-7, providing a rationale for the observation that it enhances the RNA binding properties of the core (Chowdhury et al., 2012). However, the basis for the specific recognition of U tract RNAs presenting a short oligo-A tail is currently unclear and an important question for future studies. The C-terminal extension that is characteristic of Lsm2, and the canonical Sm domains of Lsm2-Lsm3 create preformed protein-protein interaction sites. The C-terminal domain of Pat1 binds a composite surface of Lsm2 and Lsm3 with a rather rigid recognition mechanism between folded domains. We speculate that the unstructured Mid domain of Pat1 (Braun et al., 2010) might flexibly dock to an adjacent pocket of Lsm2 and enhance binding affinity. Counterintuitively, the binding determinants for Pat1 are not provided by Lsm1, the subunit of the cytoplasmic Lsm1-7 complex that differs from the nuclear Lsm2-8 complex. This finding has several implications. First, the localization of these proteins to distinct subcellular compartments (Reijns et al., 2009) is likely to provide a key contribution to binding specificity. Second, the interaction surfaces of Lsm2-3 that we identified for the cytoplasmic Lsm1-7-Pat1 complex might also be involved in protein-protein recognition in the nucleus in the context of the nuclear Lsm2-8 complex. An interesting candidate for Lsm2-8 binding is the splicing factor Prp8, which appears to contain a sequence similar to the Lsm2-Lsm3 binding region of Pat1 (data not shown). Given that, in human cells, Pat1 is a shuttling protein with transient nuclear localization (Marnef et al., 2012), it is also possible that Pat1 itself might interact with Lsm2-8, rationalizing how Pat1 might exert its nuclear functions.

EXPERIMENTAL PROCEDURES

Protein Purification and Binding Assays

S. cerevisiae Lsm1-7 complexes were formed by mixing purified Lsm1, Lsm4, Lsm2-3, and Lsm5-6-7 in a 2:2:1:1 ratio and reconstituted essentially as described previously (Zaric et al., 2005). All Pat1 fragments were cloned as either TEV-cleavable His_6-ZZ-tagged or His_6-GST-tagged proteins and purified with standard procedures. The octameric complex was reconstituted by incubating the individually purified proteins in a 1:1.5 molar ratio of Lsm1-7 and Pat1 for 1 hr at 4°C. The complex was purified further by size-exclusion chromatography (Superdex 200) in a buffer containing 20 mM Tris (pH 7.4), 150 mM NaCl, and 1 mM dithiothreitol. For in vitro pull-down experiments, point mutations were introduced with QuikChange site-directed mutagenesis according to the manufacturer's instruction (Stratagene). Mutants were purified by similar protocol as for the WT Lsm1-7 and Lsm2-3. The pull-down assays were carried out as described previously (Sharif et al., 2013). Protocols are detailed in the Supplemental Information.

Crystal Structure Determination

$Lsm1_A$-7 and Lsm_B1-7-$Pat1_C$ yielded crystals (conditions are detailed in the Supplemental Information) that diffracted to 2.3 Å and 3.7 Å resolution, respectively, with Swiss Light Source and European Synchrotron Radiation Facility synchrotron radiation. Data were processed with XDS (Kabsch, 2010), and the structures were solved by molecular replacement with Phaser (McCoy et al., 2007). The atomic models were built with Coot (Emsley et al., 2010) and refined with PHENIX (Adams et al., 2010). The data collection and refinement statistics are summarized in Figure 1B.

ACCESSION NUMBERS

The coordinates and structure factors have been deposited in the Protein Data Bank under accession numbers 4C92 for $Lsm1_A$-7 and 4C8Q for $Lsm1_B$-7-$Pat1_C$.

SUPPLEMENTAL INFORMATION

Supplemental Information contains Supplemental Experimental Procedures and four figures and can be found with this article online at http://dx.doi.org/10.1016/j.celrep.2013.10.004.

ACKNOWLEDGMENTS

We are grateful to Kiyoshi Nagai and Yasushi Kondo at the Medical Research Council Laboratory of Molecular Biology (Cambridge, UK) for sharing their

yeast Lsm2-8 expression constructs and protocols. We thank the Max Planck Institute (MPI) Crystallization Facility for screenings and optimization, the MPI Core Facility for mass spectrometry and N-terminal sequencing, and the beamline scientists at the Swiss Light Source and European Synchrotron Radiation Facility for excellent assistance with data collection. We also thank Steffen Schüssler and Marc Baumgärtner for help with purification and the members of our lab for discussions and critical reading of the manuscript. This study was supported by the Max-Planck-Gesellschaft, the European Commission (ERC Advanced Investigator grant 294371 and Marie Curie ITN RNPnet), and the Deutsche Forschungsgemeinschaft (DFG SFB646, SFB1035, GRK1721, FOR1680, and CIPSM) to E.C.

Received: September 24, 2013
Revised: October 3, 2013
Accepted: October 3, 2013
Published: October 17, 2013

REFERENCES

Achsel, T., Brahms, H., Kastner, B., Bachi, A., Wilm, M., and Lührmann, R. (1999). A doughnut-shaped heteromer of human Sm-like proteins binds to the 3′-end of U6 snRNA, thereby facilitating U4/U6 duplex formation in vitro. EMBO J. *18*, 5789–5802.

Achsel, T., Stark, H., and Lührmann, R. (2001). The Sm domain is an ancient RNA-binding motif with oligo(U) specificity. Proc. Natl. Acad. Sci. USA *98*, 3685–3689.

Adams, P.D., Afonine, P.V., Bunkóczi, G., Chen, V.B., Davis, I.W., Echols, N., Headd, J.J., Hung, L.-W., Kapral, G.J., Grosse-Kunstleve, R.W., et al. (2010). PHENIX: a comprehensive Python-based system for macromolecular structure solution. Acta Crystallogr. D Biol. Crystallogr. *66*, 213–221.

Andrade, M.A., Petosa, C., O'Donoghue, S.I., Müller, C.W., and Bork, P. (2001). Comparison of ARM and HEAT protein repeats. J. Mol. Biol. *309*, 1–18.

Bouveret, E., Rigaut, G., Shevchenko, A., Wilm, M., and Séraphin, B. (2000). A Sm-like protein complex that participates in mRNA degradation. EMBO J. *19*, 1661–1671.

Braun, J.E., Tritschler, F., Haas, G., Igreja, C., Truffault, V., Weichenrieder, O., and Izaurralde, E. (2010). The C-terminal alpha-alpha superhelix of Pat is required for mRNA decapping in metazoa. EMBO J. *29*, 2368–2380.

Chen, C.-Y.A., and Shyu, A.-B. (2011). Mechanisms of deadenylation-dependent decay. Wiley Interdiscip Rev RNA *2*, 167–183.

Chen, V.B., Arendall, W.B., 3rd, Headd, J.J., Keedy, D.A., Immormino, R.M., Kapral, G.J., Murray, L.W., Richardson, J.S., and Richardson, D.C. (2010). MolProbity: all-atom structure validation for macromolecular crystallography. Acta Crystallogr. D Biol. Crystallogr. *66*, 12–21.

Chowdhury, A., and Tharun, S. (2008). lsm1 mutations impairing the ability of the Lsm1p-7p-Pat1p complex to preferentially bind to oligoadenylated RNA affect mRNA decay in vivo. RNA *14*, 2149–2158.

Chowdhury, A., Mukhopadhyay, J., and Tharun, S. (2007). The decapping activator Lsm1p-7p-Pat1p complex has the intrinsic ability to distinguish between oligoadenylated and polyadenylated RNAs. RNA *13*, 998–1016.

Chowdhury, A., Raju, K.K., Kalurupalle, S., and Tharun, S. (2012). Both Sm-domain and C-terminal extension of Lsm1 are important for the RNA-binding activity of the Lsm1-7-Pat1 complex. RNA *18*, 936–944.

Davey, N.E., Van Roey, K., Weatheritt, R.J., Toedt, G., Uyar, B., Altenberg, B., Budd, A., Diella, F., Dinkel, H., and Gibson, T.J. (2012). Attributes of short linear motifs. Mol. Biosyst. *8*, 268–281.

Decker, C.J., Teixeira, D., and Parker, R. (2007). Edc3p and a glutamine/asparagine-rich domain of Lsm4p function in processing body assembly in Saccharomyces cerevisiae. J. Cell Biol. *179*, 437–449.

Emsley, P., Lohkamp, B., Scott, W.G., and Cowtan, K. (2010). Features and development of Coot. Acta Crystallogr. D Biol. Crystallogr. *66*, 486–501.

Garneau, N.L., Wilusz, J., and Wilusz, C.J. (2007). The highways and byways of mRNA decay. Nat. Rev. Mol. Cell Biol. *8*, 113–126.

Haas, G., Braun, J.E., Igreja, C., Tritschler, F., Nishihara, T., and Izaurralde, E. (2010). HPat provides a link between deadenylation and decapping in metazoa. J. Cell Biol. *189*, 289–302.

He, W., and Parker, R. (2001). The yeast cytoplasmic LsmI/Pat1p complex protects mRNA 3′ termini from partial degradation. Genetics *158*, 1445–1455.

Kabsch, W. (2010). Integration, scaling, space-group assignment and post-refinement. Acta Crystallogr. D Biol. Crystallogr. *66*, 133–144.

Kambach, C., Walke, S., Young, R., Avis, J.M., de la Fortelle, E., Raker, V.A., Lührmann, R., Li, J., and Nagai, K. (1999). Crystal structures of two Sm protein complexes and their implications for the assembly of the spliceosomal snRNPs. Cell *96*, 375–387.

Leung, A.K.W., Nagai, K., and Li, J. (2011). Structure of the spliceosomal U4 snRNP core domain and its implication for snRNP biogenesis. Nature *473*, 536–539.

Marnef, A., Weil, D., and Standart, N. (2012). RNA-related nuclear functions of human Pat1b, the P-body mRNA decay factor. Mol. Biol. Cell *23*, 213–224.

McCoy, A.J., Grosse-Kunstleve, R.W., Adams, P.D., Winn, M.D., Storoni, L.C., and Read, R.J. (2007). Phaser crystallographic software. J. Appl. Cryst. *40*, 658–674.

Mitchell, S.F., Jain, S., She, M., and Parker, R. (2013). Global analysis of yeast mRNPs. Nat. Struct. Mol. Biol. *20*, 127–133.

Mund, M., Neu, A., Ullmann, J., Neu, U., and Sprangers, R. (2011). Structure of the LSm657 complex: an assembly intermediate of the LSm1-7 and LSm2-8 rings. J. Mol. Biol. *414*, 165–176.

Nissan, T., Rajyaguru, P., She, M., Song, H., and Parker, R. (2010). Decapping activators in Saccharomyces cerevisiae act by multiple mechanisms. Mol. Cell *39*, 773–783.

Ozgur, S., Chekulaeva, M., and Stoecklin, G. (2010). Human Pat1b connects deadenylation with mRNA decapping and controls the assembly of processing bodies. Mol. Cell. Biol. *30*, 4308–4323.

Pilkington, G.R., and Parker, R. (2008). Pat1 contains distinct functional domains that promote P-body assembly and activation of decapping. Mol. Cell. Biol. *28*, 1298–1312.

Pomeranz Krummel, D.A., Oubridge, C., Leung, A.K.W., Li, J., and Nagai, K. (2009). Crystal structure of human spliceosomal U1 snRNP at 5.5 A resolution. Nature *458*, 475–480.

Raker, V.A., Hartmuth, K., Kastner, B., and Lührmann, R. (1999). Spliceosomal U snRNP core assembly: Sm proteins assemble onto an Sm site RNA nonanucleotide in a specific and thermodynamically stable manner. Mol. Cell. Biol. *19*, 6554–6565.

Reijns, M.A.M., Auchynnikava, T., and Beggs, J.D. (2009). Analysis of Lsm1p and Lsm8p domains in the cellular localization of Lsm complexes in budding yeast. FEBS J. *276*, 3602–3617.

Salgado-Garrido, J., Bragado-Nilsson, E., Kandels-Lewis, S., and Séraphin, B. (1999). Sm and Sm-like proteins assemble in two related complexes of deep evolutionary origin. EMBO J. *18*, 3451–3462.

Schoenberg, D.R.D., and Maquat, L.E.L. (2012). Regulation of cytoplasmic mRNA decay. Nat. Rev. Genet. *13*, 246–259.

Sharif, H., Ozgur, S., Sharma, K., Basquin, C., Urlaub, H., and Conti, E. (2013). Structural analysis of the yeast Dhh1-Pat1 complex reveals how Dhh1 engages Pat1, Edc3 and RNA in mutually exclusive interactions. Nucleic Acids Res. *41*, 8377–8390.

Tharun, S. (2009). Lsm1-7-Pat1 complex: a link between 3′ and 5′-ends in mRNA decay? RNA Biol. *6*, 228–232.

Tharun, S., and Parker, R. (2001). Targeting an mRNA for decapping: displacement of translation factors and association of the Lsm1p-7p complex on deadenylated yeast mRNAs. Mol. Cell *8*, 1075–1083.

Tharun, S., He, W., Mayes, A.E., Lennertz, P., Beggs, J.D., and Parker, R. (2000). Yeast Sm-like proteins function in mRNA decapping and decay. Nature *404*, 515–518.

Tharun, S., Muhlrad, D., Chowdhury, A., and Parker, R. (2005). Mutations in the Saccharomyces cerevisiae LSM1 gene that affect mRNA decapping and 3′ end protection. Genetics *170*, 33–46.

Totaro, A., Renzi, F., La Fata, G., Mattioli, C., Raabe, M., Urlaub, H., and Achsel, T. (2011). The human Pat1b protein: a novel mRNA deadenylation factor identified by a new immunoprecipitation technique. Nucleic Acids Res. *39*, 635–647.

Weber, G., Trowitzsch, S., Kastner, B., Lührmann, R., and Wahl, M.C. (2010). Functional organization of the Sm core in the crystal structure of human U1 snRNP. EMBO J. *29*, 4172–4184.

Wilusz, C.J., and Wilusz, J. (2005). Eukaryotic Lsm proteins: lessons from bacteria. Nat. Struct. Mol. Biol. *12*, 1031–1036.

Zaric, B., Chami, M., Rémigy, H., Engel, A., Ballmer-Hofer, K., Winkler, F.K., and Kambach, C. (2005). Reconstitution of two recombinant LSm protein complexes reveals aspects of their architecture, assembly, and function. J. Biol. Chem. *280*, 16066–16075.

Architecture of the Lsm1-7 - Pat1 complex, a conserved assembly in eukaryotic mRNA turnover

Humayun Sharif[1] and Elena Conti[1]*

Max-Planck-Institute of Biochemistry, Department of Structural Cell Biology, Am Klopferspitz 18, D-82152 Martinsried/Munich, Germany

*To whom correspondence should be addressed

E-mail: conti@biochem.mpg.de

Supplemental data items

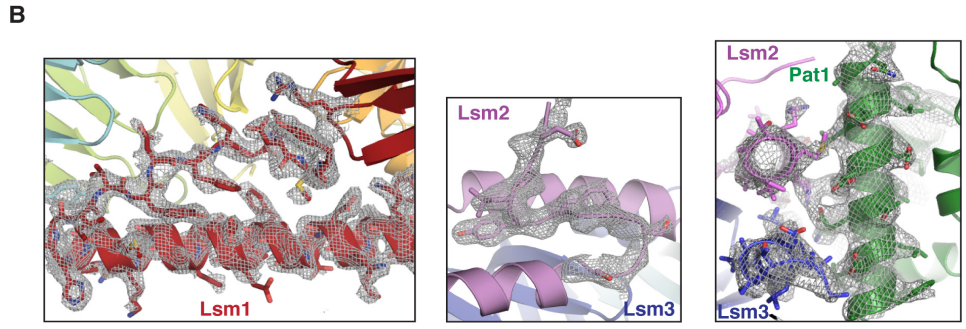

Figure S1, Related to Figure 1

Structural analysis of *S. cerevisiae* Lsm1-7 and Lsm1-7 - Pat1

A) Limited proteolysis experiment identifies the minimal interacting regions of *S. cerevisiae* Lsm1-7 and Pat1. A complex of Lsm1-7 (with all proteins full-length, with the exception of a C-terminal truncation of Lsm4, as described in the main text) was purified by size-exclusion chromatography with Pat1 residues 220-796 (including the Mid and C-terminal domains), and the peak was incubated with elastase (Roche) in a 1:10 (wt/wt) enzyme:protein ratio for 30 min at 4°C. The products of the proteolysis were resolved on 4–12% Bis–Tris NuPage gel with MES running buffer.
B) Electron densities (contoured at 1 sigma, with the final model superposed) for regions of the structures described in the text. Left panel: C-terminus of Lsm1 in the 2.3 Å resolution $Lsm1_A$-7 structure. Central panel: N-terminal tag of Lsm2 in the 2.3 Å resolution $Lsm1_A$-7 structure. Right panel: interacting region of Pat1, Lsm2 and Lsm3 in the 3.7 Å resolution $Lsm1_B$-7 - Pat1 structure.

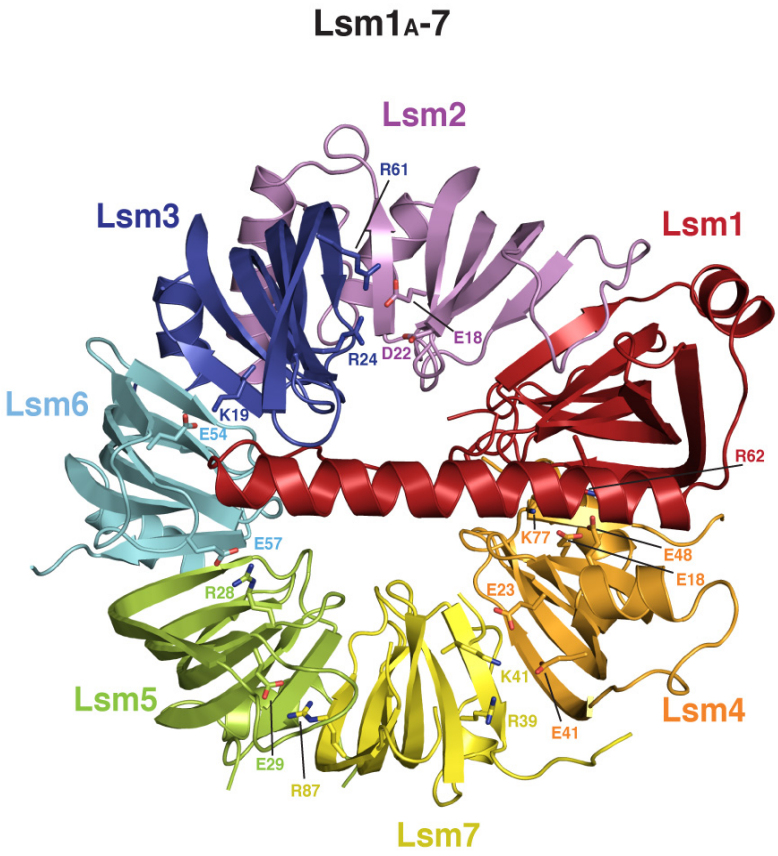

Figure S2, Related to Figure 2

Distinct inter-subunit contacts

The Lsm1-7 complex is viewed at the distal face, as in Figure 2A, left panel. Residues involved in specific intersubunit salt bridge interactions are highlighted. These interactions occur in addition to the largely hydrophobic contacts along the β-sheets of the Sm domains.

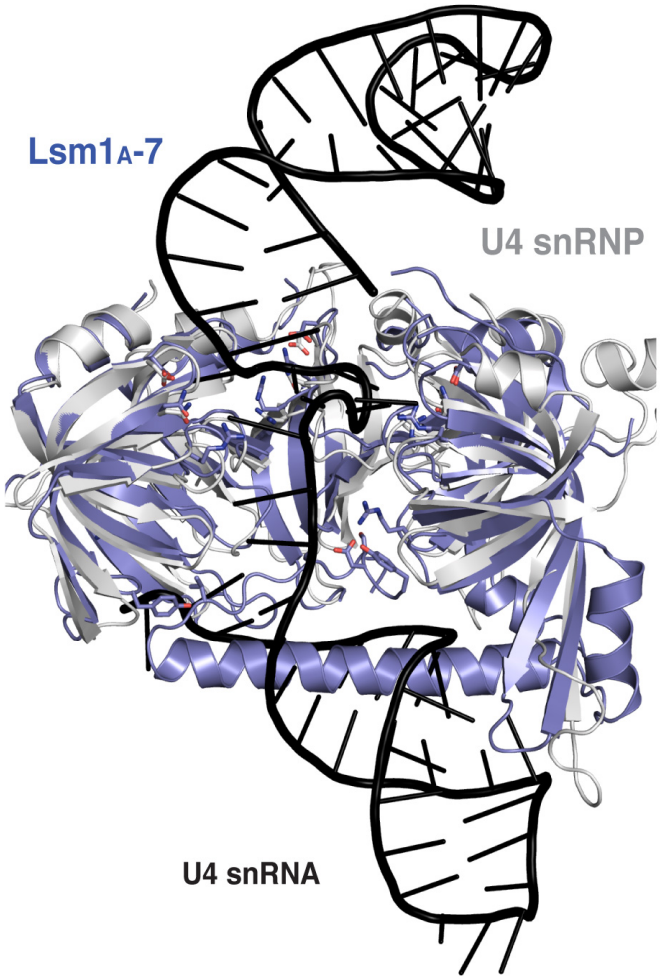

Figure S3, Related to Figure 3

Accessibility of the RNA entry site and obstruction of the RNA exit site in Lsm1-7

The superposition of the structures in Figure 3 right and left panels shows that the C-terminal extension of Lsm1 would clash against a ribonucleotide chain exiting the Sm ring with the same path observed in the U4 snRNP core (Leung et al., 2011). For clarity, $Lsm1_A$-7 structure is shown here in blue and U4 snRNP structure in gray.

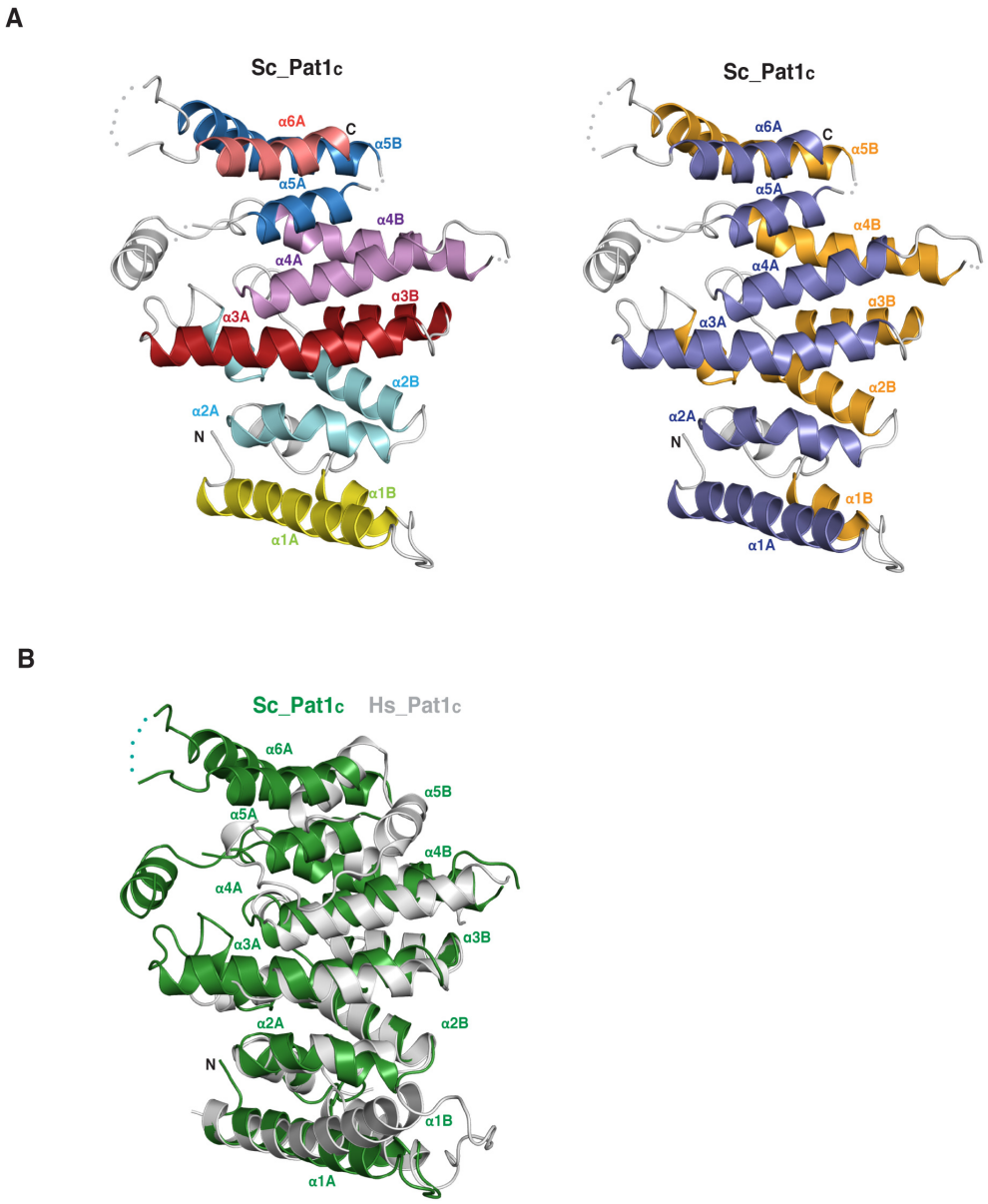

Figure S4, Related to Figure 4

The yeast Pat1$_C$ superhelix

A) Helical-hairpin architecture of *S. cerevisiae* Pat1$_C$. On the left, the structure is shown with each repeat in a different colour. On the right, the A helices of the repeats are in orange, the B helices in blue and the connecting regions in gray.

B) The structure of *S. cerevisiae* Patc1$_C$ is shown in green superposed to the corresponding structure of the human orthologue (in gray) (from (Braun et al., 2010)).

Supplemental text section

Supplemental Experiment Procedures

Protein expression and purification

S. cerevisiae Lsm1 constructs (full-length, residues 27-172 or residues 45-145) and Lsm4 (residues 1-114) were cloned as 3C-cleaveable His_6-tagged proteins and expressed in BL21-Gold (DE3) pLysS cells (Stratagene). Lsm2-3 and Lsm5-6-7 were expressed from polycistronic constructs as TEV cleavable His_6-tagged proteins (kind gift of K. Nagai and Y. Kondo) in Rosetta-gami2 (DE3) pLysS cells (Novagen). All proteins were expressed in Terrific Broth (TB) medium at 18°C. Cells expressing Lsm1, Lsm4, Lsm2-3 and Lsm5-6-7 were mixed in a ratio of 2:2:1:1, resuspended in lysis buffer (20 mM Tris pH 7.4, 500 mM NaCl, 25 mM Imidazole, 10 mM 2-Mercaptoethanol) and lysed by sonication. Proteins were purified using Nickel-based affinity chromatography. Eluted proteins were then treated in denaturing conditions at 4M Urea and 1M NaCl overnight at 4°C. On the next day proteins were incubated for 6 h at 37°C followed by gradual decrease of salt in the dialysis buffer at 4 °C for refolding and reconstitution of stoichiometric protein complex. Proteins were supplemented with TEV and 3C protease cocktail in final dialysis buffer (20 mM Tris pH 7.4, 150 mM NaCl, 10 mM 2-mercaptoethanol) for overnight at 4 °C. Proteins were further purified by ion exchange chromatography at pH 7.4 (MonoQ, GE Healthcare) followed by size-exclusion chromatography (Superdex 200, GE Healthcare).

$Pat1_{220-796}$ and $Pat1_{450-796}$ proteins (with a TEV-cleavable His_6-ZZ-tag or His_6-GST-tag) were expressed in BL21-Gold (DE3) pLysS cells (Stratagene) in TB medium at 18°C. Cells were resuspended in lysis buffer supplemented with DNase and Phenylmethylsulfonyl Fluoride (PMSF), lysed by sonifaction and subjected to Nickel affinity purification. Tags were cleaved (where necessary) overnight in dialysis buffer with TEV protease followed by ion exchange chromatography (Heparin, GE

healthcare) at pH 7.4 and size exclusion chromatography (Superdex 200, GE Healthcare).

Crystallization and structure determination

Crystallization trials were carried out at 18°C and 10°C using the vapour diffusion method by mixing equal volumes of protein complex and crystallization buffer. Crystals of Lsm_A1-7 were obtained at 10 °C at 9.3 mg/ml. The best diffracting crystals of $Lsm1_A$-7 complex were obtained in 100 mM MES pH 6.0, 40% MPD after 5-10 days. Crystals were flash-frozen in liquid nitrogen directly from the crystallization drop, which diffracted to 2.3 Å resolution. Crystals of Lsm_B1-7-$Pat1_C$ were obtained at 10 °C at a concentration of 13 mg/ml in 100 mM HEPES pH 7.0, 20% MPD, 10 mM hexamine cobalt (III) chloride in 3-4 weeks. The crystals were cryo protected by adding glycerol to crystal condition that diffracted to 3.7 Å resolution.

The $Lsm1_A$-7 structure was solved by molecular replacement with Phaser (McCoy et al., 2007) using the coordinates of Sm and Lsm proteins (Leung et al., 2011; Mund et al., 2011) as search models. The final model includes residues 43 - 172 of Lsm1, 1 - 95 of Lsm2 (and additionally 10 residues of the N-terminal tag), 1 - 79 of Lsm3, 1 - 84 of Lsm4, 4 - 87 of Lsm5, 10 - 86 of Lsm6 and 26 - 110 of Lsm7 (with the exception of a partially disordered loop between residues 72 - 81). The Lsm_B1-7-$Pat1_C$ structure was solved by molecular replacement with Lsm_A1-7 and the human Pat1 orthologue (Braun et al., 2010). The low resolution Lsm_B1-7-$Pat1_C$ structure was refined in addition with reference model restraints with a high-resolution reference model (Lsm_A1-7 at 2.3 Å resolution).

Pull-down assays

Pull downs were performed by mixing 3-5 µg of GST-tagged (bait) protein with equal molar amounts of untagged (prey) protein. Binding buffer (20 mM Tris-Cl pH 7.4, 150 mM NaCl, 10% glycerol, 1 mM DTT) was added to a final volume of 60 µl. The reaction mixtures were incubated on ice for 1 hour 17 µl of 50% (v/v) suspension of

GSH–Sepharose beads in 200 µl of binding buffer was added to each reaction mixture and incubated at 4 °C for 1 hour. Beads were washed three times with 500 µl binding buffer. Bound proteins were eluted with 20 mM reduced glutathione. Samples were resolved on SDS-PAGE and visualized by Coomassie blue stain.

4 Extended Discussion

Discussion on each of two studies is presented in Sections 3.1 and 3.2. This section deals with the extended combined discussion and elaborates on the points made earlier. First two sections deals with Dhh1, Pat1 and Edc3 interactions related discussion. Later sections deal with discussion on the Lsm1-7-Pat1 complex and a combined discussion on general mechanisms related to both Sections. In the end, a broader perspective of the projects is discussed.

4.1 Diversified functions of Dhh1 in mRNA decapping pathway

Despite the highly conserved helicase core of DEAD box proteins some of their features are highly specific (Linder and Jankowsky, 2011). The Dhh1 structure reveals similar conserved helicase core, which consists of two RecA domains but with unusual inter-domain interactions (Cheng et al., 2005; Dutta et al., 2011). DEAD box proteins hydrolyze ATP in a closed conformation triggered by RNA and ATP binding that brings the two RecA domains together to provide composite surface for interaction with RNA (Linder and Jankowsky, 2011). Inter-domain interactions restrict ATPase activity of Dhh1 which shows weaker activity when compared to canonical DEAD box proteins (Dutta et al., 2011). The weaker the ATPase activity of Dhh1 is hypothesized to be required for stringent regulation of this cytoplasmic abundant protein (Dutta et al., 2011). In Trypanosomes, Dhh1 copy number estimates to 400,000 copies per cell equals approximately six times molar excess of mRNAs (Kramer et al., 2010). This number exceeds for mammalian cells where the DDX6/Me31B is available in higher number if repressed mRNAs are taken into consideration (Ernoult-Lange et al., 2012). Due to the abundance of Dhh1, multiple copies of it can bind to mRNA. This multiple binding may suppress interaction of additional factors with mRNA for storage purposes in P-bodies or eventually for their decay (Ernoult-Lange et al., 2012).

High cellular abundance with nanomolar binding affinity for RNA and restricted ATPase activity come in perspective for high regulation during translation repression and decapping. DEAD box proteins can thus play a RNA binding-only role or as RNA clamping proteins (Dutta et al., 2011; Linder and Jankowsky, 2011). Dhh1 ATPase activity is not necessarily needed to bind RNA (Dutta et al., 2011). Domain movements of DEAD-box proteins can sometimes be achieved through binding a co-factor which would release it from an inactive state resulting in rotation of the domains, ATP hydrolysis and ultimately release of RNA (Dutta et al., 2011; Ernoult-Lange et al., 2012). Indeed recently, DDX6 interaction with CNOT1 protein (human ortholog of Not1 protein) in Ccr4-Not deadenylase complex, revealed how CNOT1 binding modulates the active conformation of DDX6 that stimulates its ATPase activity (Mathys et al., 2014).

4.2 Functions of small linear motifs in decapping protein-protein interactions

The decapping proteins interaction network contains many interactions that are mediated by small linear motifs present in intrinsically disordered regions of the proteins involved. Such regions are present in Pat1, Edc3, Scd6, Dcp1, Dcp2 and Xrn1 (Jonas and Izaurralde, 2013).

The small linear motifs (SLiMs) belong to a class of disordered regions prevalent in many decapping proteins and in several other pathways including cell-signaling networks and gene transcription (Davey et al., 2012; Jonas and Izaurralde, 2013; Tantos et al., 2012). SLiMs size range from three up to ten residues and this small size confers a relatively low binding affinity when making direct contact with the interacting partner (Davey et al., 2012). Additionally, they are complimented with flanking disordered regions having an additive effect on their binding affinities (Davey et al., 2012; Tompa, 2012). Moreover, SLiMs have higher conservation than their neighboring regions and tend to form secondary structures upon binding to their partners (Davey et al., 2012; Tompa, 2012).

SLiMs have been observed through biochemical/structural analysis combined with sequence analysis of Pat1 and Edc3 (Section 3.1). Pat1 and Edc3 contain the

FDF/DW motif implicated in binding to Dhh1/DDX6 (Section 3.1). Flanking FDF/DW motif, both proteins contain variable additional sites of interaction, which enhance their binding to Dhh1 (Dhh1 interaction surfaces, patch 2 and patch 3 involved in interaction with Edc3 and Pat1, explained in Section 3.1). Moreover, Edc3 FDF motif peptide is unstructured in solution and adopts a helical structure upon binding to Dhh1 (Tritschler et al., 2009). Furthermore, FDF motifs of both the proteins are recognized by the same surface on Dhh1 (Section 3.1). These observations explain the evolutionarily plastic nature of SLiMs and their transient interactions in decapping pathway.

4.3 Transient complex formation and mRNP remodeling during mRNA decay

Over the years, functional and structural snapshots of protein factors involved in mRNA decay provided the clues concerning this intricate mechanism. The assembly of decapping complex on the repressed mRNAs is a complicated mechanism that includes interactions of catalytic factors and decapping activators in a network of protein-protein and protein-RNA interactions. The transient nature of complex formation increases the level of complexity in elaborating the working model of decay. This can be explained by multiple mRNP remodeling steps during the degradation process.

The interactions may depend on sequence, binding preference as well as space and time (Moore, 2005). It can be argued that the interactions revise and rearrangements in mRNP take place during the decay. The proteins involved can have different function alone or when interacting with multiple partners. For example, Dhh1 directly interacts with mRNA and also functions in shuttling mRNAs to cytoplasmic foci (Dutta et al., 2011). Its interaction with Edc3 is necessary to repress the expression of mRNAs (Tritschler et al., 2009). Moreover, its interaction with Pat1 is required for the P-body formation and interaction with decapping enzyme Dcp2 at 5′-end of mRNAs (Ozgur and Stoecklin, 2013)

Similarly, Dhh1 interaction with multiple partners on the same binding surface adds complexity to the protein interaction network. The transient Dhh1 complex formation

triggered by proteins containing small linear motifs (SLiMs) may provide extra functionality for a limited time period until their interaction is not required. Structural and functional studies have shown that Dhh1 shares binding surface with RNA, Edc3, Scd6/Tral and Pat1, which give clues regarding its mutually exclusive binding to either of them (Haas et al., 2010; Ozgur et al., 2010). Switching partners also explains that Pat1 and Edc3 proteins in yeast have the capability to detach Dhh1 from interaction with RNA or vice versa. Alternatively, Dhh1, due to its abundance in the cytoplasm as compared to Pat1 and Lsm1-7, could exist in multiple interactions, in mRNA bound form, in complex with Edc3 and with Pat1 simultaneously (Section 3.1).

Certain mRNA features including AU-rich elements (AREs) and the status of the 3′-poly(A) or 5′ cap structure could guide these positional preferences (Mitchell et al., 2013). Moreover, presence of certain mRNA binding proteins at specific sequences could also guide positional specific recruitment. This site-specific recruitment has functional values as well and may regulate the protein functions during translational repression, deadenylation and decapping events (Mitchell et al., 2013).

4.4 Lessons learnt from the unusual C-terminal helix of Lsm1

The Lsm1-7 complex shows structural integrity in preserving hetero-heptameric assembly and Sm-folds in each subunit (Section 3.2). However, the most surprising finding by the structural analysis is the helical extension of Lsm1 C-terminus. It protrudes inside the channel made by heptameric complex. Structural comparison with U4 snRNP complex reveals that the helical C-terminal Lsm1 may obstruct the incoming 3′-end of RNA through the central pore made by seven subunits. Indeed, earlier biochemical evidence from *in vivo* truncation of Lsm1 and *in vitro* purified Pat1-Lsm1-7 complex lacking Lsm1 C-terminal shows severe mRNA decay impairment and weaker mRNA binding affinities respectively (Chowdhury et al., 2012).

Based on structural analysis two possible scenarios can be hypothesized for possible functions of the helical extension of Lsm1. First, it could block the channel and thus blocking the exit of 3′-end of mRNA from distal face of the complex. In this way,

helix must provide the specificity to bind 3′-end of mRNA thus providing rationality to the earlier observations. Second, unknown interaction partner(s) of Pat1-Lsm1-7 complex may induce conformational change in the Lsm1 C-terminal helix. This change in conformation may allow release of helix from blocking the channel that would allow 3′-end of mRNAs to thread through the channel.

4.5 Pat1 distinct domains provide the structural basis for interaction with Lsm1-7 and other decapping activators

Biochemical analysis of purified proteins in *in vitro* pull-downs supplemented with structural information revealed that Pat1 C-terminal interacts with composite surface provided by Lsm2 and Lsm3 in Pat1-Lsm1-7 complex structure (Section 3.2). These interactions are surprisingly different from previously proposed model of Pat1 interaction with Lsm1-7 in which cytoplasmic specific subunit Lsm1 was suggested to provide specificity to bind Pat1. Interestingly, a conserved motif in Pat1 middle domain is speculated to bind the conserved surface on Lsm2.

The unique property of Pat1-Lsm1-7 complex is the ability to distinguish and bind to oligoadenylated RNAs rather than poly or unadenylated RNAs (Chowdhury and Tharun, 2008). Specificity is predicted to be provided by the Lsm1-7 complex, which prefers binding to U-stretch near 3′ end of mRNAs (Chowdhury and Tharun, 2008). However, Pat1 also binds RNA preferably poly(U) RNA. Its C-terminal domain has a basic patch involved in RNA binding (Braun et al., 2010). The relative contribution of RNA binding ability of the complex can be envisioned as Pat1 provides extra surface for binding RNA in addition to binding specificity provided by Lsm1-7. Pat1 middle and C-terminal domains are also involved in interaction with Xrn1, Dcp1, Dcp2 and RNA and these are mediated by a conserved surface on Pat1 C-terminus, which provide the basis of simultaneous binding of these factors (Jonas and Izaurralde, 2013).

4.6 Cross-talk between mRNA decapping and deadenylation

Deadenylation dependent mRNA degradation pathways are highly conserved in all eukaryotes (Garneau et al., 2007). The association between deadenylation and decapping remains poorly understood. Only few clues can be gathered from the literature but mechanistic details of the coupling of two important events in the mRNA degradation still remain to be investigated.

Pat1 middle and P-rich domain has been shown to interact with the components of Ccr4-Not complex in *Drosophila* and human proteins (Haas et al., 2010; Ozgur et al., 2010). The fact that both the unstructured and low complexity domains are mediated in these interactions highlights the difficulty of *in vitro* purifications and characterization of these interactions (Haas et al., 2010; Jonas and Izaurralde, 2013; Ozgur et al., 2010). Furthermore, the Lsm1-7 complex preference for interaction with the deadenylated mRNAs (Chowdhury et al., 2007) hints on to that Pat1 may interact first with the deadenylase complex and then helps recruiting of the Lsm1-7 complex on the mRNAs. Similarly, interaction of Dhh1 with the components of Ccr4-Not complex has been observed (Coller et al., 2001). Indeed, recent structure of human DDX6 bound with MIF4G domain of CNOT1 revealed for the first time molecular basis of decapping activator protein interaction with the deadenylase complex (Mathys et al., 2014).

With this information in hand, Dhh1 could be regarded as a bridging protein between deadenylation and decapping because of its interaction with Pat1 and Not1 proteins. What role does Pat1 play when interacting with Ccr4-Not complex? Whether the interactions are direct or via Dhh1? What are the implications in these interactions remain yet to be identified.

4.7 Pat1 provides the link between 5' and 3'-ends of mRNA

Pat1 is a key decapping activator protein and its deletion from yeast strain shows strong defects in mRNA decapping, similar to deletion of decapping enzyme Dcp1 and Dcp2 (Nissan et al., 2010; Tharun et al., 2000). The importance of Pat1 in decapping and other associated decay processes can be explained by its plethora of

interactions with decapping proteins by providing a scaffold for interactions (Nissan et al., 2010). Dhh1, Pat1 and Lsm1-7 proteins show positional specificity relative to mRNA rather than sequence specificity. Pat1 and Lsm1-7 show binding preference towards the 3′-end and can also be purified as a separate complex together with Xrn1 (Bouveret et al., 2000). Whereas, Dhh1 has higher propensity to bind near the 5′-end of mRNAs and can be co-purified with decapping enzymes Dcp1-Dcp2 and Edc3 (Mitchell et al., 2013).

In sections, 3.1 and 3.2, Pat1 interactions with Dhh1 and Lsm1-7 complex have been shown biochemically and through structural analysis. In this way for the first time, Pat1 has been shown to interact with two distinct protein complexes known to interact at 3′ and 5′-end of mRNA respectively (Figure 4.1). In addition, it can be concluded that mRNA circular architecture is maintained until the 5′-exoribonucleotic activity of Xrn1 is taken over for mRNA degradation (Figure 4.1).

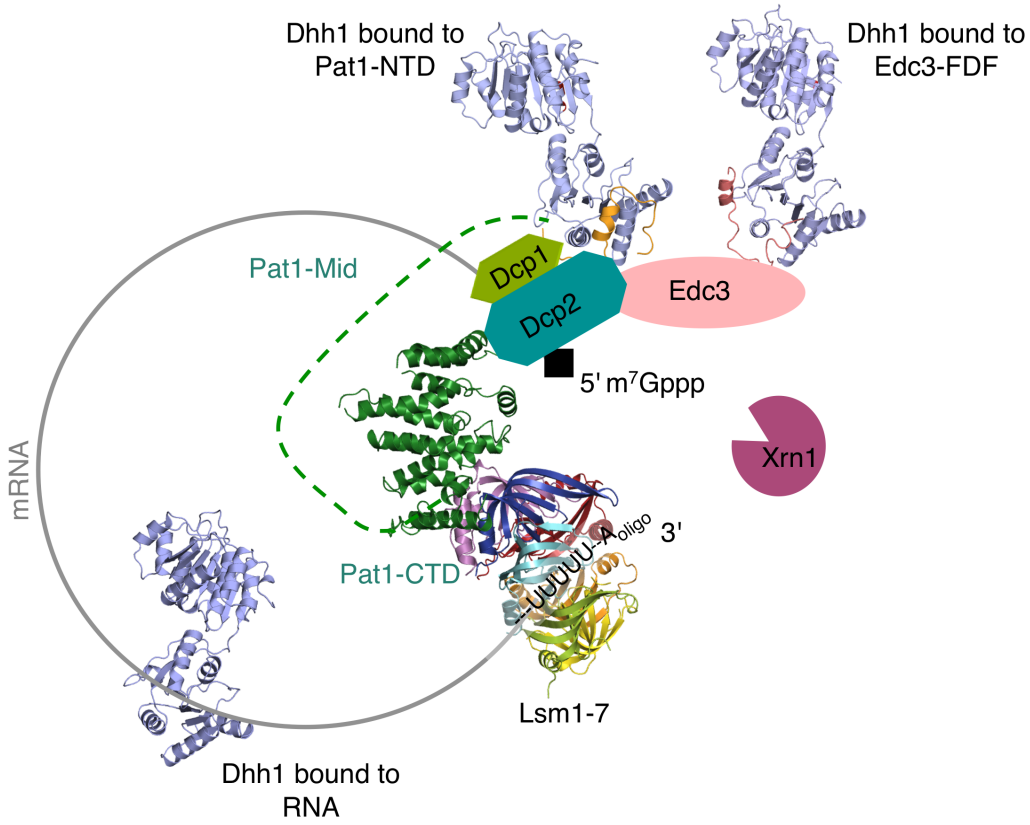

Figure 4.1: Circular mRNA model with decapping complex

Summary of the Sections 3.1 and 3.2. Dhh1 is shown in all the interactions it is involved in, i.e. bound to Pat1-NTD, Edc3-FDF and with RNA simultaneously

(Section 3.1). Pat1-Mid domain is represented as intrinsically disordered region with dashed line and its putative interaction with Lsm2. Pat1-CTD representation bound with Lsm1-7 complex (Section 3.2). Also interactions of Pat1 and Dhh1 with Dcp2 are depicted as putative interactions described in (Nissan et al., 2010). Structural information of Xrn1 interaction with Pat1 and Lsm1-7 complex is still elusive.

Additional to these interactions, Pat1 as well as Dhh1 engage in interactions with Dcp2 and enhances its decapping activity (Nissan et al., 2010). It would be interesting to understand how does these interactions remodel mRNP overall when implicated in these multiple interactions. Whether the interactions can occur simultaneously or are mutually exclusive.

5 Outlook

Recent advancements in structural understanding of decapping activators have opened a vast range of open questions regarding their role in mRNA turnover. Dhh1 involved in mutually exclusive interactions is a compelling target for further functional studies. It would be interesting to understand how mutually exclusive interactions effect the decapping process. Further dissection of Dhh1 direct interaction with other modulating factors, which are involved in imparting its functions in translation repression and deadenylation, is worthwhile.

Pat1 structure solved with Lsm1-7 complex open a wide range of questions for future studies. With further structure elucidation a number of possible questions can be answered. Structural snapshots of Lsm1-7-Pat1 and Lsm1-7 complex bound to RNA can give details regarding how this complex recognizes 3′ oligoadenylated mRNAs. In terms of larger assembly of proteins involved in mRNA decapping and decay, it would be exciting to get atomic or high resolution electron microscopy structures of complex including Pat1, Lsm1-7, Dhh1, Dcp1-Dcp2, Xrn1 and other interacting factors involved in making stable decapping complex. Moreover, snapshots of transient complexes involved in this larger assembly and how it effects the overall decapping and at what step.

From functional point of view, it is intriguing how actively translating mRNAs are brought to a repressed state and in which direct interactions Pat1 and Dhh1 are involved in during translation repression and deadenylation? The sequence of how mRNA decapping activators are recruited to the oligoadenylated mRNAs? How mRNA decapping machinery is assembled on the repressed mRNA? These questions are the foremost questions in the field.

6 Bibliography

Achsel, T., Brahms, H., Kastner, B., Bachi, A., Wilm, M., and Luhrmann, R. (1999). A doughnut-shaped heteromer of human Sm-like proteins binds to the 3'-end of U6 snRNA, thereby facilitating U4/U6 duplex formation in vitro. EMBO J *18*, 5789-5802.

Albrecht, M., and Lengauer, T. (2004). Novel Sm-like proteins with long C-terminal tails and associated methyltransferases. FEBS letters *569*, 18-26.

Allmang, C., Kufel, J., Chanfreau, G., Mitchell, P., Petfalski, E., and Tollervey, D. (1999). Functions of the exosome in rRNA, snoRNA and snRNA synthesis. EMBO J *18*, 5399-5410.

Anantharaman, V., and Aravind, L. (2004). Novel conserved domains in proteins with predicted roles in eukaryotic cell-cycle regulation, decapping and RNA stability. BMC genomics *5*, 45.

Basquin, J., Roudko, V.V., Rode, M., Basquin, C., Seraphin, B., and Conti, E. (2012). Architecture of the nuclease module of the yeast Ccr4-not complex: the Not1-Caf1-Ccr4 interaction. Mol Cell *48*, 207-218.

Beckham, C., Hilliker, A., Cziko, A.M., Noueiry, A., Ramaswami, M., and Parker, R. (2008). The DEAD-box RNA helicase Ded1p affects and accumulates in Saccharomyces cerevisiae P-bodies. Mol Biol Cell *19*, 984-993.

Beggs, J.D. (2005). Lsm proteins and RNA processing. Biochem Soc Trans *33*, 433-438.

Bhaskar, V., Roudko, V., Basquin, J., Sharma, K., Urlaub, H., Seraphin, B., and Conti, E. (2013). Structure and RNA-binding properties of the Not1-Not2-Not5 module of the yeast Ccr4-Not complex. Nat Struct Mol Biol *20*, 1281-1288.

Boeck, R., Tarun, S., Jr., Rieger, M., Deardorff, J.A., Muller-Auer, S., and Sachs, A.B. (1996). The yeast Pan2 protein is required for poly(A)-binding protein-stimulated poly(A)-nuclease activity. The Journal of biological chemistry *271*, 432-438.

Bonnerot, C., Boeck, R., and Lapeyre, B. (2000). The two proteins Pat1p (Mrt1p) and Spb8p interact in vivo, are required for mRNA decay, and are functionally linked to Pab1p. Mol Cell Biol *20*, 5939-5946.

Bouveret, E., Rigaut, G., Shevchenko, A., Wilm, M., and Seraphin, B. (2000). A Sm-like protein complex that participates in mRNA degradation. EMBO J *19*, 1661-1671.

Braun, J.E., Tritschler, F., Haas, G., Igreja, C., Truffault, V., Weichenrieder, O., and Izaurralde, E. (2010). The C-terminal alpha-alpha superhelix of Pat is required for mRNA decapping in metazoa. EMBO J *29*, 2368-2380.

Braun, J.E., Truffault, V., Boland, A., Huntzinger, E., Chang, C.T., Haas, G., Weichenrieder, O., Coles, M., and Izaurralde, E. (2012). A direct interaction between DCP1 and XRN1 couples mRNA decapping to 5' exonucleolytic degradation. Nat Struct Mol Biol *19*, 1324-1331.

Brengues, M., Teixeira, D., and Parker, R. (2005). Movement of eukaryotic mRNAs between polysomes and cytoplasmic processing bodies. Science *310*, 486-489.

Brown, C.E., and Sachs, A.B. (1998). Poly(A) tail length control in Saccharomyces cerevisiae occurs by message-specific deadenylation. Mol Cell Biol *18*, 6548-6559.

Brown, C.E., Tarun, S.Z., Jr., Boeck, R., and Sachs, A.B. (1996). PAN3 encodes a subunit of the Pab1p-dependent poly(A) nuclease in Saccharomyces cerevisiae. Mol Cell Biol *16*, 5744-5753.

Buchan, J.R., Muhlrad, D., and Parker, R. (2008). P bodies promote stress granule assembly in Saccharomyces cerevisiae. J Cell Biol *183*, 441-455.

Callahan, K.P., and Butler, J.S. (2010). TRAMP complex enhances RNA degradation by the nuclear exosome component Rrp6. The Journal of biological chemistry *285*, 3540-3547.

Carroll, J.S., Munchel, S.E., and Weis, K. (2011). The DExD/H box ATPase Dhh1 functions in translational repression, mRNA decay, and processing body dynamics. J Cell Biol *194*, 527-537.

Chang, C.T., Bercovich, N., Loh, B., Jonas, S., and Izaurralde, E. (2014). The activation of the decapping enzyme DCP2 by DCP1 occurs on the EDC4 scaffold and involves a conserved loop in DCP1. Nucleic Acids Res.

Chen, C.Y., and Shyu, A.B. (2003). Rapid deadenylation triggered by a nonsense codon precedes decay of the RNA body in a mammalian cytoplasmic nonsense-mediated decay pathway. Mol Cell Biol *23*, 4805-4813.

Chen, C.Y., and Shyu, A.B. (2011). Mechanisms of deadenylation-dependent decay. Wiley Interdiscip Rev RNA *2*, 167-183.

Cheng, Z., Coller, J., Parker, R., and Song, H. (2005). Crystal structure and functional analysis of DEAD-box protein Dhh1p. RNA *11*, 1258-1270.

Chlebowski, A., Lubas, M., Jensen, T.H., and Dziembowski, A. (2013). RNA decay machines: the exosome. Biochim Biophys Acta *1829*, 552-560.

Chowdhury, A., Mukhopadhyay, J., and Tharun, S. (2007). The decapping activator Lsm1p-7p-Pat1p complex has the intrinsic ability to distinguish between oligoadenylated and polyadenylated RNAs. RNA *13*, 998-1016.

Chowdhury, A., Raju, K.K., Kalurupalle, S., and Tharun, S. (2012). Both Sm-domain and C-terminal extension of Lsm1 are important for the RNA-binding activity of the Lsm1-7-Pat1 complex. RNA *18*, 936-944.

Chowdhury, A., and Tharun, S. (2008). lsm1 mutations impairing the ability of the Lsm1p-7p-Pat1p complex to preferentially bind to oligoadenylated RNA affect mRNA decay in vivo. RNA *14*, 2149-2158.

Cohen, L.S., Mikhli, C., Jiao, X., Kiledjian, M., Kunkel, G., and Davis, R.E. (2005). Dcp2 Decaps m2,2,7GpppN-capped RNAs, and its activity is sequence and context dependent. Mol Cell Biol *25*, 8779-8791.

Coller, J., and Parker, R. (2004). Eukaryotic mRNA decapping. Annu Rev Biochem *73*, 861-890.

Coller, J., and Parker, R. (2005). General translational repression by activators of mRNA decapping. Cell *122*, 875-886.

Coller, J.M., Tucker, M., Sheth, U., Valencia-Sanchez, M.A., and Parker, R. (2001). The DEAD box helicase, Dhh1p, functions in mRNA decapping and interacts with both the decapping and deadenylase complexes. RNA *7*, 1717-1727.

Cougot, N., Babajko, S., and Seraphin, B. (2004a). Cytoplasmic foci are sites of mRNA decay in human cells. J Cell Biol *165*, 31-40.

Cougot, N., van Dijk, E., Babajko, S., and Seraphin, B. (2004b). 'Cap-tabolism'. Trends Biochem Sci *29*, 436-444.

Davey, N.E., Van Roey, K., Weatheritt, R.J., Toedt, G., Uyar, B., Altenberg, B., Budd, A., Diella, F., Dinkel, H., and Gibson, T.J. (2012). Attributes of short linear motifs. Molecular bioSystems *8*, 268-281.

Decker, C.J., and Parker, R. (1993). A turnover pathway for both stable and unstable mRNAs in yeast: evidence for a requirement for deadenylation. Genes Dev *7*, 1632-1643.

Decker, C.J., and Parker, R. (2012). P-bodies and stress granules: possible roles in the control of translation and mRNA degradation. Cold Spring Harbor perspectives in biology *4*, a012286.

Decker, C.J., Teixeira, D., and Parker, R. (2007). Edc3p and a glutamine/asparagine-rich domain of Lsm4p function in processing body assembly in Saccharomyces cerevisiae. J Cell Biol *179*, 437-449.

Ding, L., Spencer, A., Morita, K., and Han, M. (2005). The developmental timing regulator AIN-1 interacts with miRISCs and may target the argonaute protein ALG-1 to cytoplasmic P bodies in C. elegans. Mol Cell *19*, 437-447.

Dunckley, T., and Parker, R. (1999). The DCP2 protein is required for mRNA decapping in Saccharomyces cerevisiae and contains a functional MutT motif. EMBO J *18*, 5411-5422.

Durand, S., Cougot, N., Mahuteau-Betzer, F., Nguyen, C.H., Grierson, D.S., Bertrand, E., Tazi, J., and Lejeune, F. (2007). Inhibition of nonsense-mediated mRNA decay (NMD) by a new chemical molecule reveals the dynamic of NMD factors in P-bodies. J Cell Biol *178*, 1145-1160.

Dutta, A., Zheng, S., Jain, D., Cameron, C.E., and Reese, J.C. (2011). Intermolecular interactions within the abundant DEAD-box protein Dhh1 regulate its activity in vivo. The Journal of biological chemistry *286*, 27454-27470.

Ernoult-Lange, M., Baconnais, S., Harper, M., Minshall, N., Souquere, S., Boudier, T., Benard, M., Andrey, P., Pierron, G., Kress, M.*, et al.* (2012). Multiple binding of repressed mRNAs by the P-body protein Rck/p54. RNA *18*, 1702-1715.

Eulalio, A., Behm-Ansmant, I., and Izaurralde, E. (2007a). P bodies: at the crossroads of post-transcriptional pathways. Nature reviews Molecular cell biology *8*, 9-22.

Eulalio, A., Behm-Ansmant, I., Schweizer, D., and Izaurralde, E. (2007b). P-body formation is a consequence, not the cause, of RNA-mediated gene silencing. Mol Cell Biol *27*, 3970-3981.

Eulalio, A., Huntzinger, E., and Izaurralde, E. (2008). GW182 interaction with Argonaute is essential for miRNA-mediated translational repression and mRNA decay. Nat Struct Mol Biol *15*, 346-353.

Eulalio, A., Rehwinkel, J., Stricker, M., Huntzinger, E., Yang, S.F., Doerks, T., Dorner, S., Bork, P., Boutros, M., and Izaurralde, E. (2007c). Target-specific requirements for enhancers of decapping in miRNA-mediated gene silencing. Genes Dev *21*, 2558-2570.

Eystathioy, T., Jakymiw, A., Chan, E.K., Seraphin, B., Cougot, N., and Fritzler, M.J. (2003). The GW182 protein colocalizes with mRNA degradation associated proteins hDcp1 and hLSm4 in cytoplasmic GW bodies. RNA *9*, 1171-1173.

Fairman-Williams, M.E., Guenther, U.P., and Jankowsky, E. (2010). SF1 and SF2 helicases: family matters. Curr Opin Struct Biol *20*, 313-324.

Fenger-Gron, M., Fillman, C., Norrild, B., and Lykke-Andersen, J. (2005). Multiple processing body factors and the ARE binding protein TTP activate mRNA decapping. Mol Cell *20*, 905-915.

Fischer, N., and Weis, K. (2002). The DEAD box protein Dhh1 stimulates the decapping enzyme Dcp1. EMBO J *21*, 2788-2797.

Franks, T.M., and Lykke-Andersen, J. (2008). The control of mRNA decapping and P-body formation. Mol Cell *32*, 605-615.

Fromm, S.A., Truffault, V., Kamenz, J., Braun, J.E., Hoffmann, N.A., Izaurralde, E., and Sprangers, R. (2012). The structural basis of Edc3- and Scd6-mediated activation of the Dcp1:Dcp2 mRNA decapping complex. EMBO J *31*, 279-290.

Fromont-Racine, M., Mayes, A.E., Brunet-Simon, A., Rain, J.C., Colley, A., Dix, I., Decourty, L., Joly, N., Ricard, F., Beggs, J.D.*, et al.* (2000). Genome-wide protein

interaction screens reveal functional networks involving Sm-like proteins. Yeast *17*, 95-110.

Garneau, N.L., Wilusz, J., and Wilusz, C.J. (2007). The highways and byways of mRNA decay. Nature reviews Molecular cell biology *8*, 113-126.

Gavin, A.C., Bosche, M., Krause, R., Grandi, P., Marzioch, M., Bauer, A., Schultz, J., Rick, J.M., Michon, A.M., Cruciat, C.M., *et al.* (2002). Functional organization of the yeast proteome by systematic analysis of protein complexes. Nature *415*, 141-147.

Haas, G., Braun, J.E., Igreja, C., Tritschler, F., Nishihara, T., and Izaurralde, E. (2010). HPat provides a link between deadenylation and decapping in metazoa. J Cell Biol *189*, 289-302.

Halbach, F., Reichelt, P., Rode, M., and Conti, E. (2013). The yeast ski complex: crystal structure and RNA channeling to the exosome complex. Cell *154*, 814-826.

Halbach, F., Rode, M., and Conti, E. (2012). The crystal structure of S. cerevisiae Ski2, a DExH helicase associated with the cytoplasmic functions of the exosome. RNA *18*, 124-134.

Harigaya, Y., Jones, B.N., Muhlrad, D., Gross, J.D., and Parker, R. (2010). Identification and analysis of the interaction between Edc3 and Dcp2 in Saccharomyces cerevisiae. Mol Cell Biol *30*, 1446-1456.

He, W., and Parker, R. (2000). Functions of Lsm proteins in mRNA degradation and splicing. Curr Opin Cell Biol *12*, 346-350.

He, W., and Parker, R. (2001). The yeast cytoplasmic LsmI/Pat1p complex protects mRNA 3' termini from partial degradation. Genetics *158*, 1445-1455.

Hermann, H., Fabrizio, P., Raker, V.A., Foulaki, K., Hornig, H., Brahms, H., and Luhrmann, R. (1995). snRNP Sm proteins share two evolutionarily conserved sequence motifs which are involved in Sm protein-protein interactions. EMBO J *14*, 2076-2088.

Hsu, C.L., and Stevens, A. (1993). Yeast cells lacking 5'-->3' exoribonuclease 1 contain mRNA species that are poly(A) deficient and partially lack the 5' cap structure. Mol Cell Biol *13*, 4826-4835.

Ingelfinger, D., Arndt-Jovin, D.J., Luhrmann, R., and Achsel, T. (2002). The human LSm1-7 proteins colocalize with the mRNA-degrading enzymes Dcp1/2 and Xrnl in distinct cytoplasmic foci. RNA *8*, 1489-1501.

Ito, T., Chiba, T., Ozawa, R., Yoshida, M., Hattori, M., and Sakaki, Y. (2001). A comprehensive two-hybrid analysis to explore the yeast protein interactome. Proc Natl Acad Sci U S A *98*, 4569-4574.

Jackson, R.J., Hellen, C.U., and Pestova, T.V. (2010). The mechanism of eukaryotic translation initiation and principles of its regulation. Nature reviews Molecular cell biology *11*, 113-127.

Januszyk, K., and Lima, C.D. (2014). The eukaryotic RNA exosome. Curr Opin Struct Biol *24C*, 132-140.

Jensen, T.H., Neville, M., Rain, J.C., McCarthy, T., Legrain, P., and Rosbash, M. (2000). Identification of novel Saccharomyces cerevisiae proteins with nuclear export activity: cell cycle-regulated transcription factor ace2p shows cell cycle-independent nucleocytoplasmic shuttling. Mol Cell Biol *20*, 8047-8058.

Jonas, S., and Izaurralde, E. (2013). The role of disordered protein regions in the assembly of decapping complexes and RNP granules. Genes Dev *27*, 2628-2641.

Jones, C.I., Zabolotskaya, M.V., and Newbury, S.F. (2012). The 5' --> 3' exoribonuclease XRN1/Pacman and its functions in cellular processes and development. Wiley Interdiscip Rev RNA *3*, 455-468.

Kambach, C., Walke, S., Young, R., Avis, J.M., de la Fortelle, E., Raker, V.A., Luhrmann, R., Li, J., and Nagai, K. (1999). Crystal structures of two Sm protein complexes and their implications for the assembly of the spliceosomal snRNPs. Cell *96*, 375-387.

Kedersha, N., Chen, S., Gilks, N., Li, W., Miller, I.J., Stahl, J., and Anderson, P. (2002). Evidence that ternary complex (eIF2-GTP-tRNA(i)(Met))-deficient preinitiation complexes are core constituents of mammalian stress granules. Mol Biol Cell *13*, 195-210.

Kramer, S., Queiroz, R., Ellis, L., Hoheisel, J.D., Clayton, C., and Carrington, M. (2010). The RNA helicase DHH1 is central to the correct expression of many developmentally regulated mRNAs in trypanosomes. Journal of cell science *123*, 699-711.

Kshirsagar, M., and Parker, R. (2004). Identification of Edc3p as an enhancer of mRNA decapping in Saccharomyces cerevisiae. Genetics *166*, 729-739.

Ladomery, M., Wade, E., and Sommerville, J. (1997). Xp54, the Xenopus homologue of human RNA helicase p54, is an integral component of stored mRNP particles in oocytes. Nucleic Acids Res *25*, 965-973.

Leung, A.K., Nagai, K., and Li, J. (2011). Structure of the spliceosomal U4 snRNP core domain and its implication for snRNP biogenesis. Nature *473*, 536-539.

Linder, P., and Jankowsky, E. (2011). From unwinding to clamping - the DEAD box RNA helicase family. Nature reviews Molecular cell biology *12*, 505-516.

Ling, S.H., Decker, C.J., Walsh, M.A., She, M., Parker, R., and Song, H. (2008). Crystal structure of human Edc3 and its functional implications. Mol Cell Biol *28*, 5965-5976.

Liu, H., Rodgers, N.D., Jiao, X., and Kiledjian, M. (2002). The scavenger mRNA decapping enzyme DcpS is a member of the HIT family of pyrophosphatases. EMBO J *21*, 4699-4708.

Liu, J., Rivas, F.V., Wohlschlegel, J., Yates, J.R., 3rd, Parker, R., and Hannon, G.J. (2005a). A role for the P-body component GW182 in microRNA function. Nature cell biology *7*, 1261-1266.

Liu, J., Valencia-Sanchez, M.A., Hannon, G.J., and Parker, R. (2005b). MicroRNA-dependent localization of targeted mRNAs to mammalian P-bodies. Nature cell biology *7*, 719-723.

Liu, Q., Greimann, J.C., and Lima, C.D. (2006). Reconstitution, activities, and structure of the eukaryotic RNA exosome. Cell *127*, 1223-1237.

Maillet, L., and Collart, M.A. (2002). Interaction between Not1p, a component of the Ccr4-not complex, a global regulator of transcription, and Dhh1p, a putative RNA helicase. The Journal of biological chemistry *277*, 2835-2842.

Makino, D.L., Baumgartner, M., and Conti, E. (2013). Crystal structure of an RNA-bound 11-subunit eukaryotic exosome complex. Nature *495*, 70-75.

Mangus, D.A., Evans, M.C., Agrin, N.S., Smith, M., Gongidi, P., and Jacobson, A. (2004). Positive and negative regulation of poly(A) nuclease. Mol Cell Biol *24*, 5521-5533.

Marino-Ramirez, L., and Hu, J.C. (2002). Isolation and mapping of self-assembling protein domains encoded by the Saccharomyces cerevisiae genome using lambda repressor fusions. Yeast *19*, 641-650.

Marnef, A., and Standart, N. (2010). Pat1 proteins: a life in translation, translation repression and mRNA decay. Biochem Soc Trans *38*, 1602-1607.

Marnef, A., Weil, D., and Standart, N. (2012). RNA-related nuclear functions of human Pat1b, the P-body mRNA decay factor. Mol Biol Cell *23*, 213-224.

Mathys, H., Basquin, J., Ozgur, S., Czarnocki-Cieciura, M., Bonneau, F., Aartse, A., Dziembowski, A., Nowotny, M., Conti, E., and Filipowicz, W. (2014). Structural and Biochemical Insights to the Role of the CCR4-NOT Complex and DDX6 ATPase in MicroRNA Repression. Mol Cell.

Mayes, A.E., Verdone, L., Legrain, P., and Beggs, J.D. (1999). Characterization of Sm-like proteins in yeast and their association with U6 snRNA. EMBO J *18*, 4321-4331.

Mazzoni, C., D'Addario, I., and Falcone, C. (2007). The C-terminus of the yeast Lsm4p is required for the association to P-bodies. FEBS letters *581*, 4836-4840.

Meaux, S., and Van Hoof, A. (2006). Yeast transcripts cleaved by an internal ribozyme provide new insight into the role of the cap and poly(A) tail in translation and mRNA decay. RNA *12*, 1323-1337.

Mitchell, P., Petfalski, E., Shevchenko, A., Mann, M., and Tollervey, D. (1997). The exosome: a conserved eukaryotic RNA processing complex containing multiple 3'-->5' exoribonucleases. Cell *91*, 457-466.

Mitchell, S.F., Jain, S., She, M., and Parker, R. (2013). Global analysis of yeast mRNPs. Nat Struct Mol Biol *20*, 127-133.

Moore, M.J. (2005). From birth to death: the complex lives of eukaryotic mRNAs. Science *309*, 1514-1518.

Muhlrad, D., Decker, C.J., and Parker, R. (1994). Deadenylation of the unstable mRNA encoded by the yeast MFA2 gene leads to decapping followed by 5'-->3' digestion of the transcript. Genes Dev *8*, 855-866.

Mund, M., Neu, A., Ullmann, J., Neu, U., and Sprangers, R. (2011). Structure of the LSm657 complex: an assembly intermediate of the LSm1-7 and LSm2-8 rings. J Mol Biol *414*, 165-176.

Naidoo, N., Harrop, S.J., Sobti, M., Haynes, P.A., Szymczyna, B.R., Williamson, J.R., Curmi, P.M., and Mabbutt, B.C. (2008). Crystal structure of Lsm3 octamer from Saccharomyces cerevisiae: implications for Lsm ring organisation and recruitment. J Mol Biol *377*, 1357-1371.

Nissan, T., Rajyaguru, P., She, M., Song, H., and Parker, R. (2010). Decapping activators in Saccharomyces cerevisiae act by multiple mechanisms. Mol Cell *39*, 773-783.

Orban, T.I., and Izaurralde, E. (2005). Decay of mRNAs targeted by RISC requires XRN1, the Ski complex, and the exosome. RNA *11*, 459-469.

Ozgur, S., Chekulaeva, M., and Stoecklin, G. Human Pat1b connects deadenylation with mRNA decapping and controls the assembly of processing bodies. Mol Cell Biol *30*, 4308-4323.

Ozgur, S., Chekulaeva, M., and Stoecklin, G. (2010). Human Pat1b connects deadenylation with mRNA decapping and controls the assembly of processing bodies. Mol Cell Biol *30*, 4308-4323.

Ozgur, S., and Stoecklin, G. (2013). Role of Rck-Pat1b binding in assembly of processing-bodies. RNA Biol *10*, 528-539.

Parker, R. (2012). RNA degradation in Saccharomyces cerevisae. Genetics *191*, 671-702.

Parker, R., and Sheth, U. (2007). P bodies and the control of mRNA translation and degradation. Mol Cell *25*, 635-646.

Pellegrini, O., Mathy, N., Condon, C., and Benard, L. (2008). In vitro assays of 5' to 3'-exoribonuclease activity. Methods Enzymol *448*, 167-183.

Piccirillo, C., Khanna, R., and Kiledjian, M. (2003). Functional characterization of the mammalian mRNA decapping enzyme hDcp2. RNA *9*, 1138-1147.

Pilkington, G.R., and Parker, R. (2008). Pat1 contains distinct functional domains that promote P-body assembly and activation of decapping. Mol Cell Biol *28*, 1298-1312.

Pomeranz Krummel, D.A., Oubridge, C., Leung, A.K., Li, J., and Nagai, K. (2009). Crystal structure of human spliceosomal U1 snRNP at 5.5 A resolution. Nature *458*, 475-480.

Presnyak, V., and Coller, J. (2013). The DHH1/RCKp54 family of helicases: an ancient family of proteins that promote translational silencing. Biochim Biophys Acta *1829*, 817-823.

Reijns, M.A., Alexander, R.D., Spiller, M.P., and Beggs, J.D. (2008). A role for Q/N-rich aggregation-prone regions in P-body localization. Journal of cell science *121*, 2463-2472.

Salgado-Garrido, J., Bragado-Nilsson, E., Kandels-Lewis, S., and Seraphin, B. (1999). Sm and Sm-like proteins assemble in two related complexes of deep evolutionary origin. EMBO J *18*, 3451-3462.

Seraphin, B. (1995). Sm and Sm-like proteins belong to a large family: identification of proteins of the U6 as well as the U1, U2, U4 and U5 snRNPs. EMBO J *14*, 2089-2098.

She, M., Decker, C.J., Sundramurthy, K., Liu, Y., Chen, N., Parker, R., and Song, H. (2004). Crystal structure of Dcp1p and its functional implications in mRNA decapping. Nat Struct Mol Biol *11*, 249-256.

She, M., Decker, C.J., Svergun, D.I., Round, A., Chen, N., Muhlrad, D., Parker, R., and Song, H. (2008). Structural basis of dcp2 recognition and activation by dcp1. Mol Cell *29*, 337-349.

Sheth, U., and Parker, R. (2003). Decapping and decay of messenger RNA occur in cytoplasmic processing bodies. Science *300*, 805-808.

Sheth, U., and Parker, R. (2006). Targeting of aberrant mRNAs to cytoplasmic processing bodies. Cell *125*, 1095-1109.

Sonenberg, N., and Hinnebusch, A.G. (2009). Regulation of translation initiation in eukaryotes: mechanisms and biological targets. Cell *136*, 731-745.

Song, M.G., and Kiledjian, M. (2007). 3' Terminal oligo U-tract-mediated stimulation of decapping. RNA *13*, 2356-2365.

Steiger, M., Carr-Schmid, A., Schwartz, D.C., Kiledjian, M., and Parker, R. (2003). Analysis of recombinant yeast decapping enzyme. RNA *9*, 231-238.

Stevens, A. (1980). Purification and characterization of a Saccharomyces cerevisiae exoribonuclease which yields 5'-mononucleotides by a 5' leads to 3' mode of hydrolysis. The Journal of biological chemistry *255*, 3080-3085.

Stevens, A., and Poole, T.L. (1995). 5'-exonuclease-2 of Saccharomyces cerevisiae. Purification and features of ribonuclease activity with comparison to 5'-exonuclease-1. The Journal of biological chemistry *270*, 16063-16069.

Tantos, A., Han, K.H., and Tompa, P. (2012). Intrinsic disorder in cell signaling and gene transcription. Molecular and cellular endocrinology *348*, 457-465.

Teixeira, D., Sheth, U., Valencia-Sanchez, M.A., Brengues, M., and Parker, R. (2005). Processing bodies require RNA for assembly and contain nontranslating mRNAs. RNA *11*, 371-382.

Tharun, S. (2009). Lsm1-7-Pat1 complex: a link between 3' and 5'-ends in mRNA decay? RNA Biol *6*, 228-232.

Tharun, S., He, W., Mayes, A.E., Lennertz, P., Beggs, J.D., and Parker, R. (2000). Yeast Sm-like proteins function in mRNA decapping and decay. Nature *404*, 515-518.

Tharun, S., and Parker, R. (2001). Targeting an mRNA for decapping: displacement of translation factors and association of the Lsm1p-7p complex on deadenylated yeast mRNAs. Mol Cell *8*, 1075-1083.

Tompa, P. (2012). Intrinsically disordered proteins: a 10-year recap. Trends Biochem Sci *37*, 509-516.

Topisirovic, I., Svitkin, Y.V., Sonenberg, N., and Shatkin, A.J. (2011). Cap and cap-binding proteins in the control of gene expression. Wiley Interdiscip Rev RNA *2*, 277-298.

Tourriere, H., Chebli, K., Zekri, L., Courselaud, B., Blanchard, J.M., Bertrand, E., and Tazi, J. (2003). The RasGAP-associated endoribonuclease G3BP assembles stress granules. J Cell Biol *160*, 823-831.

Tritschler, F., Braun, J.E., Eulalio, A., Truffault, V., Izaurralde, E., and Weichenrieder, O. (2009). Structural basis for the mutually exclusive anchoring of P body components EDC3 and Tral to the DEAD box protein DDX6/Me31B. Mol Cell *33*, 661-668.

Tritschler, F., Eulalio, A., Helms, S., Schmidt, S., Coles, M., Weichenrieder, O., Izaurralde, E., and Truffault, V. (2008). Similar modes of interaction enable Trailer Hitch and EDC3 to associate with DCP1 and Me31B in distinct protein complexes. Mol Cell Biol *28*, 6695-6708.

Tritschler, F., Eulalio, A., Truffault, V., Hartmann, M.D., Helms, S., Schmidt, S., Coles, M., Izaurralde, E., and Weichenrieder, O. (2007). A divergent Sm fold in EDC3 proteins mediates DCP1 binding and P-body targeting. Mol Cell Biol *27*, 8600-8611.

Tucker, M., Staples, R.R., Valencia-Sanchez, M.A., Muhlrad, D., and Parker, R. (2002). Ccr4p is the catalytic subunit of a Ccr4p/Pop2p/Notp mRNA deadenylase complex in Saccharomyces cerevisiae. EMBO J *21*, 1427-1436.

Tucker, M., Valencia-Sanchez, M.A., Staples, R.R., Chen, J., Denis, C.L., and Parker, R. (2001). The transcription factor associated Ccr4 and Caf1 proteins are components of the major cytoplasmic mRNA deadenylase in Saccharomyces cerevisiae. Cell *104*, 377-386.

Uetz, P., Giot, L., Cagney, G., Mansfield, T.A., Judson, R.S., Knight, J.R., Lockshon, D., Narayan, V., Srinivasan, M., Pochart, P.*, et al.* (2000). A comprehensive analysis of protein-protein interactions in Saccharomyces cerevisiae. Nature *403*, 623-627.

Unterholzner, L., and Izaurralde, E. (2004). SMG7 acts as a molecular link between mRNA surveillance and mRNA decay. Mol Cell *16*, 587-596.

van Dijk, E., Cougot, N., Meyer, S., Babajko, S., Wahle, E., and Seraphin, B. (2002). Human Dcp2: a catalytically active mRNA decapping enzyme located in specific cytoplasmic structures. EMBO J *21*, 6915-6924.

Wahle, E., and Winkler, G.S. (2013). RNA decay machines: deadenylation by the Ccr4-not and Pan2-Pan3 complexes. Biochim Biophys Acta *1829*, 561-570.

Wang, L., Lewis, M.S., and Johnson, A.W. (2005). Domain interactions within the Ski2/3/8 complex and between the Ski complex and Ski7p. RNA *11*, 1291-1302.

Wang, X., Watt, P.M., Louis, E.J., Borts, R.H., and Hickson, I.D. (1996). Pat1: a topoisomerase II-associated protein required for faithful chromosome transmission in Saccharomyces cerevisiae. Nucleic Acids Res *24*, 4791-4797.

Wang, Z., Jiao, X., Carr-Schmid, A., and Kiledjian, M. (2002). The hDcp2 protein is a mammalian mRNA decapping enzyme. Proc Natl Acad Sci U S A *99*, 12663-12668.

Weber, G., Trowitzsch, S., Kastner, B., Luhrmann, R., and Wahl, M.C. (2010). Functional organization of the Sm core in the crystal structure of human U1 snRNP. EMBO J *29*, 4172-4184.

Weir, J.R., Bonneau, F., Hentschel, J., and Conti, E. (2010). Structural analysis reveals the characteristic features of Mtr4, a DExH helicase involved in nuclear RNA processing and surveillance. Proc Natl Acad Sci U S A *107*, 12139-12144.

Wells, S.E., Hillner, P.E., Vale, R.D., and Sachs, A.B. (1998). Circularization of mRNA by eukaryotic translation initiation factors. Mol Cell *2*, 135-140.

Wilusz, C.J., and Wilusz, J. (2008). New ways to meet your (3') end oligouridylation as a step on the path to destruction. Genes Dev *22*, 1-7.

Yamashita, A., Chang, T.C., Yamashita, Y., Zhu, W., Zhong, Z., Chen, C.Y., and Shyu, A.B. (2005). Concerted action of poly(A) nucleases and decapping enzyme in mammalian mRNA turnover. Nat Struct Mol Biol *12*, 1054-1063.

Yu, J.H., Yang, W.H., Gulick, T., Bloch, K.D., and Bloch, D.B. (2005). Ge-1 is a central component of the mammalian cytoplasmic mRNA processing body. RNA *11*, 1795-1802.

Zaric, B., Chami, M., Remigy, H., Engel, A., Ballmer-Hofer, K., Winkler, F.K., and Kambach, C. (2005). Reconstitution of two recombinant LSm protein complexes reveals aspects of their architecture, assembly, and function. The Journal of biological chemistry *280*, 16066-16075.

Zheng, D., Ezzeddine, N., Chen, C.Y., Zhu, W., He, X., and Shyu, A.B. (2008). Deadenylation is prerequisite for P-body formation and mRNA decay in mammalian cells. J Cell Biol *182*, 89-101.

Zuo, Y., and Deutscher, M.P. (2001). Exoribonuclease superfamilies: structural analysis and phylogenetic distribution. Nucleic Acids Res *29*, 1017-1026.

7 Acknowledgements

First of all special gratitude goes to my Mom, for being a role model and for teaching me how to survive in tough situations. To my dad, glimpse of memories with him has always been very special to me. Thanks to my brothers Fahad, Fawad and my sisters Rashida, Shazia and Zubaria, whose encouragement and affection kept me on going even during the hard times.

Special thanks to Elena for supporting me and giving the projects that I worked on. Her positive and encouraging attitude towards science and the energy she puts into it is inspirational.

Thanks to the lab members for making a pleasant atmosphere in the lab. To Varun, with whom I shared most of the problems related to graduate life. Sutapa (Shoots), for advices regarding future endeavors and help in postdoc applications. Both of you, Varun and Shoots for discussing the similarities we enjoy being neighbors back in south East Asia in our native languages. Ben for joining in our great Thursday lunches every week and initial help with structure modeling. To Ajla, for all her positive energies, bright smile that cheered me up. To our little group including Shoots, Varun, Ajla, Ben and Marco for occasional sub-continent food gatherings and our “All you can E(at)! ” slogan. To Christian, for making the synchrotron trips enjoyable. To Rajan, for help with crystallography related problems. To Sebastian, for being so expressive and for answering scientific questions. Masami and Eva, what a great trip to Turkey we had together! Special thanks to Eva and Sebastian for reading my thesis and commenting on it. To Sevim, for an unforgettable experience of attending your Turkish wedding. To Ingmar, for great discussions on politics and life in general. To Ksenia, for heads up on many topics especially mTOR during thesis defense preparations. Thanks to Joerg, Marc, Katharina, Gretel, Walter, Judith, Jerome, Claire, Fabien, Jerome, Karina, Sabine, Petra and Tatjana for help when I started in lab and for all little assistances necessary to keep going in the lab. Thanks to all those previous lab members, especially JP, Uma and Felix, who left leaving good memories. Thanks to second floor people, Ira, Justine, Malanie, Julia and Sagar for occasional conversations and sharing the grief of graduate life.

Very special thanks to Prof. Soo Hyun Eom for introducing me to X-ray crystallography and whose support and teaching kept me in this field. To Dr. Esben Lorentzen and Dr. Katja Strasser, for their valuable comments during TAC meetings. Thanks to our collaborators, Kundan Sharma and Prof. Henning Urlaub. To my teacher Tayyaba, whom I always feel indebted to for her finanial support during my schooling. Thanks to Ashiq and Javaid for inspiring me to keep on working hard.
Last but not the least thanks to Zarish, for keeping her calm when I wasn't there with her. Special love to my nieces and nephews for cheering me up with their beautiful conversations.

In the end, a very special gratitude to the Almighty Allah for his countless blessings!